THERMAL DECOMPOSITION CHARACTERISTICS OF MISCANTHUS AND ULVA DURING PYROLYSIS

Y.G. ZABEL
DELFT UNIVERSITY OF TECHNOLOGY

18 October 2018

THERMAL DECOMPOSITION CHARACTERISTICS OF MISCANTHUS AND ULVA DURING PYROLYSIS

By

Y.G. Zabel

To obtain the degree of

Master of Science
in Sustainable Process and Energy Technology

at the Faculty of Mechanical Engineering
Delft University of Technology
to be defended on 13 November 2018 at 15:00

Student number: 4234804
Project duration: September 2017 — November 2018

Thesis committee:

Prof.dr.ir. W. De Jong	TU Delft, supervisor
Prof.dr. D.J.E.M. Roekaerts	TU Delft
Dr. P.V. Aravind	TU Delft
C. Tsekos, MSc	TU Delft, daily supervisor

TU Delft Delft University of Technology

Preface

This master thesis report is the product of a year of research in order to graduate and obtain the degree of Master of Science in Sustainable Process and Energy Technology at the faculty of Mechanical Engineering at the Technical University of Delft, the Netherlands.

The choice for the subject “Thermal decomposition characteristics of Miscanthus and Ulva during pyrolysis”, is due to my interest in renewable energy sources. One of the most important advantages of the use of renewable energy sources is that it contributes to the reduction of greenhouse gases in the atmosphere and it thus counteracts global warming. By choosing this subject I got the opportunity to research the thermal decomposition processes of the renewable energy source ‘biomass’. Extensive research on the decomposition of biomass during pyrolysis contributes to the knowledge that is required to make the use of biomass as a renewable energy source more efficient and thus more feasible for application at large-scale.

The purpose of this thesis is to extend the currently available knowledge of the decomposition characteristics of biomass species and the biomass pyrolysis process in general. In order to achieve this, a literature review was conducted to summarise currently available knowledge on biomass pyrolysis. Furthermore, for various slow heating rates, the decomposition of two biomass species, Miscanthus and Ulva, was investigated experimentally using a thermogravimetric analyser. To study the decomposition characteristics of the two biomass species at fast heating rates experimental research has been carried out in a Pyroprobe reactor.
The effect of the final pyrolysis temperature on the product yields was investigated in the range of 500 to 1000 °C. The yields provide useful information about the decomposition processes occurring during pyrolysis of the particular biomass type. To determine the gas composition the gaseous products from the Pyroprobe experiments were further examined using a micro gas chromatograph. The solid and liquid products were stored carefully and are ready for further examination. The decomposition rates of the two biomass species were modelled with the independent parallel reaction model to obtain kinetic constants corresponding to the decomposition rates of the main biomass components present in Miscanthus and Ulva.

I would like to thank Professor Wiebren de Jong for being my supervisor and giving me the opportunity to conduct this master thesis project under his wing. Furthermore, I would like to thank my daily supervisor Christos Tsekos for his support and for guiding me in the right direction whenever this was necessary.

Yorrit Zabel
Delft University of Technology
18 October 2018

Abstract

Global warming, caused by the excessive release of greenhouse gases due to the use of fossil fuels, is the main reason why a switch to renewable energy sources is becoming a necessity. A renewable energy source with a high potential to contribute to the energy needs worldwide is biomass. Biomass can be used for the production of electricity and heat or for the production of chemicals for a wide range of applications.

The overall challenge for the thermal conversion of biomass is the development of robust and efficient technologies to process biomass with a high conversion efficiency into a useful and clean product. Biomass pyrolysis has great potential to convert a wide range of biomass species into various products.

In this project, the decomposition characteristics of two high-potential biomass feedstocks, Miscanthus and Ulva, were investigated. The grass species Miscanthus has been in the spotlight as a potential biomass feedstock due to its rapid growth, high biomass yield potential and high calorific value. There is a growing interest in the seaweed species Ulva as a potential biomass feedstock due to its rapid growth and due to the fact its use may lead to a reduction of ecological problems (Ulva is a major sea pollutant).

Decomposition characteristics of Miscanthus and Ulva at slow heating rates were investigated with a thermogravimetric analyser. Proximate analysis results and mass loss rate graphs were obtained. The shapes (peaks) of the mass loss rate graphs were linked to the different biomass components present in Miscanthus and Ulva.

For the decomposition at fast heating rates pyrolysis experiments were carried out in a Pyroprobe reactor. The solid, liquid and gaseous product yields were analysed for different final pyrolysis temperatures. The compositions of the gas fractions were analysed using a micro gas chromatograph. The influences of pyrolysis temperature and biomass feedstock composition on the product yields and compositions were linked to different pyrolysis mechanisms

In order to determine the role of different biomass components in the pyrolysis process, the decomposition of the biomass feedstocks and pyrolysis kinetics are further investigated by modelling the mass loss rates of Miscanthus and Ulva during slow pyrolysis obtained from thermogravimetric analysis. For this purpose, the independent parallel reaction (IPR) model was used.
For Miscanthus the mass loss rate was modelled in the temperature range of 100 – 900 °C at different (slow) heating rates using three independent reactions, one for each of its main biomass components hemicellulose, cellulose and lignin. Kinetic constants (activation energies and pre-exponential factors) were obtained for each independent reaction together with the fractions of volatiles of the main components. This resulted in calculated graphs for the mass loss rate of Miscanthus, that deviated less than 1% from the experimentally obtained graph. A Matlab application was built to conduct the modelling of Miscanthus. This application can be used to model the mass loss rates of any lignocellulosic biomass.
For Ulva it was tried to model the mass loss rate using five and ten independent reactions, without success. At first it was tried to model the whole temperature range (100-1200 °C), which had as a consequence that ten independent reactions had to be used in order to model all the different peaks. As this was found to be impossible due to the infinitely long computation times, it was tried to model only the mass loss rate in the temperature range of 100-550 °C. For this, five independent reactions were required. This did not result in valuable kinetic constants as well due to insufficient knowledge of the ranges of the kinetic constants for the different independent reactions.

The experimental and modelling results obtained in this study for Miscanthus and Ulva help characterising the two biomass species. Based on the decomposition rates, product yields and gas compositions, a better understanding of the pyrolysis reaction mechanisms of the different constituents of Miscanthus and Ulva is gathered. This is a contribution to the knowledge required to optimise thermal conversion processes for different biomass species.

Contents

List of Abbreviations

a.r.	As Received
DAF	Dry Ash Free
d.b.	Dry Biomass
DEV	Deviation
ECN	Energy research Centre of the Netherlands
GA	Genetic Algorithm
GC	Gas Chromatography
HPLC	High-Performance Liquid Chromatograph
IPR	Independent Parallel Reactions
LSQ	Least Squares
mGC	Micro Gas Chromatograph
MxG	Miscanthus x giganteus
OF	Objective function
PAH	Polycyclic Aromatic Hydrocarbons
STDEV	Standard Deviation
TGA	Thermogravimetric Analysis
w.b.	Wet Biomass

List of Symbols

Symbol	Parameter	Unit
A	Pre-exponential factor	1/min
a	Conversion	-
b	Heating rate	°C/min
c	Fraction of volatiles	-
D	Diameter	mm
d	Particle size	μm
E_a	Activation energy	kJ/mol
HHV	Higher Heating Value	MJ/kg
k	Reaction rate constant	1/min
LHV	Lower Heating Value	MJ/kg
M	Molecular weight	mol
m	Mass	mg
n	Number of individual reactions	-
O	Reaction order	-
P	Number of experimental points	-
p	Pressure	Pa
R	Universal gas constant	kJ/mol/K
t	Residence time	s
T	Temperature	°C
V	Volume	mL
X	Vector component	-
Y	Mass fraction	-
Greek letters		
φ	Flow rate	mL/min
Subscripts		
i	Index for different parameters	-
j	Index for experimental points	-

Phase 1

1. Introduction

Fossil fuels, such as natural gas, oil and coal, are currently the largest source of energy in the world. It can be seen from chart “A” in *figure 1.1*, that fossil fuels had a global share of 81.5% of the total primary energy supplied in 2015. In the Netherlands the share of fossil fuels was 92.5% of the total primary energy supplied in the same year, as can be seen from chart “B” in *figure 1.1*. Renewable energy sources had a global share of 13.7% of the total primary energy supplied in 2015. In the Netherlands the share of renewable energy was only 6.1% [1, 2].

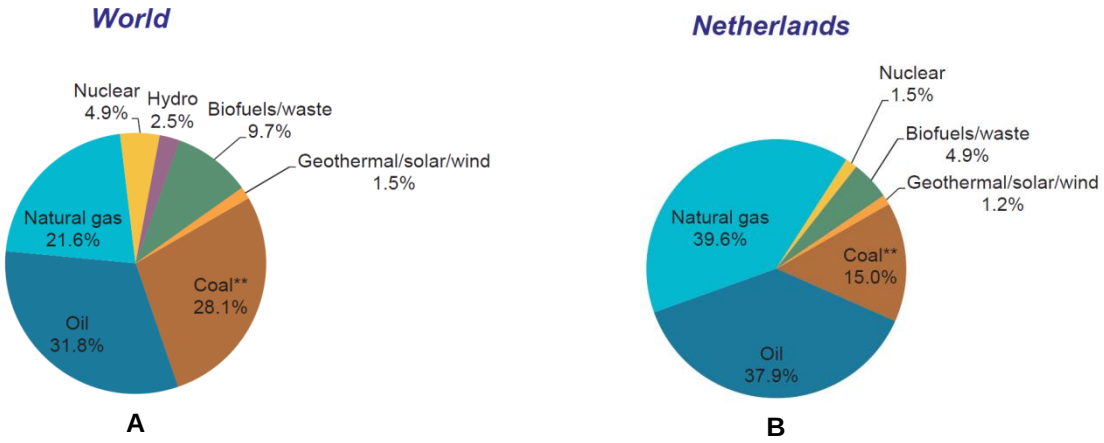

Figure 1.1: Shares of total primary energy supply: the world and the Netherlands (2015) [1, 2].

Progressive depletion of fossil fuel reserves, world's growing energy requirements and global warming – caused by the excessive release of greenhouse gases due to the use of fossil fuels – make a switch to renewable energy sources a necessity.

A renewable energy source with a high potential to contribute to the energy needs worldwide is biomass. Biomass can be used for the production of electricity and heat or for the production of chemicals for a wide range of applications. A significant advantage compared to fossil fuels is the fact that the conversion of biomass feedstocks is carbon neutral, which means that the net carbon emission is zero: the carbon dioxide released into the atmosphere during the conversion of biomass is balanced by the carbon dioxide removed from the atmosphere via photosynthesis during the lifespan of the plants. Therefore, the use of biomass for the production of energy has a minimal contribution to the greenhouse effect compared to the use of fossil fuels. For this reason, extensive research has been carried out to improve thermal conversion processes of biomass materials [3].

Thermal conversion methods, such as combustion, gasification and pyrolysis can be used to convert biomass into useful products. The relatively large amount of volatile matter in biomass means that lower temperatures are required for conversion of these feedstocks compared to conversion of fossil fuels [4]. Biomass combustion is already widely practised. Efficiencies are low at small capacities and fouling and emissions are problematic in many applications. Biomass gasification can obtain higher energy efficiencies than direct combustion at all scales of operation. Biomass pyrolysis, the thermal degradation of biomass by heat in the absence of oxygen, is the subject of many different studies, as it is found to be the primary decomposition stage of both combustion and gasification [5, 6]. Biomass fast pyrolysis (pyrolysis at high heating rates) is gaining attention due to advantages of producing liquid fuels (liquid fuels are easier to store and to transport). The liquid fuel, called bio-oil, can be used as an energy carrier or as a source for various chemicals [7].

2. Research Direction

2.1 Problem Statement

Biomass pyrolysis has great potential to produce energy and/or a wide range of fuels and chemicals. The overall challenge for this biomass conversion method is the development of robust and efficient technologies to process biomass with a high conversion efficiency into a useful and clean product [8].

To be able to optimise thermal conversion methods of biomass, a better understanding of the pyrolysis reaction mechanisms is desired. More research needs to be done in characterising the devolatilisation reactions of potential biomass feedstocks and their main components. Extensive knowledge about the decomposition rates, product yields and product compositions of potential biomass feedstocks is required to determine technical parameters of the pyrolysis process, but also to determine for what purposes the particular biomass species can be used best. Knowledge of the pyrolysis characteristics of the main components is the basis and thus essentially important for a better understanding of biomass thermal conversion.

2.2 Research Question

In the present study the decomposition characteristics of two high-potential biomass species, Miscanthus and Ulva, were analysed during the pyrolysis process and pyrolysis kinetics were studied using the independent parallel reaction model. The aim of this study was to answer the following research question:

"Can the decomposition of Miscanthus and Ulva during pyrolysis be explained based on the decomposition of their main components and can this decomposition be predicted using the independent parallel reaction model?"

The following sub-questions have been studied in order to find a complete answer to the research question:

- *"What is the influence of the biomass composition on the slow pyrolysis for Miscanthus and Ulva?"*
- *"What is the effect of the heating rate on the slow pyrolysis of Miscanthus and Ulva?"*
- *"What is the influence of the biomass composition on the fast pyrolysis of Miscanthus and Ulva?"*
- *"What is the effect of the final pyrolysis temperature on the fast pyrolysis of Miscanthus and Ulva?"*
- *"Can kinetic parameters be found for the decomposition of the main components of Miscanthus and Ulva during slow pyrolysis using the independent parallel reaction model?"*
- *"What is the effect of the heating rate on the kinetic parameters for slow pyrolysis?"*

2.3 Project Scope

To find a thorough answer to the research question, the decomposition characteristics of Ulva and Miscanthus during the pyrolysis process were investigated in the following way:

- In order to determine the role of the main biomass components in the pyrolysis process, the decomposition of the biomass feedstocks is studied based on (non-isothermal) thermogravimetric analysis, which is employed as one of the best methods available for the study and understanding of the thermal behaviour of biomass slow pyrolysis.
- Fast pyrolysis was investigated as well by performing experiments in a Pyroprobe reactor. The solid, liquid and gaseous product yields were analysed as well as the compositions of the gaseous products.
- The pyrolysis kinetics of Miscanthus and Ulva during slow pyrolysis were analysed using the independent parallel reaction (IPR) model. The study of pyrolysis kinetics provides necessary information regarding the engineering design of pyrolysis reactors. The IPR model was used to model the decomposition rates of the biomass species at different heating rates based on the results from thermogravimetric analysis.

3. Biomass Feedstocks

Among different types of biomass feedstocks the grass species Miscanthus and the seaweed species Ulva appear to have numerous promising characteristics for the use as a sustainable energy source, including rapid growth, good yield and simple cultivation and harvesting. One of the main reasons to look into these biomass species is that they can both be cultivated on non-arable land and therefore they do not contribute to the land usage issues. In *paragraph 3.1* the characteristics of Miscanthus are discussed and in *paragraph 3.2* the characteristics of Ulva are reviewed.

3.1 Miscanthus

In this project one of the biomass feedstocks used is Miscanthus. Miscanthus is a perennial, rhizomatous grass originating from East Asia. It is becoming widely cultivated across Europe, as it can be used for the sustainable production of renewable fuels and chemicals [9]. The genus 'Miscanthus' consists of approximately 17 species, such as Miscanthus tinctorius, Miscanthus sinensis and Miscanthus sacchariflorus. The most common species is Miscanthus x giganteus (MxG). This species is a sterile hybrid genotype, which means that it cannot form fertile seeds and that it is a cross between two species, namely Miscanthus sacchariflorus and Miscanthus sinensis. It was formed in order to maximise the productivity and adaptive range of the crop and to prevent proliferation [9, 10].

Miscanthus has been in the spotlight as an alternative energy source due to its rapid growth, high biomass yield potential, high calorific value (20 MJ/kg of dry matter) and high carbon capture. These advantages are due to the fact that MxG possesses the C_4 photosynthetic pathway, which allows for high rates of photosynthesis (most plants are C_3-plants). Furthermore, Miscanthus is easily cultivated under a range of European climatic conditions due to its good adaptability to different climates and soils, simple harvesting and its low requirement of pesticide and fertiliser [11-15]. The fact that Miscanthus is sterile is a disadvantage as well, since it requires vegetative propagation, which is expensive. Therefore, the crop must remain productive for several years, so that establishment costs can be recovered. The lifespan of productive Miscanthus is estimated to be 15 to 20 years [16].

3.1.1 Composition

Miscanthus is a lignocellulosic biomass species and therefore (in general) its main cell wall constituents are cellulose (40-60 wt%), hemicellulose (20-40 wt%) and lignin (10-30 wt%) [9]. Moisture is found to be between 8 and 9 wt% [6]. Also some extractives (compounds such as fatty acids, sterols, and other aromatics) are present in Miscanthus (2.2-4.2%) [9, 17]. In general, the major elemental composition of Miscanthus based on dry matter includes 47-50 wt% carbon, 40-45 wt% oxygen and 5-6 wt% hydrogen. Furthermore, minerals, such as potassium, nitrogen, chlorine and sulphur are present in its composition. The elemental composition of Miscanthus is reported to be 0.5-1.2 wt% potassium, 0.2-0.7 wt% nitrogen, 0.1-0.2 wt% chlorine and 0.1-0.2 wt% sulphur [6, 18]. When biomass is thermally decomposed, the minerals will end up in the ash (ash is the solid residue of thermally decomposed material). According to Lewandowski et al. Miscanthus ash (2.5 wt% [6]) consists of 25-40 wt% SiO_2 (silica or silicon dioxide), 20-25 wt% K_2O (potassium oxide), 5 wt% P_2O_5 (phosphorus pentoxide), 5 wt% CaO (calcium oxide) and 5 wt% MgO (magnesium oxide) [18].

The heating value is an important parameter in defining the biomass feedstock energy content and in evaluating the combustion quality. It is a measure of the thermal energy released upon conversion and it is a key property for determining energy balances. One can distinguish the higher heating value (HHV) and the lower heating value (LHV). The HHV takes into account the latent heat of vaporisation of water (originally present or chemically formed) in the products. The LHV assumes that the latent heat of vaporisation of the water in the reaction products is not recovered. Biomass heating value is tightly connected to the elemental composition and the variation in cell wall composition of the biomass species. Once one knows the biomass ultimate analysis, which determines the elemental composition of the biomass, the HHV can be calculated with the formula presented in *equation 3.1* [19]. The reported HHV for Miscanthus is 17–20 MJ/kg [9].

$$HHV = 34.91Y_C + 117.83Y_H + 10.05Y_S - 1.51Y_N - 10.34Y_O - 2.11Y_{ash} \quad (3.1)$$

in which Y_i is the mass fraction of element i on a dry fuel basis.

The LHV can be calculated from the HHV in two steps, see *equation 3.2* and *equation 3.3*. The first step corrects for the hydrogen content in the dry (0 wt% moisture) fuel [19]:

$$LHV^{db} = HHV - 2.4 \times 8.9 Y_H \ [MJ \cdot kg^{-1}] \quad (3.2)$$

Here, 2.4 MJ/kg is the latent heat of vaporization of water and 8.9 [kg/kg] is the stoichiometric water to H ratio. The second step is to correct for the wet fuel's moisture content as follows [19]:

$$LHV^{wb} = LHV^{db} (1 - Y_{moisture}) - 2.4\, Y_{moisture} \quad (3.3)$$

3.1.2 Cultivation Characteristics

When planting Miscanthus rhizomes in a controlled environment, experimental results show that Miscanthus begins to growth from the dormant winter rhizome when soil temperatures reach 10 to 12 °C. The threshold temperature for leaf expansion of plants ranges from 5 to 10 °C. In the first winter after planting the rhizomes, the rather shallow and underdeveloped rhizomes can be destroyed by cold and wet conditions. These overwintering problems do not occur in the second and subsequent winters. It takes at least two growing seasons before vigorous shoot growth occurs. The full establishment of a Miscanthus stand takes 3 to 5 years [18]. From that moment on, Miscanthus can grow up to 4 meters tall. The height of the plant will depend on the growth conditions [15]. Miscanthus has a low water requirement (270–300 L/kg/year) and weeding is not necessary due to the leaf rug that is formed after 2 years [20].

Miscanthus is harvested annually when the stems are dead, which is determined by the minimum temperatures in colder climates. This is normally in late winter or early spring. Although harvesting before winter would give 30-60 wt% higher yield, Miscanthus is usually harvested from February to April to improve the combustion quality: over the winter moisture content and mineral content decline as a result of leaf loss, the wash out of minerals and extra drying due the wind. Late harvesting reduces the need for mineral removal, which reduces input costs [14, 16, 18].

One of the great benefits of Miscanthus is its large biomass yield. The yield increases in each successive year. In addition, the yield is greatly influenced by location and by the date and method of harvest. There have been huge differences in biomass yields from 2 t/ha to 44 t/ha: Yield above 30 t/ha dry matter have been reported for locations in southern Europe. In central and northern Europe yields without irrigation range usually between 10-25 t/ha dry matter. The main reasons for this are the lower global radiation and average temperature values. Yield variation could also occur due to different by soil types and soil water availability. Although stands are easier to establish on lighter soils, in the long run yields are higher on heavy soils. This is explained mainly by the improved water availability in heavy soils [18]. The energy output of Miscanthus in comparison with energy input has been reported to be circa 15–20:1 [16].

Generally, it should also be noted that biomass characteristics can vary considerably from year to year and between different locations. Weather conditions and soil conditions have a strong influence on biomass quality and composition as well. Overall, a delayed harvest appears to be the most important management tool to improve the biomass quality of Miscanthus [18].
In *figure 3.1 "A"* a picture of Miscanthus can be found.

A **B**

Figure 3.1: Pictures of Miscanthus giganteus (A) and Ulva lactuca (B).

3.2 Ulva

The other feedstock used in this project is the marine biomass called Ulva, also known as sea lettuce. Ulva is a green seaweed species with profusely branching tubular networks, widely encountered in intertidal zones of shores and estuaries [21]. It is a genus of marine and brackish water green macroalgae. The most common species is Ulva lactuca [22]. Other common green seaweeds from the Ulvaceae family are Ulva pertusa, Ulva prolifera and Ulva rigida. Ulva species have a relatively high growth rate compared to other algae. Due to its rapid growth, Ulva is known to be a major sea pollutant causing ecological problems in several oceans worldwide. Its use as a biomass feedstock could reduce environmental problems in seas and oceans [23].

Apart from the high growth rates, Ulva has multiple other desirable features for it to be used as a biomass feedstock. As Ulva is cultivated in a saline water environment, there is less competition with conventional agriculture compared to terrestrial biomass feedstocks. Various unconventional water sources, such as seawater, brackish water and wastewater, can be used in their cultivation [24, 25]. The average photosynthetic efficiency of aquatic biomass is 6–8%, which is much higher than that of terrestrial biomass (1.8–2.2%) [26].
A disadvantage could be that the cultivation of Ulva is energy intensive and requires a high input of nutrients. Therefore, the cost efficiency of the cultivation process is doubtful in case the sole product is energy. Moreover, the production of Ulva in temperate regions will, due to the irradiation, result in a seasonally fluctuating delivery of biomass, and hence pre-treatment and storage costs will have to be considered [27].

3.2.1 Composition

Seaweeds have a different composition than terrestrial biomass species. Their biochemical composition depends strongly on the growth conditions. Ulva has dry matter content of approximately 50 wt%. The dry matter is composed of 31-62 wt% carbohydrates, 8-40 wt% protein and starch, and 0.1-8 wt% lipids [25, 27-29]. The carbohydrates can be divided into 20-28 wt% soluble and 24-35 wt% insoluble carbohydrates. The soluble carbohydrates consist of mainly ulvan (8-29 wt%), a family of sulfated polysaccharides introduced for Ulva species [30]. The insoluble carbohydrates are mainly hemicellulose (17-20 wt%), but also small amounts of cellulose (9 wt%) and lignin (1-14 wt%) [27, 28, 31-33]. The elemental composition is approximately 47 wt% oxygen, 35 wt% carbon, 5 wt% hydrogen and 4 wt% nitrogen [25]. Furthermore, Ulva has large contents of minerals: 3.1-3.4 wt% sulphur, 3.2 wt% sodium, 0.6-2.5 wt% potassium and 1.1 wt% chlorine on dry matter basis. The ash content in Ulva lactuca can range from 10−40 wt% db. [22, 25, 27, 31, 33]. The lower heating value of Ulva lactuca is reported to be between 12.7 and 16.8 MJ/kg [34].

3.2.2 Cultivation Characteristics

Ulva is common from tropical to polar climates, although the strains most likely vary among regions. Despite reports of natural growth rates in northern temperate regions, cultivation has yet only taken place in warmer regions of lower latitudes. Ulva can be harvested from ocean farms, land-based cultivation or natural populations in shallow coastal areas or eutrophic waters. Cultivation in waste water from land-based aquaculture is particularly promising as it can recycle nutrients for terrestrial crop production [27, 35].

Ulva has a lifecycle of one year that peaks in abundance in late spring. The ash-free calorific content increases by 28 wt% over the year, from a June minimum to an October maximum. Ash content showed a similar trend with a June minimum (18.7 wt%) and an October maximum (31.8 wt%). Wet weight calorific content varies over the year with an April minimum followed by an 82.9 wt% increase to a May peak [36].

Ulva gets good scores when considering biomass yields and growth rates. It grows attached to stones or other substrates, but it easily detaches and grows well free floating, often forming dense mats, sometimes called “green tides”. The biomass yield of Ulva lactuca is estimated at 45 tons of dry matter per hectare per year. This is 2–6.5 times the production potential of conventional terrestrial energy crops and three times the production of brown algae in temperate waters [22, 27, 31].
In *figure 3.1 “B”* a picture of Ulva can be found.

4. Biomass Pyrolysis

Pyrolysis is the thermal decomposition occurring in the absence of oxygen. Besides the fact that pyrolysis can be used as an autonomous conversion process, it is also the first step in combustion and gasification processes, where it is followed by total or partial oxidation of the primary products. Lower process temperatures and long vapour residence times favour the production of char coal. High temperatures and moderate residence times increase the biomass conversion to gas and moderate temperatures and short vapour residence times are optimal for producing liquids [37].

4.1 Pyrolysis Process

Pyrolysis is defined as “the thermal decomposition of carbonaceous matter into a range of useful products, in the absence of oxygen”. It consists of a series of complex physical and chemical processes. The pyrolysis process is initiated at around 200 °C, when the thermally unstable components begin to break down (devolatilisation) and evaporate. Large hydrocarbon molecules of biomass are converted into smaller molecules of solid, liquid and gaseous products [38-40].

There are six general steps that occur during the pyrolysis process [41]:

1. Heat transfer from a heat source increases the temperature of the feedstock;
2. The initiation of primary pyrolysis reactions at this higher temperature releases volatiles and forms char;
3. The flow of hot volatiles towards not yet volatilised solids results in heat transfer between the hot volatiles and the solid feedstock;
4. Condensation of some of the volatiles in the colder parts of the feedstock leads to secondary reactions, which can produce tar (tar is a complex mixture of condensable hydrocarbons);
5. Autocatalytic secondary pyrolysis reactions of the volatiles proceed while primary pyrolysis reactions simultaneously occur;
6. Thermal decomposition, reforming, water gas shift reactions, recombination of radicals and dehydration can also occur, which are a function of the residence time and temperature profile of the process.

4.1.1 Pyrolysis Operating Conditions

The pyrolysis products depend mainly on the following operating conditions:
The *(final) pyrolysis temperature* is one of the most important pyrolysis parameters. The different temperature profiles cause different yields and characteristics of the pyrolysis products [42].
The higher the pyrolysis temperature, the higher the amount of volatiles produced (higher liquid and gas yields) and the lower the char production [37].

An increase in *pressure*, leading to a higher degree of secondary and tertiary reactions, results in an increase in the concentration of gases inside the reactor [43]. A higher pressure also favours the formation of char [44].

The *biomass composition* plays an important role in the pyrolysis process. As mentioned before, the major constituents of lignocellulosic biomass are cellulose, hemicellulose and lignin. The weight percentage of these constituents varies for different biomass species. Biomass pyrolysis products are a complex combination of on the one hand the individual pyrolysis reactions of cellulose, hemicellulose and lignin, and on the other hand secondary reactions of primary pyrolysis products. Cellulose degradation produces anhydrocellulose and levoglucosan, which can contribute to char, liquid and gas production. Hemicellulose decomposition produces more volatiles, less tar and less char than cellulose. Lignin pyrolysis yields mostly phenols. It produces more residual char than the pyrolysis of cellulose [41]. More information on the decomposition characteristics of the three main biomass components can be found in *paragraph 4.2*.

The *heating rate* is a very important parameter as well. For a high char production, a low heating rate process should be chosen. A high heating rate provides a shorter time for reactions that induce char production. Rapid heating of the biomass thus favours the formation of volatiles [37].

The *particle size* affects the heat flux in the biomass feedstock. The heat flux is higher for smaller particle sizes due to the higher homogeneity of the feedstock. For smaller biomass particles the reactivity of char is higher as well and the char yield is lower [37]. The yield of volatiles increases with a decrease in particle size, especially in the case of fine particles (<1 mm). For larger particle sizes the liquid yield decreases due to the fact that secondary reactions within the particles become more significant [45].

An increase in *residence time* results in an increase of the gas yield. This could be explained by the (secondary) cracking reactions of the primary pyrolysis product. The longer the residence time, the more cracking reactions can take place. The residence time has only little influence on the primary reactions, since most of the volatile content is quickly released from the biomass, especially if the heating rate is very high [37, 46].

To conclude, if the purpose is to maximise the yield of gaseous products resulting from biomass pyrolysis, a high final pyrolysis temperature, a low heating rate and a long gas residence time would be preferred. If the purpose is to maximise the yield of liquid products, moderate temperatures, a high heating rate and a short gas residence time would be required. For a high char production, a low temperature and a low heating rate should be chosen together with a very long residence time [37].

4.1.2 Types of Pyrolysis

Depending on the operating conditions, the pyrolysis process can be divided into four subclasses: slow (or conventional) pyrolysis, fast pyrolysis, flash pyrolysis and pyrolysis in the presence of a medium. Slow pyrolysis is carried out under relatively low pyrolysis temperatures (250-650 °C). The heating rate in slow pyrolysis (5-100 °C/min) is typically much slower than that used in fast pyrolysis (500-10000 °C/min). A feedstock can be slowly heated or can be held at a constant temperature. Vapours can be continuously removed from the process as they are formed. Fast pyrolysis is a high-temperature (500-1000 °C) process in which biomass is rapidly heated. Biomass decomposes to generate vapours, aerosols, and some charcoal-like char. There are four characteristic conditions of a fast pyrolysis process: a very high heating rate, a carefully controlled pyrolysis reaction temperature, short vapour residence times and rapid cooling of the pyrolysis vapours and aerosols to give bio-oil [41]. Flash pyrolysis of biomass is a promising process for the production of solid, liquid and gaseous fuel, which can achieve up to 75 wt% of bio-oil yield. This process can be characterised by rapid devolatilisation in an inert atmosphere, very high heating rates (>60000 °C/min), very high reaction temperatures (800-1200 °C) and very short gas residence times [47]. In *table 4.1* the range of the main operating conditions is summarised for the different pyrolysis types mentioned above.

A special type of pyrolysis is pyrolysis in the presence of a medium. It uses either hydrogen or water as a medium in the pyrolysis process. When the medium is hydrogen, the process is called hydro-pyrolysis. Hydro-pyrolysis is typically carried out under high-pressure conditions. It can increase the volatile yield and the proportion of lower-molar-mass hydrocarbons. When high-temperature water is used in the thermal cracking of biomass, the process is called hydrous pyrolysis [38].

Table 4.1: Range of main operating conditions for the different pyrolysis types [5].

	Conventional pyrolysis	Fast pyrolysis	Flash pyrolysis
Pyrolysis temperature (°C)	250-650	500-1000	800-1200
Heating rate (°C/min)	5-100	500-10000	>60000
Particle size (mm)	5-50	<1	<0.2
Solid residence time (s)	450-550	0.5-10	<0.5

4.2 Pyrolysis Reaction Mechanisms

Pyrolysis of biomass is very complex due to the diversity, the heterogeneity and the limited thermal stability of some of the components. It is most frequently considered as the superposition of three main primary mechanisms: char formation, depolymerisation and fragmentation. For sufficient reaction times also secondary mechanisms can occur.
Lignocellulosic biomass species mainly consists of three components: 30–60 wt% cellulose, 20–35 wt% hemicellulose and 15–30 wt% lignin, together with some resins and minerals. Pyrolysis of biomass yields approximately the products expected from the pyrolysis of its three main components separately, despite synergetic effects. The study of the individual components thus forms the basis of the expected reaction pathways and determines the occurring primary and secondary reactions. However, for a same component, significant differences in the product yields can be found, due to the variety in the origin of the component and of the operating conditions imposed. The temperature of the reactor, the heating rate, the particle size of the material and the gas residence time are the most important parameters that affect the yields [48, 49].

4.2.1 Primary Mechanisms

Primary mechanisms are reaction mechanisms that affect the biomass feedstock directly. the released As mentioned previously, in the case of biomass pyrolysis the three main primary mechanisms are char formation, depolymerisation and fragmentation [49].:

Char formation is the conversion of biomass into a solid residue named char, which presents an aromatic polycyclic structure. This pathway is generally favoured by intra- and intermolecular rearrangement reactions, which result in a higher degree of reticulation and in a higher thermal stability of the residue. The main steps of this pathway are the formation of benzene rings and the combination of these rings into a polycyclic structure. All these rearrangement reactions are generally accompanied by the release of water and non-condensable gases [49].

Depolymerisation is the breaking of the bonds between the monomer units of the polymers. After each rupture, stabilisation reactions of the two new chain ends occur. Depolymerisation results in a decrease in the degree of polymerisation of the chains until the produced molecules become volatile. These molecules, which are condensable at ambient temperatures, are most frequently found in the liquid fraction in the form of derived-monomer, dimer or trimer [49].

Fragmentation is the breaking of the covalent bonds within the monomer units of the biomass polymers and results in the formation of non-condensable gases and a diversity of small-chain organic compounds, which are condensable at ambient temperatures [49].

The distribution of volatile compounds highly depends on the temperature in the reactor. While char formation reactions and depolymerisation reactions are favoured between 250 °C and 500 °C, fragmentation reactions on this temperature range only concern a few types of chemical bonds. As a consequence, the optimum liquid yields are obtained in processes where the temperature in the reactor is generally between 450 and 550 °C. When the temperature rises above 550 °C, more and more fragmentation reactions happen, which result in the formation of low molecular weight (MW) compounds, some of which are non-condensable [49]. An overview of the primary reaction mechanisms can be found in *figure 4.1*.

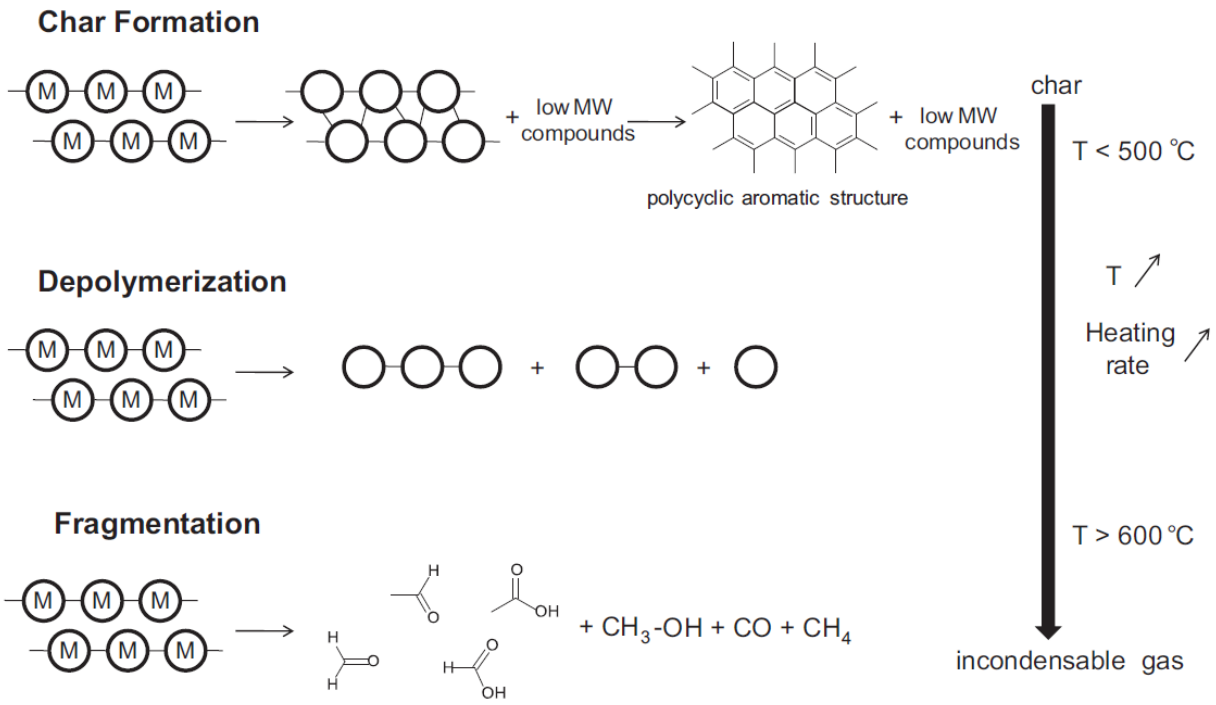

Figure 4.1. Overview of the primary pyrolysis reaction mechanisms [49].

4.2.2 Secondary Mechanisms

Secondary mechanisms are reaction mechanisms that affect the products of the primary reaction mechanisms. In the case of biomass pyrolysis, the released volatiles can undergo secondary reactions if they are not stable at the current reactor temperature. The two main secondary mechanisms in biomass pyrolysis are cracking and recombination [49].

Cracking reactions consist of the breaking of chemical bonds within the volatile compounds and result in the formation of lower MW molecules. As the breaking of the same chemical bonds can undergo either within the polymers or within the volatile compounds, there are similarities in the products obtained from fragmentation and cracking reactions and it is sometimes difficult to figure out which pathway is mainly responsible for the formation of low MW compounds [49].

Recombination (or recondensation) is the combination of volatile compounds to give a higher MW molecule, which sometimes is no longer volatile under the conditions in the reactor. Recombination reactions inside the pores of a polymer can lead to the formation of a secondary char. The presence of polycyclic aromatic hydrocarbons (PAH) in the gas phase is characteristic for favourable conditions for recombination reactions. With very high heating rates (>5000 °C/min), many types of chemical bonds are simultaneously broken, which leads to the release of many volatile compounds before rearrangement reactions are likely to happen [49].

The influence of the cracking of volatile compounds on product yields becomes significant for temperatures above 600 °C, while the appearance of PAH, characteristic for recombination reactions, is generally observed at much higher temperatures (≥800 °C). These secondary reactions are more likely to happen with longer residence times of the volatile compounds in the reactor [49].

4.3 Conversion of Lignocellulosic Biomass Components

Lignocellulosic biomass is mainly composed of macromolecular substances – cellulose, hemicellulose and lignin – together with smaller amounts of low molecular weight substances: extractives and inorganics (salts or minerals). Moisture is also present in biomass in the cell walls, void areas and in the vapour phase. Extractives are organic compounds, such as waxes, fats, resins and starches. Inorganics are the species that form the ashes, such as minerals [49]. Despite the promotion of the devolatilisation at the low-temperature range (catalytic effect), mineral matter promotes the formation of char [50]. Biomass has a porous structure and consists of cells. In a typical cell, cellulose represents an important structural element that is surrounded by other substances that function as matrix (hemicellulose) and encrusting (lignin) materials [49].

Generally, the thermal degradation profiles of lignocellulosic biomass are interpreted as the addition of the independent degradations of their main components. Therefore, lignocellulosic biomass pyrolysis can be divided into four individual stages: moisture evolution (0–100 °C), hemicellulose decomposition (200-350 °C), cellulose decomposition (300–400 °C) and lignin decomposition (100–900 °C). The differences in the inherent structures and chemical nature of the three components possibly account for the different behaviours observed. Hemicellulose, consisting of various saccharides, appears to have a random, amorphous structure, rich of branches, which are very easy to remove from the main stem and to degrade to volatiles evolving out (CO, CO_2, and some hydrocarbons, etc.). Different to hemicellulose, cellulose consists of a long polymer of glucose without branches, its structure is in a good order and very strong. Lignin is full of aromatic rings with various branches. The chemical bonds in lignin covered an extremely wide range, causing a high thermal stability. This is the reason why the degradation of lignin occurs in a wide temperature range [51].

To clarify the weight loss characteristics of the individual biomass components hemicellulose, cellulose and lignin, the TGA plots of these components for a temperature range of 0–900 °C are shown in *figure 4.2*.

It should be noted that the pyrolysis behaviour of algal biomass is quite different from that of lignocellulose biomass. Algal biomass consists of proteins, lipids and carbohydrates, which can be pyrolysed more easily than the cellulose, lignin and hemicellulose that are usually present in terrestrial biomasses. Moreover, the different compositions of biomass may lead to different optimum pyrolysis temperatures, as well as product distributions and compositions [52]. This will be discussed in more detail in *chapter 7*.

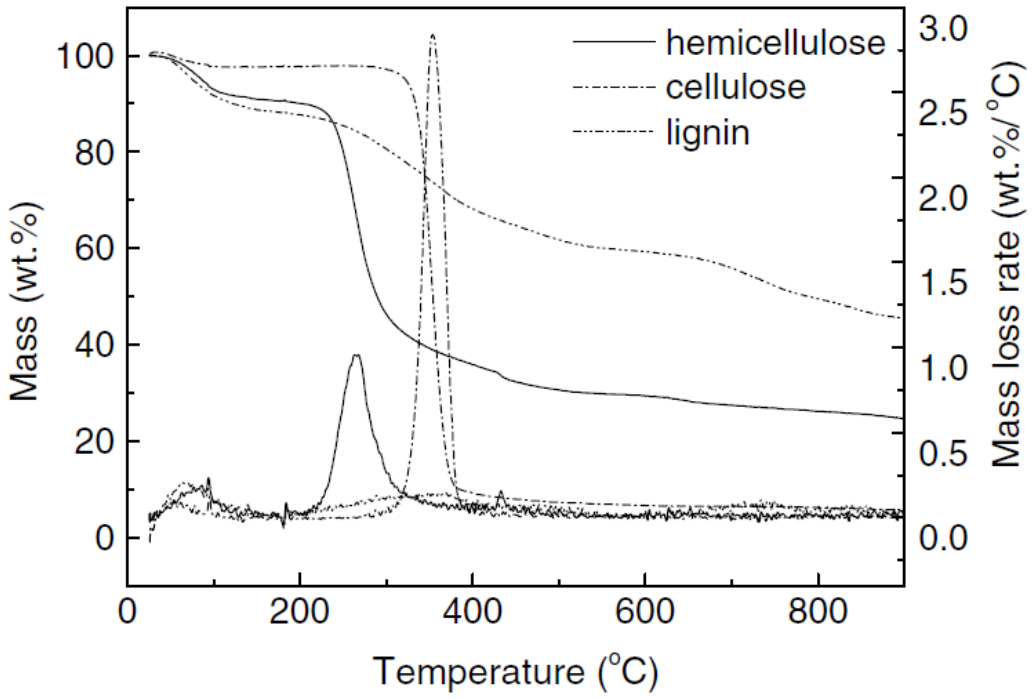

Figure 4.2. TGA curves of individual hemicellulose, cellulose and lignin decomposition [51].

4.3.1 Hemicellulose Conversion

Hemicellulose is a complex component of biomass, interconnected together with cellulose by physical intermixing, and linked to lignin by covalent bonds. Hemicellulose is thermally the least stable component of biomass. For that reason, hemicellulose decomposes faster and at lower temperatures than cellulose and lignin. The main hemicellulose components are xylan and glucomannans. The main decomposition products from xylan are acetic acid, furfural, 1-hydroxy-2-propanone, CO_2, CO and H_2O [53, 54].

The conversion of hemicelluloses mainly occurs in the temperature range 200–350 °C. Hemicellulose is decomposed by dehydration at low temperatures and depolymerisation at higher temperatures. Inorganic impurities cause fragmentation effects. Dehydration yields anhydride fragments, water soluble acids, char, gases and water, while depolymerisation yields volatile organics, levoglucosan and other anhydrohexoses, levoglucosenone and furans. For temperatures higher than 350 °C, the weight loss is associated with the rearrangement of the residue during the secondary charring process. This may be caused by the difference in thermal stability of the monomer units (or the linkages between these units) and in the crystallinity of the constituents [48, 49]. The main reactions occurring during xylan pyrolysis are shown in *figure 4.3*. A commercial hemicellulose can hardly be purchased whereas xylan, although it might have different physical and chemical properties, has been widely used as the representative component of hemicellulose in pyrolysis processes [51].

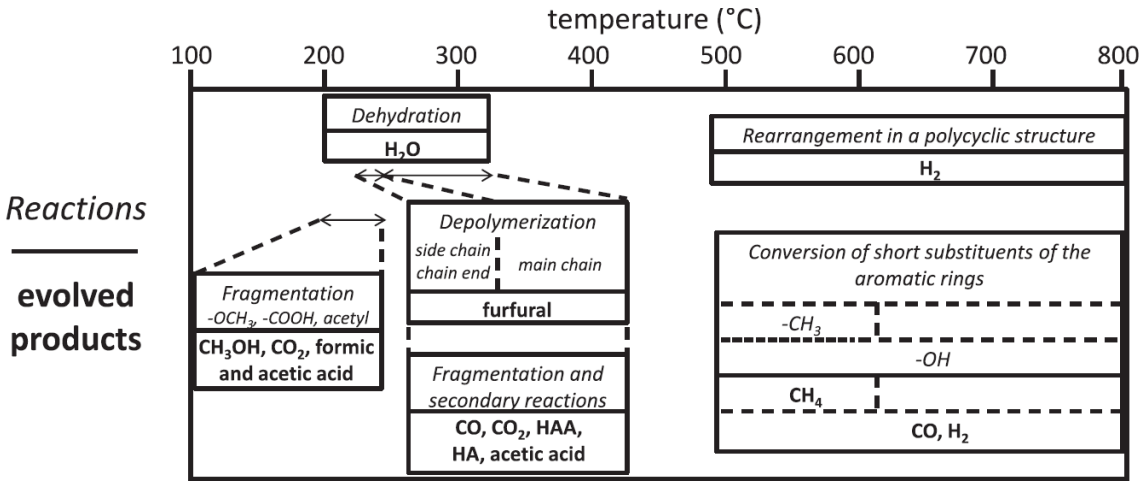

Figure 4.3. Main reactions occurring during xylan (hemicellulose) pyrolysis [49].

4.3.2 Cellulose Conversion

Cellulose, $(C_6H_{10}O_5)_n$, is the main component of plant cell walls and consists of anhydroglucose units, connected by glycoside bonds. Of all lignocellulosic components, the thermal decomposition of cellulose is mostly investigated and best understood. The three competitive primary reactions are described below:

- Dehydration into char, gases and water.
- Depolymerisation into levoglucosan and other primary anhydrosugars.
- Fragmentation into hydroxyacetaldehyde and other carbonyls, acids and alcohols.

Dehydration dominates at low temperatures (<100 °C) and slow heating rates. At higher temperatures, depolymerisation and fragmentation are dominant. Depolymerisation dominates at temperatures between 300 and 450 °C, while fragmentation has its optimum at around 600 °C [48].

The main conversion of cellulose occurs between 300 and 390 °C with a highest decomposition rate generally comprised between 330 and 370 °C. During this step, most of the evolved products are condensable organic compounds. For temperatures higher than 400 °C, the residue becomes more and more aromatic [49].

Experimental studies have shown that cellulose pyrolysis produces levoglucosan as an intermediate product, which is then converted into tar compounds. Besides levoglucosan, other primary tar components are produced during cellulose pyrolysis as well, such as furfural, glycolaldehyde, hydroxyacetone, formic acid and acetic acid. Increasing yields of CO, CH_4 and H_2 were linked to decreasing yields of levoglucosan, glycolaldehyde, formic acid and furfural [53].

The products of primary pyrolysis can further undergo secondary reactions in the condensed phase or outside the cellulosic matrix. Recombination can lead to secondary charring, which is associated with the production of H_2O, CO_2 and the formation of volatile PAH. Secondary charring is favoured at low temperatures and enhanced with increasing residence time of the volatiles, increasing pressure and increasing presence of inorganics. Cracking of the volatiles can be induced inside (heterogeneously) or outside (homogeneously) the cellulosic matrix. Homogeneous tar cracking in the gas phase, which produces mainly CO, is relevant for temperatures above 500 °C [54]. The main reactions occurring during cellulose pyrolysis are shown in *figure 4.4*.

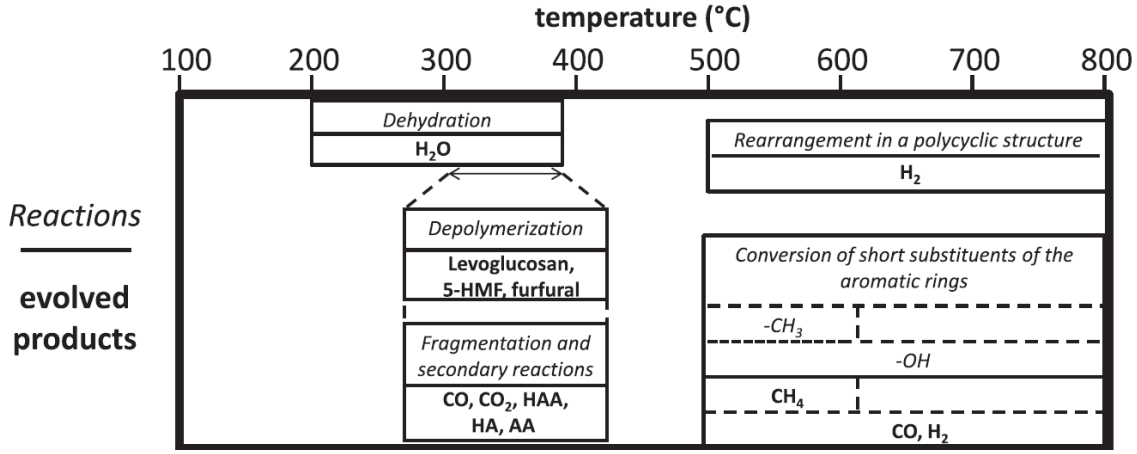

Figure 4.4. Main reactions occurring during cellulose pyrolysis [49].

4.3.3 Lignin Conversion

Lignin is the strengthening component of the cell wall. The fraction normally consists of 20–40 wt% of the dry biomass. Lignin is a complex racemic polymer of hydroxyl and is composed of p-hydroxyphenyl, guaiacyl and syringil units. The complexity of the structure depends on the plant species and due to its structural diversity, lignin pyrolysis yields various products, such as catechols, vanillins and aromatic hydrocarbons [48, 53].

Lignin pyrolysis is known to produce char, condensable tars and non-condensable gases. During primary pyrolysis 'pyrolytic lignin' is produced together with permanent gases and light condensable species, such as water, carbonyls and alcohols. Primary tars consist of guaiacol and syringol units, which resemble the original lignin structure [53, 54].

In secondary reactions, that may take place inside the matrix or in the gas phase, pyrolytic lignin can further react, producing not only other phenolic oligomers, but also phenolic monomers, char, gases and light condensable species. Examples of secondary tars from lignin are phenols, catechols, pyrogallols, cresols and xylenols. The reduction of tar yield from lignin due to secondary reactions is slower than the reduction of tar yield from holocellulose (cellulose and hemicellulose). This is caused by the higher stability of the aromatic (ring-shaped) structure of the tars from lignin. Since only the lignin fraction of the biomass is aromatic in nature, lignin represents a potential precursor for PAH formation. The formation of PAH is enhanced at high temperatures (>800 °C) due to (secondary) recombination reactions [54].

The decomposition of lignin occurs in a wide temperature range (100–900 °C) due to the broad range of activity of the chemical bonds in lignin aromatic rings. At low temperatures dehydration dominates, while at higher temperatures a diversity of lignin monomers is formed. The highest decomposition rate generally occurs between 360 and 400 °C. The instability of the propyl chains, linkages between monomer units and methoxy-substituents of the aromatic rings is responsible for the release of volatile compounds. After this main step of primary volatile release, a charring process occurs, which consists of the rearrangement of the char skeleton in a polycyclic aromatic structure. The volatile compounds released by these rearrangement reactions are mostly low MW non-condensable gases. Throughout the reaction the concentration of benzene rings within the residue tends to increase. Under inert atmosphere, the benzene rings are very stable. Most of the aromatic rings that will form the char are already present in the initial lignin [49, 53]. The main reactions occurring during lignin pyrolysis are shown in *figure 4.5*.

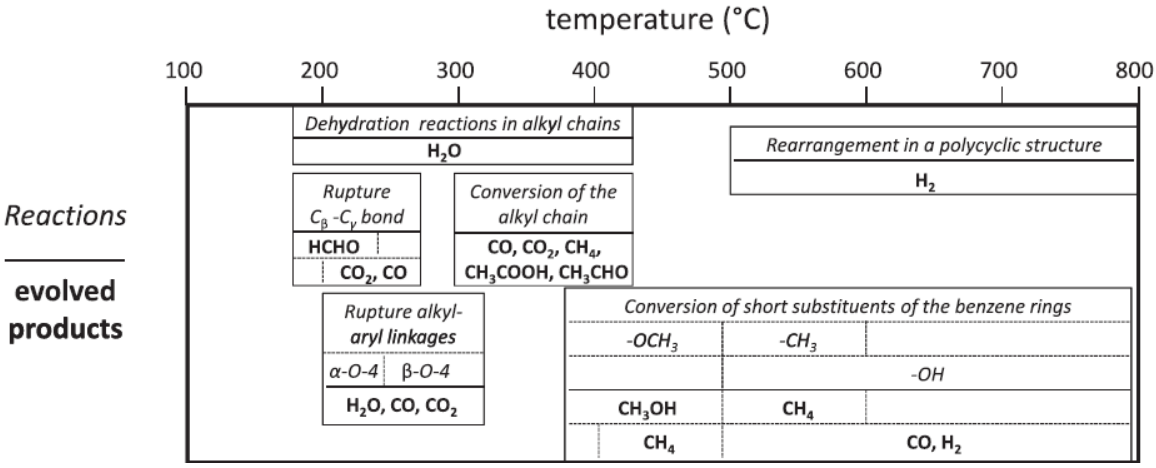

Figure 4.5. Main reactions occurring during lignin pyrolysis [49].

4.4 Pyrolysis Products

Pyrolysis generally produces the following three products: a solid product called char, which is a solid residue mainly containing carbon; a liquid product called bio-oil, which is a viscous and corrosive liquid composed of condensable hydrocarbons and water; and a gaseous product, which contains permanent gases, such as H_2, CO, CO_2, CH_4.

4.4.1 Solid product

Bio-char is the solid product of pyrolysis. It is primarily carbon (~85 wt%), but it can also contain some oxygen and hydrogen. Unlike fossil fuels, biomass contains very little inorganic ash. The heating value of biomass char is about 32 MJ/kg, which is substantially higher than that of the parent biomass or its liquid product. It is characterised by large pore surface area [38].

4.4.2 Liquid product

The liquid fraction produced during the pyrolysis process, also called pyrolysis oil or bio-oil, is a black, tarry fluid with an acrid or smoky odour. It is the desired product of the fast pyrolysis process and it can be used for many different applications. Bio-oil is a mixture of complex hydrocarbons, called tar, with large amounts of oxygen and water (15-30%) [55].

Tar is a complex mixture of condensable hydrocarbons. In detail, the compounds are mainly olefins, phenolics, mono- and poly-nuclear aromatics, heterocyclic aldehydes and alkyl derivatives of aromatics [56]. When studying tar composition and formation, most of the attention should go to the polyaromatic and phenolic fractions of tar, as these compounds not only cause the most problems in downstream applications, but also contain a significant fraction of the total heating value of the product gas stream [57]. Phenolics are aromatic hydrocarbons with at least one OH group (e.g. phenols, cresols, guaiacols, catechols and light gases e.g. carbon oxides) also described as oxygen-containing hetero-atomic compounds. Phenols are typical products of lignin pyrolysis identified from experimental work [53, 56, 58]. Polycyclic aromatic hydrocarbons (PAH), also known as polyaromatic hydrocarbons or polynuclear aromatic hydrocarbons, are hydrocarbons that are composed of multiple aromatic rings. PAH constitute a very extensive and probably the most structurally assorted group of organic compounds [59].

Bio-oils are complex mixtures of compounds that are derived from the depolymerisation of cellulose, hemicellulose and lignin. It can be divided into two phases: an aqueous phase containing a wide variety of organo-oxygen compounds of low molecular weight and a non-aqueous phase containing insoluble organics (mainly aromatics) of high molecular weight. The chemical compositions of bio-oils are determined by many factors, such as biomass type, feedstock pre-treatment (particle size and shape, moisture and ash contents), pyrolysis conditions (temperature, heating rate, residence time, pressure, gaseous environment) as well as vapour filtration and condensation (filter type, condensing method and medium, cooling rate). Therefore, bio-oils produced from different materials and by different pyrolysis reactors may differ greatly from one another. As a result, the fuel properties of different bio-oils usually vary in wide ranges. While the original biomass has a lower heating value (LHV) in the range of 19.5-21 MJ/kg dry basis, its liquid yield has an LHV in the range of 13-18 MJ/kg wet basis [38, 55].

Bio-oils have some promising properties: they usually possess some lubricity and they are less toxic and more biodegradable than petroleum fuels. A significant characteristic of bio-oils is the high percentage of alkylated compounds, especially methyl derivatives. At elevated pyrolysis temperatures, the amount of these oxygenated organic components decreases, and more aromatic components survive, which results in a greater heating value [55, 60]. Compared to traditional biomass fuels, such as black liquor or hog fuel, bio-oil presents a much better opportunity for high-efficiency energy production, and significant effort has been spent on research and development directed to the application of bio-oil for the generation of heat and power and for use as a transport fuel. Furthermore, bio-oil can be readily stored and transported [7].

Besides the good properties, bio-oils have some poor properties as well: they are low-grade liquid fuels when compared with petroleum fuels. The poor fuel properties include the complex multiphase structures, high contents of oxygen, water, solids and ash, low heating values, high viscosity and surface tension, chemical and thermal instability, low pH values, incompatibility with conventional fuels, incomplete volatility, and poor ignition and combustion properties [55]. Furthermore, the variability of the bio-oil composition due to different feedstocks, reactor configurations, and recovery systems that results in differences in physical and chemical properties as well as combustion behaviour makes large-scale applications difficult [7].

Bio-oil has received extensive recognition around the world for its characteristics as a substitute for fuel oil or diesel in many static applications including boilers, furnaces, diesel engines and turbines for electricity generation. If used as a fuel, upgrading of the bio-oil is necessary due to problems with the high water content, the presence of organic acids and the char that is still in the liquid product. After upgrading to methanol or ethanol, it can be used as non-fossil transportation fuels that can be easily integrated into existing fuel distribution networks. Ethyl and methyl alcohol derived from biomass can power vehicles by direct combustion or by operating a fuel cell. Both methods significantly reduce harmful emissions when compared with fossil fuels [60, 61].
Alternatively, bio-oil could serve as a raw material for the production of chemicals. Chemicals can be produced either by using the bio-oil as a whole or from fractionation of the bio-oil. Adhesives (e.g. asphalt bio-binder), phenol-formaldehyde-type resins (e.g. agri-chemicals, fertilisers, acids and emission control agents) and anhydro-sugars, like levoglucosan, can be produced, which can be used for the manufacturing of for instance pharmaceuticals, surfactants, and bio-degradable polymers. Other, more specific chemicals can also be produced from the bio-oils after further processing and separation [7, 61].

4.4.3 Gaseous product

Primary decomposition of biomass produces both condensable and non-condensable gases (primary gas). The vapours which are made of heavier molecules condense upon cooling, adding to the liquid yield of pyrolysis. The non-condensable gas mixture contains lower-molecular-weight gases like hydrogen, carbon monoxide, carbon dioxide, methane, ethane, and ethylene. These do not condense on cooling. Additional non-condensable gases are produced through secondary cracking of the vapour at higher temperature. These are called secondary gases. The final non-condensable gas product is thus a mixture of both primary and secondary gases. The LHV of primary gases is typically 11 MJ/Nm3, but that of pyrolysis gases formed after severe secondary cracking of the vapour is much higher: 20 MJ/Nm^3 [38].

Figure 4.6 gives an overview of the possible applications of fast pyrolysis products.

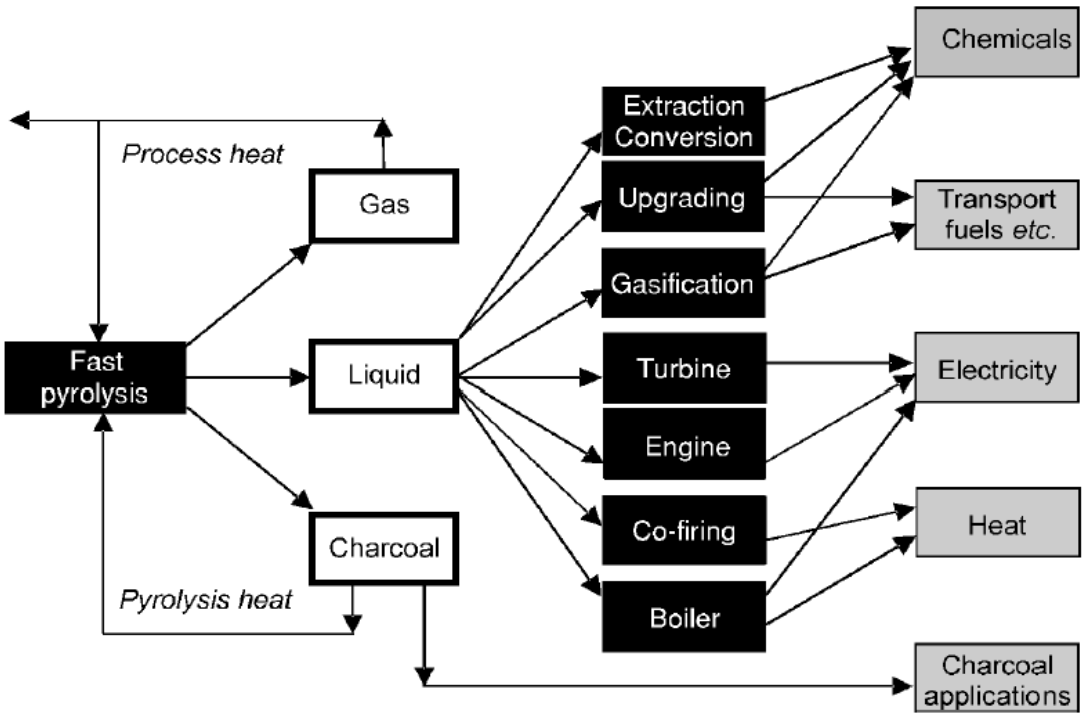

Figure 4.6. Overview of the possible applications of fast pyrolysis products [7].

5. Pyrolysis Kinetics

5.1 Introduction to Pyrolysis Kinetics

Chemical kinetics is the study of chemical processes and reaction rates. Since pyrolysis is a key step in all thermal processes, such as combustion and gasification, the understanding of pyrolysis kinetics is important for the improvement of process efficiency. Therefore, improved understanding of the reaction kinetics of pyrolysis process is required for designing combustors, gasifiers or pyrolysis reactors [62].

Kinetic modelling of reaction rates is based on the Arrhenius equation, see *equation 5.1*. The formula provides insight in the influence of temperature on reaction rates. To be more specific, it gives a relationship between reaction rate and activation energy dependent on temperature. The Arrhenius equation can be used to model temperature variation for many thermally-induced processes and reactions, including thermal degradation during pyrolysis.

$$k = A \cdot e^{-\frac{E_a}{R \cdot T}} \tag{5.1}$$

where,

- k is the reaction rate constant in $1/min$,
- T is the temperature in $Kelvin$,
- A is the pre-exponential factor in $1/min$,
- E_a is the activation energy in kJ/mol,
- R is the universal gas constant ($R = 8.314 \cdot 10^{-3}\ \frac{kJ}{mol \cdot K}$).

The activation energy, E, can be regarded as the energy threshold that must be overcome before molecules can get close enough to react and form products. Only those molecules with adequate kinetic energy to surmount this energy barrier will react. The pre-exponential factor, *A*, provides a measure of the frequency at which all molecular collisions occur regardless of their energy level. Although the pre-exponential factor does exhibit a slight temperature dependency, the main temperature dependence in the Arrhenius equation arises from the exponential term. The exponential term can be thought of as the fraction of collisions having sufficient kinetic energy to induce a reaction. The reaction rate constant, *k*, quantifies the rate of a chemical reaction. It gives the relation between the rate of the reaction and the concentration of the reactant in the reaction. Being a product of the pre-exponential factor and the exponential term, the rate constant yields the frequency of successful collisions [63, 64].

5.2 Kinetic Models for Biomass Pyrolysis

The processes comprising pyrolysis frequently are described as proceeding along concurrent (i.e. competitive and independent parallel) routes, consecutive (or sequential) routes or combinations of the two [64]. Various types of kinetic models can be used to achieve kinetic parameters for thermal decomposition rates of different biomass species. There are two main mathematical approaches used to analyse the data in order to obtain the kinetics data: model-fitting (model-based) and isoconversional (model-free) methods [54].

5.2.1 Model-fitting Methods

In model-based methods, a reaction model must be postulated first. The most appropriate reaction model can solely be selected on the basis of the quality of the regression fit. Nonlinear least squares fitting is the method most commonly employed in the biomass community to fit experimental data and evaluate the Arrhenius parameters. First and *n*th order reaction models are usually selected [54].

The model-fitting methods can be divided into two model types, distributed models and lumped models. In distributed models, it is considered that the pyrolysis products are formed by infinite number of independent parallel reactions having different activation energies given using Gaussian distribution function [62]. In lumped models, the different reaction products of biomass and individual components of biomass are lumped into three product classes: gas, tar and char, for which several kinetic schemes have been proposed for primary degradation of biomass as well as secondary decomposition of volatile products (mainly tar or higher molecular weight hydrocarbons). The lumped

models are further divided to study individual components as well as single homogeneous species decomposition of biomass [62]. A distinction can be made between one-component and multi-component models:

- One-component mechanisms describe the overall rate of devolatilisation from the biomass sample. They generally consist of three parallel reactions, as proposed by Shafizadeh and Chin, for the formation of the three classes of pyrolysis products: char, gas and tars (or liquids). One-component mechanisms have provided reasonable agreement with experimentally observed kinetic behaviour. The advantage of one-component mechanisms is that, when coupled with transport equations, both the yields of products and the decomposition rate can be predicted. However, the assumption of one-component behaviour for composite fuels, such as wood and biomass, unavoidably produces inaccuracies in the details of the decomposition rates [65]. The usefulness of one-component mechanisms is also limited by the assumption of a fixed mass ratio between pyrolysis products (i.e. volatiles and chars), which prevents the forecasting of product yields based on process conditions. Furthermore, in most pyrolysis systems the kinetic pathways are simply too complex to yield a meaningful global apparent activation energy [64].
- Multi-component mechanisms, for the large majority, simply describe the devolatilisation process (the global devolatilisation rate on dependence of time). They can be used to predict only the rate of weight loss, provided that the total amount of matter to be released in the gas/vapour phase is already known (assigned or measured). The most used mechanisms usually comprise parallel reactions for the decomposition of the volatile fractions of pseudo-components, although consecutive reactions can also be applied, owing to significant overlap between the different evolution times. In the former case, each pseudo-component, whose volatile fraction is among the model parameters, acts as if there were no interactions. The number of pseudo-components or zones, in the majority of the cases, is three and again coincides with hemicellulose, cellulose and lignin (three-component devolatilisation mechanisms). In a few cases, the contribution of extractives or more than one reaction stage in the decomposition of components, especially hemicellulose and lignin, are also taken into account. An important aspect is represented by the mathematical treatment of the experimental data to formulate reaction mechanisms and to estimate the related kinetic parameters. The use of multi-component models is recommended for differential (versus integral) measurements, because the details of the devolatilisation process are better shown. Numerical solutions of the conservation equations coupled with minimisation methods of objective functions, adequately defined, are advised [65].

In the present study the independent parallel reaction (IPR) model was used. The IPR model is a multi-component model that separates the total decomposition rate of the biomass into separate decomposition rates for each main biomass component (i.e. cellulose, hemicellulose and lignin for lignocellulosic biomass). A broader explanation of the IPR model can be found in *paragraph 6.4*.

5.2.2 Isoconversional Methods

Isoconversional (model-free) methods can be used to compute kinetic parameters during conversion without model-based assumptions, such as an a priori first order reaction. In these methods the activation energies are calculated at fixed conversions, taking advantage of the fact that the reaction rate depends exclusively on the reaction temperature. There are differential methods, such as the Friedman method, and there are integral isoconversional methods, such as the Kissinger–Akahira–Sunose (KAS), Flynn–Wall– Ozawa (FWO) or Vyazovkin methods [54]. It is noteworthy to distinguish the KAS method from the widely used Kissinger method. The Kissinger method only focuses on the maximum reaction rate during pyrolysis. Therefore, the Kissinger method is not classified as an isoconversional method [66]. Isoconversional approaches eliminate the need to initially hypothesise a form and rate order for the kinetic equation. Hence, isoconversional methods do not require previous knowledge of the reaction mechanism for biomass thermal degradation. Another advantage of isoconversional approaches is that the systematic error resulting from the kinetic analysis during the estimation of the Arrhenius parameters is eliminated [64].

Phase 2

6. Materials & Methods

The materials and methods used to perform the experiments that were performed in order to get valuable answers to the research question and sub-questions are reported in *chapter 6.*

6.1 Thermogravimetric Analyser

Thermogravimetric analysis (TGA) is a technique in which the mass of a substance is monitored as a function of temperature or time as the sample specimen is subjected to a controlled temperature program in an inert atmosphere [67]. TGA is used in this project to study the decomposition of Miscanthus and Ulva during slow pyrolysis. The chemical composition of the biomass feedstocks is investigated via proximate analysis, which divides the biomass compounds into four categories: moisture, volatile compounds, fixed carbon and ash content.

6.1.1 Experimental Set-up

The TGA experiments were performed in an SDT Q600 V20.9 thermobalance, with an alumina cup and a 100 ml/min nitrogen purge flow. The front view of the SDT Q600 is shown in *figure 6.1*. The specifications are stated below [68]:

- Maximum temperature: 1400 °C
- Maximum sample weight: 100 mg
- Maximum heating rate: 100 °C/min
- Balance sensitivity: 0.1 microgram

6.1.2 Procedure

In the TGA, a sample is heated with a programmed thermal history and under controlled atmosphere and the weight loss is continuously monitored. Therefore, the behaviour of a sample under pyrolysis conditions, in a nitrogen (inert) atmosphere, can be studied. The instrument also offers the possibility of the conduction of experiments in the presence of other agents such as air, CO_2 and He (helium). The method employed for each experiment followed the sequence described below [69]:

- Insert sample (sample sizes were between 13–15 mg for Miscanthus and between 34–37 mg for Ulva (to guarantee the uniformity of the Ulva sample)).
- Increase of temperature until 110°C under a 10°C/min heating rate.
- Isothermal operation for 10 min in order to remove the sample's moisture.
- Increase of temperature until final temperature for various heating rates (5, 10, 20° C/min).
- Isothermal operation for 10 minutes to ensure the sample has fully devolatilised
- Isothermal operation for 10 min in order to combust the remaining char. For this interval the nitrogen flow rate is replaced by air with the same flow rate (100 ml/min).
- Cooling off the machine.

Figure 6.1. Front view of the SDT Q600 Thermogravimetric Analyser [68].

6.2 Pyroprobe Reactor

A Pyroprobe is a device that uses resistive heating to thermally decompose (pyrolyse) small samples of solid material carried away by a carrier gas in an oxygen-free environment. The pyrolysis conditions, such as heating rate, final temperature and holding time, are easily controllable using the Pyroprobe software. The pyrolysis products can be examined further with a Micro Gas Chromatograph (for the gaseous products) or a High-Performance Liquid Chromatograph (for the liquid products) [70].

6.2.1 Experimental Set-up

In this project, the CDS Analytical Pyroprobe 5200 pyrolyser was used. The Pyroprobe 5200 is a multiple step, platinum filament pyrolysis instrument which prepares samples for analysis by gas chromatography, mass spectrometry or FTIR. The microprocessor of the Pyroprobe 5200 controls the temperature of the filament by calculating the resistance of the filament at set point temperature and supplying the correct voltage to achieve that temperature. The filament used for pyrolysis of samples in a quartz tube is a coil probe.

The pyrolysis filament may reach the temperatures up to 1400 °C and the heating rates may range from 0.01 °C per minute to 20.0 °C per second. For the interface, temperatures may be set to 350 °C. All programming, temperature selection, calibration and run initiation are performed through the PC interface of the Pyroprobe 5200. Selecting the Pyroprobe, Accessory or Sequence icon displays the required fields for those functions. One method includes the Pyroprobe initial, ramp and final set points, and Interface set points. Methods are saved, edited and recalled as with any other Windows based program. During a run, the actual temperatures for both the probe and interface are displayed on the screen, and set points may be examined in other program methods [71].

An overview of the Pyroprobe reactor is shown in *figure 6.2*.

Figure 6.2. Overview of the Pyroprobe reactor [72].

6.2.2 Procedure

Performing an experiment with the Pyroprobe starts with preparing a biomass sample. A fixed amount of biomass is inserted into a 2.1 mm fire-polished quartz tube, which serves as a sample holder. The biomass is held in place by two pieces of seared quartz wool closing both sides of the holder, see *figure 6.3, left*. The biomass sample should be in the centre of the quartz tube where the maximum amount of heat can be supplied by the platinum filament. The full sample holder has to be weighed before and after the experiment to be able to calculate the amount of volatiles escaped and the amount of char produced. This was done using a RADWAG WAX 110 scale with a sensitivity of up to 0.01 mg and a maximum error of 1 mg. When the sample is ready, the Pyroprobe set-up has to be prepared. The flow rate of the carrier gas can be checked by measuring the flow rate with a test tube or with a syringe connected to the Pyroprobe exit.

A clean trap (*figure 6.3, right*) has to be inserted into the Pyroprobe. An impinger bottle has to be connected to the trap functioning as a condenser. 2 ml of isopropanol is added to the impinger bottle to dissolve tar species that pass the trap. The trap has to be weighed before and after the experiment to be able to calculate the amount of condensed tars produced. Tar species that are not condensed, pass the trap and cause a gap in the mass balance, as will be explained later on in *paragraph 7.2*.
The biomass sample has to be inserted into the Pyroprobe filament. It must be made sure that the probe coils are positioned correctly. Any needed adjustments can be made using a tweezers.
When the probe is put back into place, it has to be closed tightly. The desired conditions for the experiment have to be inserted in the Pyroprobe software. By pressing 'Run' in the Pyroprobe software, the experiment will begin.

The Pyroprobe process starts with heating the interface to 300 °C, from an initial temperature of 50 °C. This takes approximately 2,5 minutes. When the interface temperature is approaching 300 °C, a syringe has to be connected to the impinger bottle to be ready for the collection of the product gases at pyrolysis initiation. When the interface reaches the temperature of 300 °C, the filament is heated to the set pyrolysis temperature. After a fixed holding time the heat supply to the filament is stopped and the experiment continues for approximately 5 minutes in order to achieve complete collection of the tar and gaseous products. During this period the interface remains heated at 300 °C. When the Pyroprobe experiment is done, the gas collected in the syringe can be further examined in the micro-GC. The volume of the collected gases in the syringe should be noted as it will be used in the determination of the weight of the product gases.
To collect the tar product from the trap, the trap has to be put into a test tube with 3 ml of isopropanol. The tube has to be left in a standing position for at least 30 minutes creating a tar solution. The tar solution has to be emptied through a Whatman filter paper (90 mm Ø) and collected in a small vial. It can be further examined with a High-Performance Liquid Chromatograph (HPLC) to identify the different compounds present in the solution.
When the temperature of the accessory falls below 50 °C, the probe can be opened safely and the sample holder can be removed. After removing the wool, the char product can be collected and stored for further examination. Once the experiment is done, all the used vessels and tubes are cleaned with acetone. The traps have to be cleaned with isopropanol and dried with pressurised air. The holder is seared with a torch and subsequently cleaned with pressurised air before a new sample can be prepared.

When blockages occur in the Pyroprobe tubes due to for instance condensed tar – this is noticed when the nitrogen flow decreases – the Pyroprobe itself needs to be cleaned. This is done by performing so-called 'blank runs'. These are runs with an empty holder at a pyrolysis temperature of 800 °C. After a blank run the trap and the product gas can contain contaminants. This implies that the Pyroprobe is actually being cleaned. Blank runs should be performed until the traps are as clean as before the run and until the collected gas consists of nothing but nitrogen. The operating protocol for the Pyroprobe can be found in *Appendix A.*

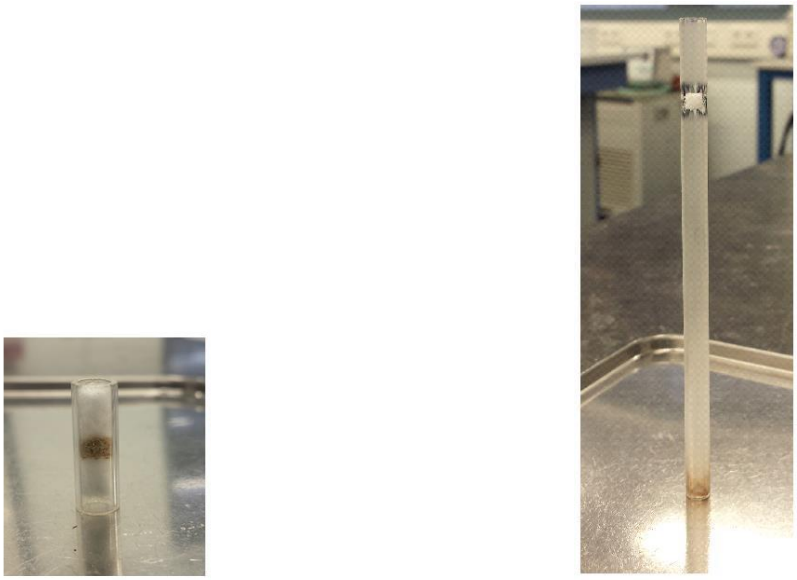

Figure 6.3: A sample holder with a biomass sample in between two quartz wool pieces (left) and a clean trap (right) [69].

Experiments were repeated at the same temperature until two experiments gave results that were similar to each other, so-called 'duplicates'.
When looking for duplicates, in the first place attention is paid to the fractional char yields, since the char yields should be the least fluctuating between experiments compared to the tar and gas yields. Char yields can only deviate per experiment due to possible non-uniformity of the biomass sample, for instance when the sample in one of the experiments has a different composition. This can happen due to the high particle sizes of the biomass samples in the experiments, reducing the uniformity.
Secondly, the tar yields are compared. Tar yields can deviate per experiment mainly as a result of tar condensing in the condenser. Other deviations could be caused by for instance differently compressed biomass samples and non-uniformity of the biomass sample. If the values of the fractional tar yields are similar as well, the two experiments are still potential duplicates.
The final test result that has to be checked is the gas fraction. The gas may not deviate much for different experiments at the same pyrolysis temperature. A deviation in the flow rate caused by a blockage in the Pyroprobe tubes could influence the gas fraction: not only the residence time of the product gas is different, but more importantly if the blockages are caused by condensed tars, these tars could react when the warm flow passes producing more gases. If the gas fraction deviates substantially, there is most likely a problem with the Pyroprobe set-up. For instance, gas leakages (a leakage can happen for instance when the flow circuit is not tightly closed), could result in substantial differences in the gas fractions of two experiments carried out under the same conditions. If the difference in gas yield is minimal, the two experiments meet all the requirements and are therefore chosen as duplicates.
To check if the experiments chosen as duplicates are well executed, one can also look at the mass balances. The mass balance is the sum of the three product fractions. In theory, the value of the mass balance should always be 100% due to principle of mass conservation, but in practice this is never achieved. Reasons for this are explained in *subparagraph 7.2.2*. If experiments are well-executed, the mass balance should not be inexplicably low and the losses should be accounted for.

6.2.3 Operating Conditions

The biomass samples in all the experiments had a weight of 30±0.3 mg. For the experiments with Miscanthus the particle size was ≤80 μm. For the experiments with Ulva the particle size was ≤250 μm. The particle sizes differed due to practical reasons: not enough Ulva was available to make different particle sizes. Nitrogen was the carrier gas. A nitrogen flow rate between 15 and 20 ml/min was used. The pressure in all the experiments was atmospheric.

The final pyrolysis temperatures were chosen to be between 500 and 1000 °C with 100 °C intervals in order to analyse the whole temperature range of fast pyrolysis. Since the actual temperature in the sample holder is lower than the temperature set in the software, the set temperature should be adjusted according to the values stated in *table 6.1* in order to obtain the correct actual temperature. The relation between the two different temperatures was obtained from measurements with thermocouples inserted in the quartz tube (not performed by the author) [69].

Table 6.1: Relationship between actual and set filament temperatures.

Actual Temperature (°C)	Set Temperature (°C)
100	120
200	248
300	375
400	503
500	630
600	758
700	885
800	1013
900	1141
1000	1268

The heating rate was set to 600 °C/s for every experiment in order to achieve fast pyrolysis conditions. The holding time, the time that the Pyroprobe remains at the final pyrolysis temperature, had a fixed value of 10 seconds for all the experiments. The holding time that was set in the Pyroprobe software is converted by the software into the holding time plus the time required for the filament to reach its final temperature using the heating rate of 600 °C/s. In practice, the heating rate of the filament turns out to decrease a bit as the final temperature is approached. Therefore, the calculated holding times are inaccurate and the correct holding times need to be measured manually. To obtain the desired holding time of 10 seconds for each final pyrolysis temperature blank Pyroprobe runs – runs with an empty sample holder – were performed. The results are shown in *table 6.2*. The temperature of the Pyroprobe interface is desired to be as high as possible without harming the equipment. The purpose of a high interface temperature is to facilitate heat transfer and drying. Therefore, it was set to 300 °C. The tubing in the back of the Pyroprobe (behind the reactor chamber), called the 'valve oven', was kept at 325 °C during the experiments.

Table 6.2: Pyroprobe holding time for each pyrolysis temperature.

Actual Temperature (°C)	Holding Time (s)
500	11.2
600	11.5
700	11.9
800	12.5
900	12.9
1000	13.5

Gas Residence Time

The time required for the produced gases to leave the Pyroprobe reactor and enter the trap is called the gas residence time. The gas residence time is an important parameter as it has an influence on the reactions taking place, and thus on the yields and compositions of the pyrolysis products. In order to find the gas residence time it is required to know what pathway the gases take inside the Pyroprobe reactor. An overview of this pathway is shown in *figure 6.4.*

To be able to calculate the gas residence time in the Pyroprobe reactor the volume of the reactor chamber and the valve oven have to be calculated. With a measured diameter of 1.5 cm and a length of 13.8 cm, the volume of the reactor chamber turned out to be 24.39 mL. To get the volume of the reactor chamber during an experiment, the volume of the probe rod and the volume of the probe coil with a full holder inside has to be subtracted from the volume of the empty reactor chamber. The probe rod with an outer diameter of 0.5 inch (1.27 cm) [71] and a length of 11.8 cm has a volume of 14.95 mL. The full holder has a volume of 1.27 mL, calculated with the length of the holder (2 cm) and the outer diameter of the probe coil (estimated to be 0.9 cm, space between coils neglected). Subtracting these values from the volume of the empty reactor chamber results in a volume of 8.17 mL for the reactor chamber during an experiment [71]. The volume of the valve oven was calculated as a straight cylinder with an inner diameter of 0.0345 inch (0.08763 cm) and turned out to be 0.25 mL. The total volume of the pathway of the product gas, which is the reactor chamber plus the tube representing the valve oven, is thus $8.17 + 0.25 = 8.41\, mL$.

To calculate the gas residence time, the total volume of the pathway of the product gas, has to be divided by the flow rate. The flow rate used in the experiments was always between 15 and 20 mL/min. This results in gas residence times between 24.50 s (at 20 mL/min) and 32.67 s (at 15 mL/min). The contribution of the produced gas to the flow rate is negligible, since the volume of the produced gas is very low compared to the volume of the nitrogen carrier gas.

It must be noted that the product gas residence time is probably lower than the residence times calculated above, since the product gases arise at the end of the reactor chamber. When only taking account the volume of the part of the reactor chamber around the probe coil, which has a diameter of 1.5 cm and a length of 2 cm, the total volume becomes $2.26 + 0.25 = 2.51\, mL$. This results in gas residence times between 7.54 s (at 20 mL/min) and 10.05 s (at 15 mL/min). These residence times are more realistic than the ones calculated for the whole volume of the reactor chamber.

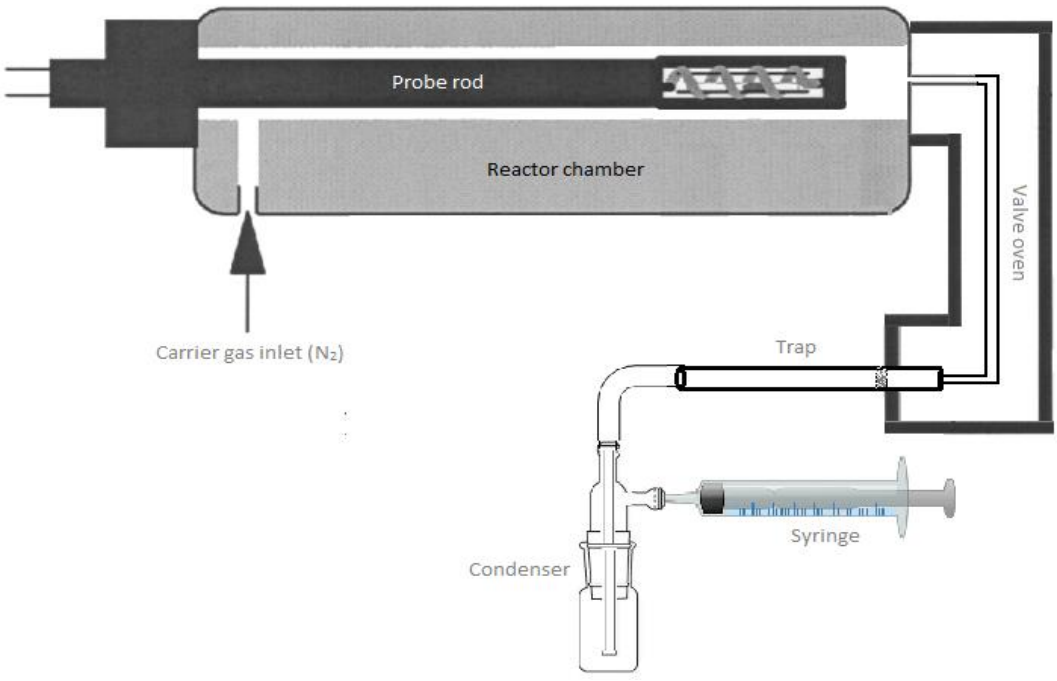

Figure 6.4. Schematic top view of the Pyroprobe reactor set-up.

6.3 Micro Gas Chromatograph

A gas chromatograph is a chemical instrument used to analyse gas samples. A gas chromatograph consists of a column (a narrow tube), which contains a microscopic layer of liquid or polymer on a solid support (stationary phase). Transported by a carrier gas (mobile phase), the gas sample flows through this column at different rates depending on their chemical and physical properties and their interaction with a specific column filling. The components are identified based on their different retention times (the times for the components to exit the column). In the present study, a micro gas chromatograph, also micro-GC or mGC, is used for the analysis of the gas components produced during the pyrolysis experiments.

6.3.1 Experimental Set-up

In this project, the Varian CP-4900 Micro-GC was used. With this chromatograph sample components of interest can be analysed while eliminating others. A gas sample of approximately 200 μL is supplied to the instrument via an injector. The micro-GC is controlled via a computer using the associated workstation software package (Galaxie software). The front panel of the micro-GC consists of information about the status of the apparatus, as can be seen in *figure 6.5*. The status of the micro-GC can either be 'Ready', 'Run', 'Error', or 'Power'. This is shown by led lights that are either on, off or blinking [73, 74].

6.3.2 Procedure

To collect the gaseous product from the pyrolysis experiment a syringe is connected to the Pyroprobe set-up. To supply the product gas to the micro-GC the syringe is transferred to the inlet of the micro-GC. This has to be done quickly in order to not let the gas escape and to not contaminate the gas with air. A small gas sample has to be supplied to the micro-GC. This is done by slightly pressing the syringe. The analysis takes approximately four minutes. After that the results are shown in a table in the micro-GC software, containing information on the volume fractions of the gases found. The micro-GC can be set up to find only the expected gas components. In the case of this study, the gas components expected to be found were hydrogen, nitrogen, carbon monoxide, carbon dioxide and methane. The other gas components found in the mixture were labelled as 'unknown'. The total amount of nitrogen present was assumed to be carrier gas and was therefore left out of the eventual results. With the measured volume fractions of H_2, CO, CO_2 and CH_4 the masses of the individual gas components were calculated using the ideal gas law (see *equation 6.1*).

$$(p \cdot V_i = \frac{m_i}{M_i} \cdot R \cdot T) \tag{6.1}$$

where p is the atmospheric pressure (100 kPa), V_i is the volume fraction of a gas component i, M_i is the molecular weight of gas component i, R is the gas constant ($8.314 \cdot 10^{-3}$ kJ/K/mol) and T is the ambient temperature (293 K). With the weight of the individual gas components the total mass of the product gas could be calculated as well. To obtain the most accurate results and due to the fact that a sufficient amount of gas was available after each experiment, the micro-GC was run four times for the same gas sample.

Figure 6.5. Front view of the micro-GC.

6.4 Kinetic Model Implementation

6.4.1 Independent Parallel Reaction Model

In the present study the independent parallel reaction (IPR) model was used to model the decompositions rates of the biomass feedstocks. The IPR model separates the total decomposition rate of the biomass into three separate decomposition rates for each main biomass component, i.e. cellulose, hemicellulose and lignin. The kinetics of biomass decomposition are routinely predicated on a single reaction (derived from the Arrhenius equation) and can be expressed under isothermal conditions by the first order differential equation shown in *equation 6.2* [64, 75].

$$\frac{da_i}{dt} = \underbrace{A_i \cdot e^{-\frac{E_{a,i}}{R \cdot T}}}_{k} \cdot f(a) \tag{6.2}$$

where,

- *da/dt* is the conversion rate,
- *f(a)* is a function of the conversion *a*,
- *i* is the index of the reaction ($i = 1$ for hemicellulose, $i = 2$ for cellulose, $i = 3$ for lignin),
- *k* is the reaction rate constant in $1/min$.

For O^{th} order reactions the function f(*a*) is equal to $(1–a)^O$. Temperature T can be written as a vector with index *j*, where j corresponds to an experimental point. *Equation 6.2* can now be written as follows:

$$\frac{da_{i,j}}{dt} = A_i \cdot e^{-\frac{E_{a,i}}{R \cdot T_j}} \cdot (1 - a_{i,j})^O \tag{6.3}$$

where

- *da/dt* is the conversion rate as a fraction of the total mass in $1/min$.
- $a_{i,j}$ is the conversion of the *i*th reaction and the *j*th experimental point of the mass sample.
- *O* is the reaction order, which is chosen to be 1 for all reactions in this study

For constant heating rate $dT/dt = b$, *equation 6.3* [75] can be multiplied by the derivative *dt/dT* to obtain the integrable formula in *equation 6.4* [75]:

$$\frac{da_{i,j}}{dT} = \frac{A_i}{b} \cdot e^{-\frac{E_{a,i}}{R \cdot T_j}} \cdot (1 - a_{i,j}) \tag{6.4}$$

Equation 6.4 needs to be integrated by parts to obtain an expression for the conversion $a_{i,j}$. This yields the following expression [75]:

$$a_{i,j} = 1 - \exp\left(\frac{A_i}{b} \int_{T(1)}^{T(p)} \exp\left(-\frac{E_{a,i}}{R \cdot T_j}\right)\right) \tag{6.5}$$

where,

- *T(1)* is the temperature at the start of the heating process,
- *T(p)* is the temperature at the end of the heating process.

In general the indefinite integral $\int_1^\infty exp(-\frac{const}{x_1})$ is equal to $x_1 \cdot \exp\left(-\frac{const}{x_1}\right) - const \cdot E_1(\frac{const}{x_1})$. In the case of this study the constant is equal to $E_{a,i}/R$ and x_1 is equal to T. This results in the following equation [75]:

$$\int_{T(1)}^{T(p)} exp\left(-\frac{E_{a,i}}{R \cdot T_j}\right) = \left\{T_j \cdot \exp\left(-\frac{E_{a,i}}{R \cdot T_j}\right) - \frac{E_{a,i}}{R} \cdot E_1\left(\frac{E_{a,i}}{R \cdot T_j}\right)\right\} - \left\{T(1) \cdot \exp\left(-\frac{E_{a,i}}{R \cdot T_1}\right) - \frac{E_{a,i}}{R} \cdot E_1\left(\frac{E_{a,i}}{R \cdot T_1}\right)\right\} \tag{6.6}$$

where,

- $E_1(x)$, with $x = \frac{const}{x_1} = \frac{E_a}{RT}$, is an exponential integral of the form $E_1(x) = \int_1^\infty \frac{\exp(-z \cdot x)}{z} dx$.

$E_1(x)$ can be solved using Hasting's approximation [76]:

$$x \cdot \exp(x) \cdot E_1(x) = \frac{x^4 + f_1 \cdot x^3 + f_2 \cdot x^2 + f_3 \cdot x + f_4}{x^4 + g_1 \cdot x^3 + g_2 \cdot x^2 + g_3 \cdot x + g_4}, \quad valid\ for\ x \geq 1 \tag{6.7}$$

where,

- $x = \frac{const}{x_1} = \frac{E_a}{RT}$; The restriction $x \geq 1$ is satisfied for all temperatures investigated in this study (up to 1200°C) as long as the activation energies are larger than 12.24 kJ/mol.
- f and g are constants used in Hasting's approximation. Values for *f* and *g* are obtained from [76] and stated in *table 6.3*.

Now, $E_1(x)$ can be calculated using *equation 6.7* and substituted into *equation 6.6*. Then *equation 6.6* can be substituted into *equation 6.5* to obtain the conversion $a_{i,j}$. The solution of *equation 6.5* is used in *equation 6.3* to finally be able to calculate the mass loss rate with one variable, namely the temperature *T*.

Table 6.3: Values of *f* and *g* used in Hasting's Approximation [76].

$f_1 = 8.5733287401$	$g_1 = 9.5733223454$
$f_2 = 18.0590169730$	$g_2 = 25.6329561486$
$f_3 = 8.6347608925$	$g_3 = 21.0996530827$
$f_4 = 0.2677737343$	$g_4 = 3.9584969228$

Eventually the overall mass loss rate, $\left(\frac{dm_j}{dt}\right)_{calc}$ in mg/min, calculated for n reactions and p experimental points is described by *equation 6.8* [75]:

$$\left(\frac{dm_j}{dt}\right)_{calc} = \sum_{i=1}^{n} c_i \frac{da_{i,j}}{dt} \tag{6.8}$$

where,

- c_i is the fraction of volatiles in the *i*th reaction. The sum of the fractions of volatiles should be equal to one: $\sum_1^n c_i = 1$.
- *n* is the number of individual reactions. In the case of lignocellulosic biomass species there is a reaction for each of the main biomass components, i.e. hemicellulose, cellulose and lignin. Therefore, the value of *n* is 3.

In essence this is an algebraic parameter estimation problem with $3 \cdot n$ unknown constants. In the case of lignocellulosic biomasses, n = 3, and thus there are 9 unknown constants: 3 activation energies, 3 pre-exponential factors and 3 fractions of volatiles, one for each of the three main biomass components. The constants can be calculated by introducing a so called "objective function", which describes the square of the difference between the experimental vector values for the overall mass loss rate and the calculated ones. By minimising the objective function globally the desired constants can be achieved. The objective function is stated in *equation 6.9* [75].

$$O.F. = \sum_{j=1}^{P} \left[\left(\frac{dm_j}{dt}\right)_{exp} - \left(\frac{dm_j}{dt}\right)_{calc}\right]^2 \tag{6.9}$$

where,

- $\left(\frac{dm_j}{dt}\right)_{exp}$ is a P-dimensional vector containing experimental data about the mass loss rate of the investigated biomass type.

The objective function value was adjusted in order to account for each experiment by defining the deviation (DEV) between the experimental and calculated curves, as a percentage of the maximum experimental mass loss rate value [75]:

$$DEV\ (\%) = \frac{100}{\max\left[\left(\frac{dm}{dt}\right)_{exp}\right]} \sqrt{\frac{O.F.}{P-3 \cdot n}} \tag{6.10}$$

The goal of the optimisation is to get values for the deviation between experimentally obtained graph and calculated graph as low as possible as long as the values for the constants make physically sense [75].

6.4.2 Implementation of the IPR Model in Matlab

MATLAB R2018a® was used to implement the IPR model. The formula for calculating the total mass loss rate, *equation 6.8*, was implemented in Matlab. *Equations 6.3* and *6.5–6.9* were substituted into *equation 6.8* in order to be able to calculate this total mass loss rates, using the temperature vector as input variable. To be able to find the optimal kinetic constants, the objective function, *equation 6.9*, had to be minimised. This was done by using a solver from the global optimisation toolbox, a package available in Matlab for solving global optimisation problems. Since global solvers compute global minima, it is essential to use a global solver to minimise the objective function in order to try to find the best solution possible. Therefore, in the case of this study, it was best to use a solver from the global optimisation toolbox.

The global optimisation toolbox in Matlab contains several global solvers, such as 'PatternSearch', 'Genetic Algorithm' (GA) and 'GlobalSearch'. In this study the (global) 'GA' solver was used. This is a solver that finds the global minimum of a function using a genetic algorithm. A genetic algorithm is a method for solving optimisation problems based on a natural selection process that mimics biological evolution. The algorithm repeatedly modifies a population of individual solutions. At each step the genetic algorithm selects individuals from the current population and uses them as parents to produce the children for the next generation. Over successive generations, the population "evolves" towards an optimal solution [77]. The GA solver was chosen, since it is known for finding a solution within a reasonable amount of time for functions with many variables and a large search range.
The solver searches for a solution between lower and upper boundaries indicated by the user. Since the formulas for the independent parallel reactions modelling the different biomass components are the same, the ranges of the kinetic constants are the only input data that deviate them from one another. Thus, in order to get valuable results, it is important to use ranges that characterise the main biomass components.

Since the solver could only create a single output variable *X*, the 9 variables (if three parallel reactions are used) had to be written as vector components *X(1)* to *X(9)*, where *X(1), X(2) and X(3)* correspond to the activation energies $E_{a,1}$, $E_{a,2}$ and $E_{a,3}$. *X(4), X(5)* and *X(6)* correspond to A_1, A_2 and A_3. *X(7), X(8)* and *X(9)* correspond to c_1, c_2 and c_3.
The pre-exponential factors had a potential range of multiple orders of magnitude. To prevent time loss running the solver, the pre-exponential factors were programmed as a function of their exponent. This means that the exponents of the pre-exponential factors were the variables, and not the pre-exponential factors themselves.
The fraction of volatiles c_i was used as a constraint for the model to actually use an independent reaction for every single biomass component that had to be modelled. Without this constraint, the solver tried to model the experimental graph with a lower amount of independent reactions than desired. The ranges for c_i can be based on the amounts of biomass component present in the particular biomass species.

The GA solver also has some disadvantages:

- The results obtained from the GA solver vary a bit for every run, due to the random number generator employed.
- The results obtained from the GA solver approach the global minimum fairly quickly, but they do not reach the absolute minimum within a reasonable amount of computation time.

To overcome these problems, the local optimisation solver called 'LSQ curvefit' is used after the GA solver to further minimise the objective function and optimise the results. The LSQ curvefit solver solves data fitting problems using the (nonlinear) least squares method. The solver computes the optimal kinetic constants by minimising the objective function, just like the GA solver. However, the LSQ curvefit solver requires an initial guess to be able to find a minimum. With this initial guess, the LSQ curvefit solver finds the absolute minimum closest to this initial guess. When using the results from the GA solver as the initial guess for the LSQ curvefit solver, the minimum that was approached by the GA solver is actually found. Therefore, the use of the LSQ curvefit solver improves the reproducibility of the results and the accuracy of the results significantly.

To run the Matlab code with the model and the two solvers in an easy way, a Matlab application with a user-friendly interface was built. The Matlab application can be used to model all kinds of lignocellulosic biomass species, as long as the mass loss rate can be modelled with three independent parallel reactions. The interface is shown in *figure 6.6*. The modelling of Ulva was performed in a separate Matlab file due to the different amount of parallel reactions used, see *subparagraph 6.4.4*.

The interface of the application contains several boxes that need to be filled in to import the experimental data from the corresponding excel file. There are boxes to input the filename, the name of the excel tab, the excel rows and columns that contain the temperatures and mass loss rates, and the units of both quantities. Furthermore, the heating rate used in the TGA experiments has to be filled in together with the total fraction of volatiles produced. The total fraction of volatiles should be calculated from the excel file and this calculated value has to be set in the interface. The sum of the individual fractions of volatiles, $\sum c_i$, always ads up to the set value for the total fraction of volatiles. Two options for the GA solver, the function tolerance and the population size, were also included in the interface. The pre-entered values for these two options were found to obtain optimal results from the solver, but since there could be reasons to try different values, they were added to the interface. More details about the optimal solver settings can be found in *subparagraph 6.4.3*.
The search ranges for the 9 variables (in the case of lignocellulosic biomass species) were included in the interface as well, so that the user can narrow them down according to results obtained from running at the widest search ranges. The pre-entered values are the values for the widest search ranges possible for lignocellulosic biomass species. When all options are set, the 'Run' button, located in the middle of the interface, can be used to start the run.
Apart from all the input boxes, the results are also displayed on the interface. The final results for the 9 variables are displayed at the bottom of the interface together with the value for the deviation of the calculated graph from the experimental graph. The plots with the mass loss rates of the individual reactions, the calculated mass loss rate and the experimental mass loss rate can be found at the right side of the interface. The operating protocol for the Matlab application can be found in *Appendix B*.

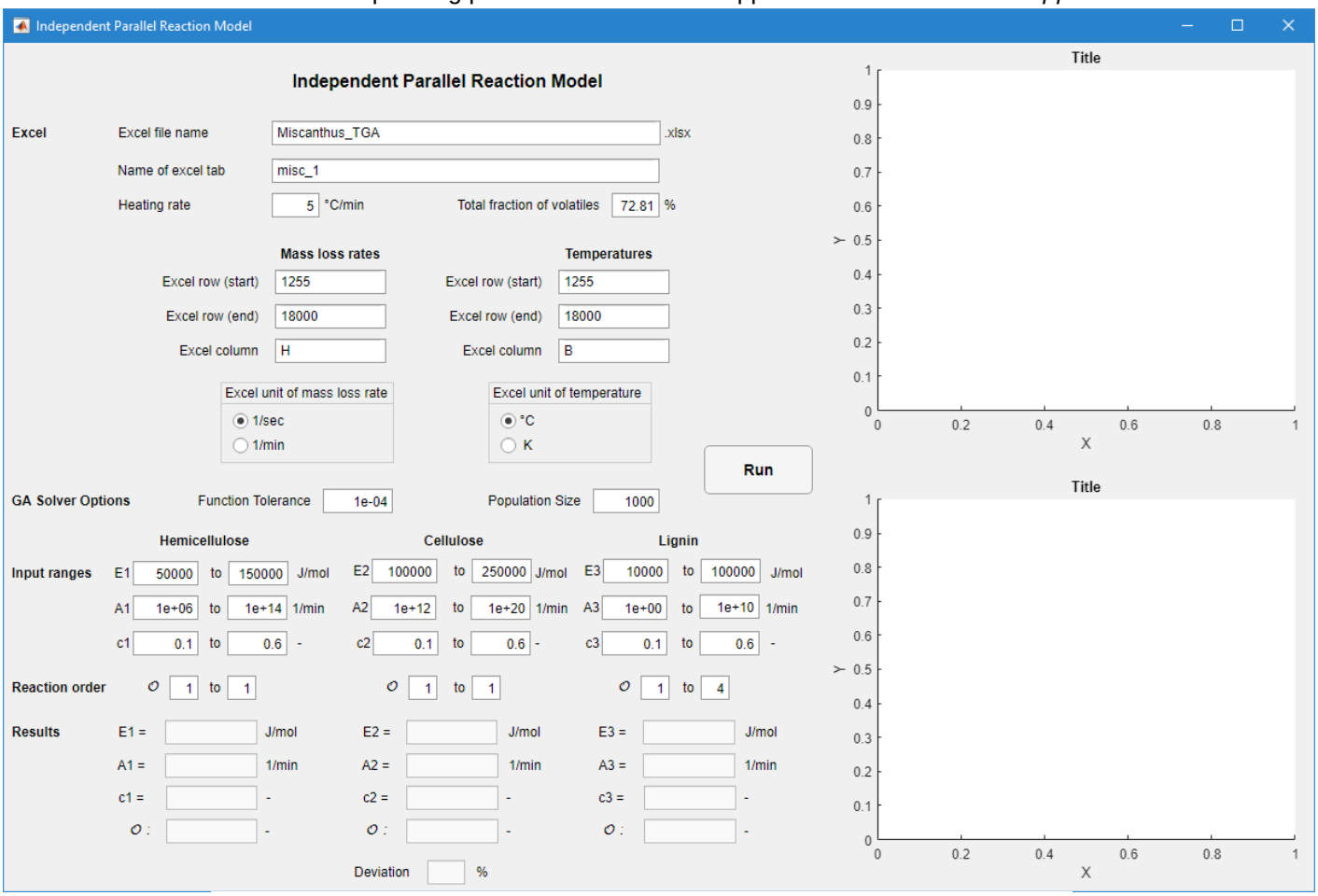

Figure 6.6. Interface of the Matlab application used to model Miscanthus.

6.4.3 Operating Conditions of the Matlab Solvers

When using the GA solver in Matlab, it is very important to explore how the settings can be adapted to have the highest chance of obtaining the best possible results. The most important setting concerning this matter is the *population size*. The population size is the amount of random solutions (combination of the variables) in a generation. From these random solutions, only a few of the best solutions are chosen to explore further with a new generation. So, when using a higher population size, there is a larger chance of having better random solutions to explore, and thus the chance is higher to find the global minimum. On the other hand, a higher population size results in a higher computation time, since more random solutions are produced in every generation. It was found that the computation time increased linearly with the population size. The default value for the population size is 200. Population sizes between 200 and 5000 were tested. For the Matlab application the value of the population size is recommended to be set to 2000. For this population size, the best results were found repeatedly, while the computation time was still decent (between 30 and 60 minutes).

During the modelling with the GA solver and the LSQ curvefit solver, the stopping criterion that was used to evaluate whether or not the results found by the solvers were good enough to stop looking further for better results, was the *function tolerance*. The function tolerance represents the average relative change in the best fitness function value. In the present case, this means that if the change in the value of the computed objective function relative to its previous value is less than the function tolerance, the solver would stop. Since the objective function had values in the order of 10^{-2} or 10^{-3}, a function tolerance of 10^{-4} was chosen for the GA solver. A function tolerance of 10^{-12} was used for the LSQ curvefit solver. This function tolerance was found experimentally to give the best solution possible for the same initial guess accurate to four decimals Requesting higher function tolerances resulted in an exponential increase of the computation time, while the solutions did not improve. Furthermore, different settings for the mutation and the crossover (two settings for the GA solver) were tested. However, after a short time of testing the default settings turned out to give the best results, so no changes were made regarding the settings of the mutation and the crossover.

The ranges of the variables are very important as they are the only input that deviates the independent reactions from one another. The initial ranges in the Matlab application were chosen so that they would cover solutions for the mass loss rates of many different (lignocellulosic) biomass species. The initial lower and upper boundaries used in the Matlab application are given in *table 6.4.* The ranges for the activation energies were chosen based on the activation energies for hemicellulose (subscript 1), cellulose (subscript 2) and lignin (subscript 3) reported in literature [54]. For lignin, assumptions about the temperature range had to be made, because lignin reacts very differently under different circumstances and in different biomass species. Most articles state that the decomposition of lignin starts between 100 and 200 °C [31, 49, 51, 78, 79]. However, there are other articles that suggest that the decomposition starts at around 300 °C [62, 80]. Since more articles stated that the decomposition of lignin starts between 100 and 200 °C, this was assumed in the present study. The assumption resulted in the fact that the maximum range explored for the activation energy of lignin had lower values (up to 100 kJ/mol) than the range that would have been explored if the decomposition of lignin was assumed to start at around 300 °C.
The ranges for the pre-exponential factors were based on several studies reporting kinetic constants of hemicellulose, cellulose and lignin in different lignocellulosic biomass species [75, 81-84]. The initial ranges for the fractions of volatiles were chosen as general as possible, but can be adjusted based on information about the content of hemicellulose, cellulose and lignin present in the modelled biomass species.
For Miscanthus, the chemical composition was found to be 20-35% hemicellulose, 27-50% cellulose and 10-22% lignin (see *paragraph 3.1*). The fractions of volatiles can be based on these values.
As mentioned earlier, the ranges can be narrowed down as the modelling results get improved. The final lower and upper boundaries used for modelling the mass loss rates of Miscanthus can be found in *paragraph 7.3*.

Table 6.4: Initial boundaries for modelling the mass loss rates of lignocellulosic biomass species.

Activation Energies			Pre-exponential Factors		Fractions of Volatiles		
$E_{a,1}$	$50 - 200$	kJ/mol	A_1	$1 \cdot 10^{6} - 1 \cdot 10^{14}\ 1/min$	c_1	$1 - 40$	%
$E_{a,2}$	$150 - 300$	kJ/mol	A_2	$1 \cdot 10^{10} - 1 \cdot 10^{22}\ 1/min$	c_2	$1 - 60$	%
$E_{a,3}$	$10 - 100$	kJ/mol	A_3	$1 \cdot 10^{0} - 1 \cdot 10^{8}\ \ 1/min$	c_3	$1 - 30$	%

6.4.4 Modelling of Ulva

In the present study, it was also tried to model the decomposition rate of Ulva based on its main components with the independent parallel reaction model. The modelling of Ulva with the IPR model was different from the modelling of Miscanthus, since the composition of algal biomass is very different from that of lignocellulosic biomass.
To be able to determine the amount of independent parallel reactions required for the modelling of Ulva, it first had to be investigated which biomass components were responsible for the different peaks in the mass loss rate curves of Ulva. This could be based on TGA results of Ulva and its main components, see *paragraph 7.1*.

Analysing the results presented in *paragraph 7.1*, it was first tried to model the mass loss rate of Ulva with ten independent parallel reactions: five reactions in the temperature range of 100 to 550 °C (attributed to soluble and insoluble carbohydrates, protein, starch and lipids), and five reactions in the temperature range of 550 to 1200 °C (attributed to inorganic components).
As modelling ten reactions would result in very long computation times for the model, it was also tried to model only the first five reactions (in the temperature range of 100 to 550 °C).
Since a different amount of parallel reactions has to be used than for modelling lignocellulosic biomass, a separate Matlab file was used to model the mass loss rates of Ulva instead of the Matlab application that was built.

As modelling of algal biomass was not done before with the IPR model (according to the authors knowledge), the ranges of the kinetic constants for the different components, required as an input for the model, could not be based on literature (as was done for lignocellulosic biomass species). Therefore, very large ranges were tried, as can be seen in *table 6.5*.

Table 6.5: Initial boundaries for modelling the mass loss rates of Ulva.

Activation Energies			Pre-exponential Factors			Fractions of Volatiles		
$E_{a,1}$	$10 - 100$	kJ/mol	A_1	$1 \cdot 10^5 - 1 \cdot 10^{10}$	$1/min$	c_1	$1 - 10$	%
$E_{a,2}$	$10 - 250$	kJ/mol	A_2	$1 \cdot 10^{16} - 1 \cdot 10^{26}$	$1/min$	c_2	$1 - 20$	%
$E_{a,3}$	$10 - 250$	kJ/mol	A_3	$1 \cdot 10^6 - 1 \cdot 10^{14}$	$1/min$	c_3	$1 - 20$	%
$E_{a,4}$	$10 - 250$	kJ/mol	A_4	$1 \cdot 10^4 - 1 \cdot 10^{12}$	$1/min$	c_4	$1 - 20$	%
$E_{a,5}$	$10 - 250$	kJ/mol	A_5	$1 \cdot 10^0 - 1 \cdot 10^8$	$1/min$	c_5	$1 - 20$	%
$E_{a,6}$	$100 - 400$	kJ/mol	A_6	$1 \cdot 10^4 - 1 \cdot 10^{14}$	$1/min$	c_6	$1 - 20$	%
$E_{a,7}$	$100 - 400$	kJ/mol	A_7	$1 \cdot 10^8 - 1 \cdot 10^{18}$	$1/min$	c_7	$1 - 20$	%
$E_{a,8}$	$200 - 500$	kJ/mol	A_8	$1 \cdot 10^2 - 1 \cdot 10^{12}$	$1/min$	c_8	$1 - 20$	%
$E_{a,9}$	$200 - 500$	kJ/mol	A_9	$1 \cdot 10^4 - 1 \cdot 10^{14}$	$1/min$	c_9	$1 - 20$	%
$E_{a,10}$	$200 - 500$	kJ/mol	A_{10}	$1 \cdot 10^0 - 1 \cdot 10^6$	$1/min$	c_{10}	$1 - 20$	%

7. Experimental Results & Discussion

In *chapter 7* the results are shown and discussed for the pyrolysis experiments with Miscanthus and Ulva. Results for the slow pyrolysis experiments conducted in a TGA can be found in *paragraph 7.1*. Results for the fast pyrolysis experiments conducted in a Pyroprobe reactor can be found in *paragraph 7.2.* The compositions of the gaseous products were examined in the micro-GC. Results of the different gas compositions can be found in *paragraph 7.3.* Results for the kinetic modelling of the mass loss rate curves from slow pyrolysis can be found in *paragraph 7.4.*

7.1 Biomass Slow Pyrolysis in a Thermogravimetric Analyser

Knowledge of the pyrolysis characteristics of the main components is the basis and thus essentially important for a better understanding to biomass thermal chemical conversion. The individual components play significant roles in determining the pyrolysis characteristics of biomass. The way in which components are chemically bound is not as important as the actual amounts of individual components present in a particular biomass. However, the chemical structure of the individual components, for example the type of cellulose, does have an effect on the pyrolysis characteristics of biomass [51, 85].

TGA for Miscanthus was performed at a temperature range of 0 to 900 °C and different heating rates of 5, 10 and 20 °C/min. The proximate analysis is shown in *table 7.1*. According to De Jong et al. pyrolysis of Miscanthus produces higher yields of char and lower yields of volatile matter as compared to wood. This different behaviour may be explained in terms of different biochemical composition between the two different biomass types. Generally, in biomass, lignin shows a relatively large contribution to the production of fixed carbon than other main constituents, such as cellulose or hemicellulose. However, precise data for Miscanthus have not been determined, thus making it unsure whether or not the differences in char yields can be related unequivocally to the diverse lignin content of the biomass types [6].

As was mentioned in *paragraph 4.3*, lignocellulosic biomass pyrolysis can be divided into four individual stages: moisture evolution, hemicellulose decomposition, cellulose decomposition and lignin decomposition. In *figure 7.1* the results from the present study on the slow pyrolysis of Miscanthus for these heating rates are presented. The mass loss rate curves are shown versus the temperature.

Table 7.1: Proximate analysis of Miscanthus from TGA.

Heating rate	5 °C/min		10 °C/min		20 °C/min		AVG (wt%)		STDEV (wt%)
	a.r. (wt%)	d.b. (wt%)	a.r. (wt%)	d.b. (wt%)	a.r. (wt%)	d.b. (wt%)			
Moisture	6.82	-	8.14	-	8.06	-	7.67	(a.r.)	0.74
Volatiles	72.80	78.12	73.19	79.68	71.40	77.66	78.49	(d.b.)	1.06
Fixed Carbon	16.47	17.67	16.35	17.80	16.60	18.05	17.84	(d.b.)	0.19
Ash	3.92	4.20	2.32	2.52	3.94	4.29	3.67	(d.b.)	1.00

As depicted in *figure 7.1,* the peak below 100 °C was due to the release of moisture in the sample and the peak observed over 100 °C can be attributed to the pyrolysis process. Devolatilisation occurs mainly between 200 and 600 °C, completed with the evolution of secondary gases, leading to the formation of char [86]. The shoulder at approximately 260, 280 and 300 °C for the different heating rates of 5, 10 and 20 °C/min, respectively, can be linked to the decomposition on hemicellulose. The main peaks at 320, 334 and 346 °C for the different heating rates, respectively, resulted from the decomposition of cellulose. In contrast to hemicellulose and cellulose, it was difficult to attribute a particular peak to lignin decomposition. This is because pyrolysis of lignin has been shown to take place continuously from 200 to 800 °C [51, 87].

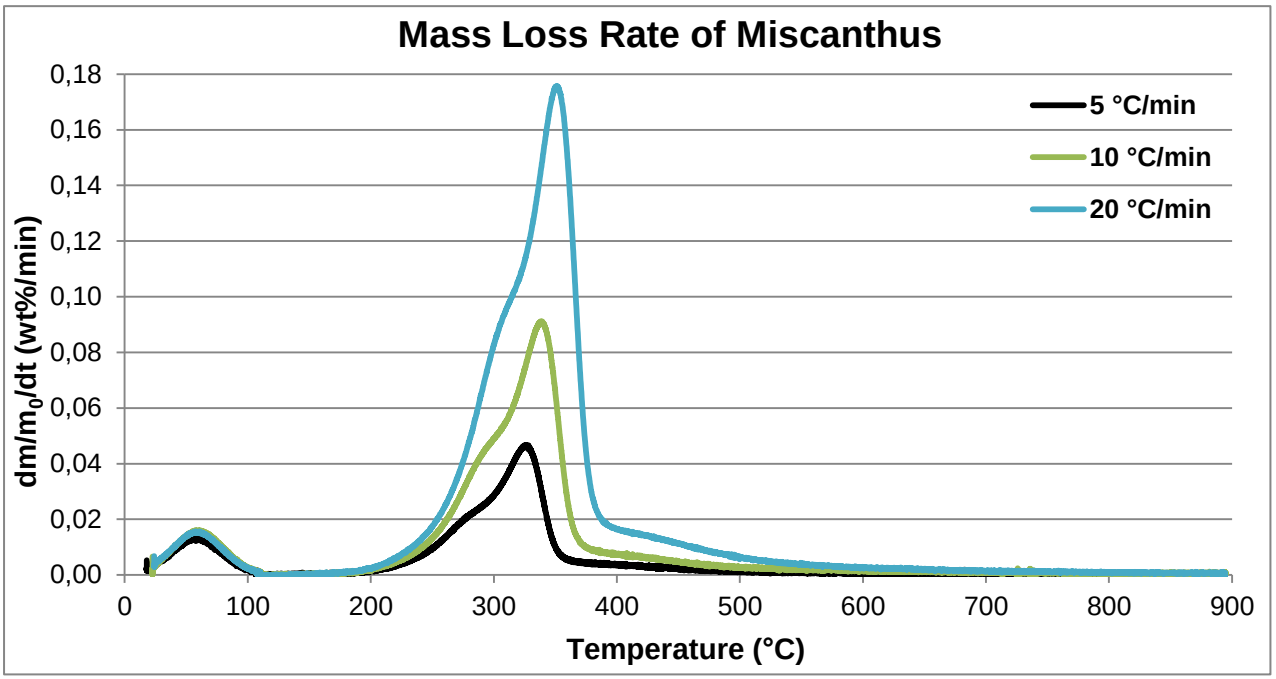

Figure 7.1. Mass loss rates of Miscanthus at heating rates of 5, 10 and 20 °C/min.

TGA for Ulva was performed at a temperature range of 0 to 1200 °C and different heating rates of 5, 10 and 20 °C/min. The proximate analysis is shown in *table 7.2*. As was mentioned in *paragraph 3.2*, Ulva – and macro-algae in general – have very different compositions compared to lignocellulosic biomass species. Apart from the insoluble carbohydrates, also soluble carbohydrates, protein, starch and lipids play a role in the devolatilisation of macro-algae. In *figure 7.2* the results from the present study on the slow pyrolysis of Ulva for these heating rates are presented. The mass loss rate curves are shown versus the temperature.

Table 7.2: Proximate analysis of Ulva from TGA.

Heating rate	5 °C/min		10 °C/min		20 °C/min		AVG (wt%)		STDEV (wt%)
	a.r. (wt%)	d.b. (wt%)	a.r. (wt%)	d.b. (wt%)	a.r. (wt%)	d.b. (wt%)			
Moisture	9.90	-	14.54	-	14.41	-	12.95	(a.r.)	2.65
Volatiles	71.13	78.94	68.20	79.81	69.09	80.72	79.82	(d.b.)	0.89
Fixed Carbon	9.22	10.23	8.46	9.90	7.91	9.24	9.79	(d.b.)	0.50
Ash	9.75	10.83	8.80	10.29	8.59	10.04	10.39	(d.b.)	0.40

Compared to Miscanthus it is less obvious for Ulva which mass loss rate peak corresponds to which biomass component. Again, the peak below 100 °C was due to the release of moisture in the sample. The small peaks at 133, 138 and 145 °C for the different heating rates of 5, 10 and 20 °C/min, respectively, are most likely indicative of the release of strongly bonded hydrated compounds releasing water upon heating [88, 89]. According to Trinh et al. the main mass loss rate peaks, found at 205, 210 and 220 °C for the different heating rates, respectively, can be attributed to the decomposition of hemicellulose and cellulose. Furthermore, the overlapping peaks from 250 to 550 °C are due to the decomposition of protein, starch and possibly lignin [31]. Zhao et al. argue that the main peak can be attributed to the decomposition of soluble carbohydrates and protein and that the two shoulder-like peaks in the temperature range from 250 to 550 °C can be attributed to the insoluble carbohydrates [90]. the peaks above 550 °C (710, 725 and 745, respectively for increasing heating rate) to the release of inorganic compounds, especially sodium, sulphur, nitrogen and chlorine [31].

To get a better understanding of the peaks in the temperature range of 180 to 550 °C in the mass loss rate graph of Ulva, TGA curves of the individual components present in Ulva are investigated. The decomposition of hemicellulose and cellulose was already found to be in the range of 250 – 500 °C, see *figure 4.2*. Alves et al. presented TGA results for separated ulvan. The main peak for the soluble carbohydrate ulvan is found at a temperature of 230 °C, which is at a similar temperature as the main peak obtained for Ulva decomposition (presented in *figure 7.2*) [89]. The decomposition of protein is found to be in the range of 250 – 500 °C with a peak for the maximum decomposition rate between 350 and 360 °C. The decomposition rate of lipids is found to be at 250 – 500 °C as well, with two decomposition rate peaks at 300 °C and 410 °C [91]. The above leads to the conclusion that the main peak can be attributed to the decomposition of soluble carbohydrates. The overlapping shoulder-like peaks between 250 and 550 °C can be attributed to the decomposition of the insoluble carbohydrates (mostly hemicellulose), protein and lipids.

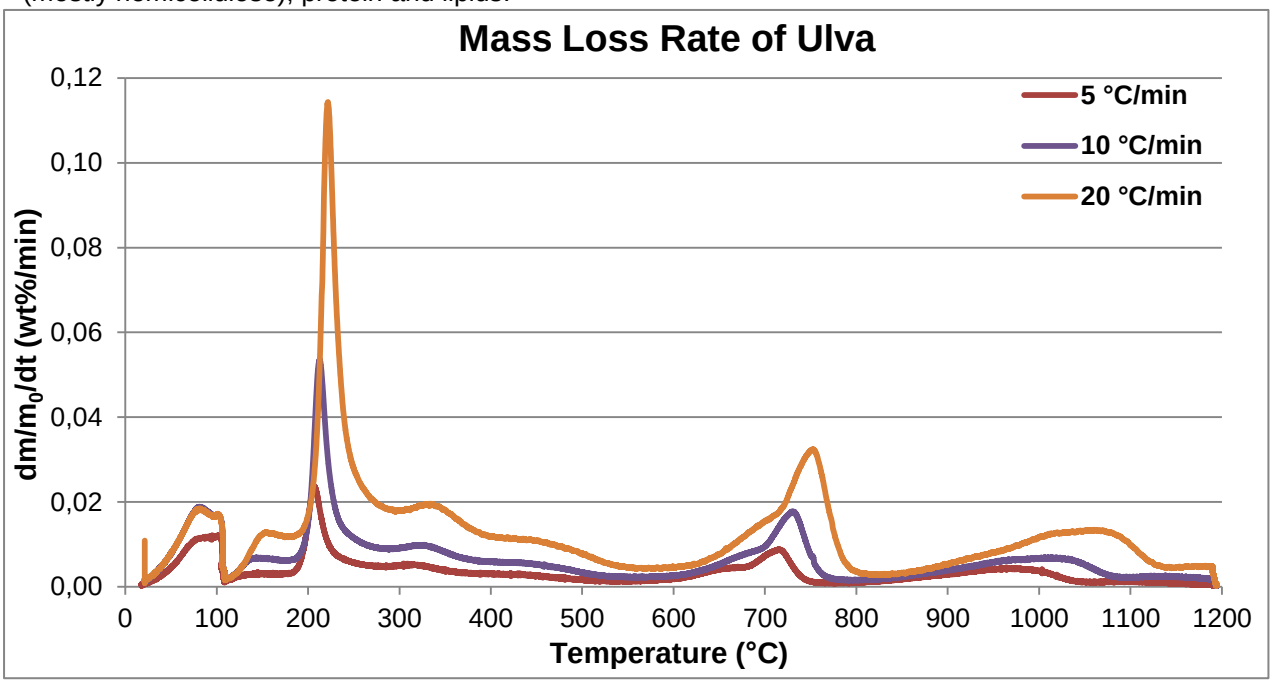

Figure 7.2. Mass loss rates of Ulva at heating rates of 5, 10 and 20 °C/min.

There are several studies that have investigated the slow pyrolysis of Miscanthus [87, 92-98] and the slow pyrolysis of Ulva [21, 31, 33, 99-102] at heating rates of 5, 10 and 20 °C/min. From the small differences between the results presented in these studies and the current study, it can be concluded that the reproducibility of TGA results can be obstructed by differences in the composition between different crops of the same biomass species: The moisture content can differ due to different uptake during storage. Also, mineral content can differ greatly due to for instance different harvest times or different geological origin. The reproducibility can also be influenced by TGA operating variables, such as calibration, furnace cleanliness, sample preparation or sample atmosphere [67].

From the proximate analysis results in *table 7.1* and *table 7.2* it can be concluded that, for slow heating rates, the heating rate does not have a significant effect on the product yields. However, as can be seen in *figure 7.1* and *figure 7.2*, different heating rates do result in different mass loss rate graphs. The first difference noticed is the increase of the mass loss rate with increasing heating rate at a certain temperature stage, which seems to be linearly correlated. At higher heating rates the particles devolatilise over a less long time, accounting for the same total mass fraction conversion, but causing a variance in the mass loss rates [21].
The second difference that stands out is the lateral shift of the graphs with higher heating rates towards higher temperatures, which means that the pyrolysis temperature needed to get the same weight loss is higher for higher heating rates. This phenomenon is called ‘thermal lag’. The thermal lag can be assigned to the combined effects of heat and mass transfer limitations, which cause temperature gradients inside the sample and inside each particle [98]. However, with the low sample sizes and particle sizes used, it can be argued that heat and mass transfer limitations are negligible. If heat and mass transfer limitations don’t play a role, the mass loss can be regarded to be dominated by chemical kinetics [103]. The thermal lag could then be explained by the endothermicity of the pyrolysis reactions. In particular the decomposition of cellulose is known to be strongly endothermic [80].

7.2 Biomass Fast Pyrolysis in a Pyroprobe reactor

In *paragraph 7.2* the results of the pyrolysis experiments performed in this study are presented. Fast pyrolysis experiments were performed for Miscanthus and Ulva in a Pyroprobe reactor. The char (solid residue), tar (liquid product) and gas yields were measured for varying pyrolysis temperature.

7.2.1 Fractional Yields of Miscanthus and Ulva Fast Pyrolysis

Pyrolysis temperature is a significant parameter that affects the amount and composition of the pyrolysis products. In this study the effects of pyrolysis temperature on the product yields from fast pyrolysis of Miscanthus and Ulva were investigated. As was mentioned in *chapter 6*, experiments were performed at a heating rate of 600 °C/sec for six different temperatures: 500, 600, 700, 800, 900 and 1000 °C. A summarising graph of the average fractional product yields (solid, liquid and gaseous products) of Miscanthus pyrolysis for all the tested temperatures can be found in *figure 7.3*. A summarising graph of the average fractional yields for the products of Ulva pyrolysis for all the tested temperatures can be found in *figure 7.4*. The tables of all the experiments at the different temperatures can be found in *Appendix C*.

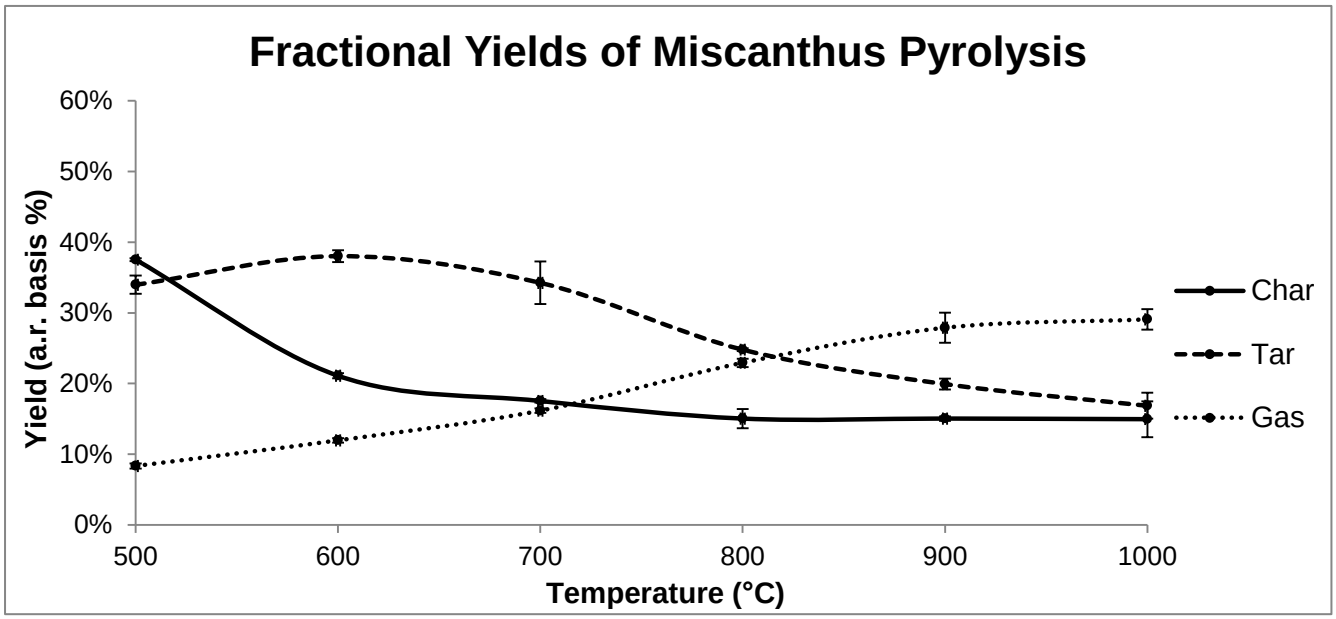

Figure 7.3. Fractional yields of Ulva pyrolysis for different pyrolysis temperatures.

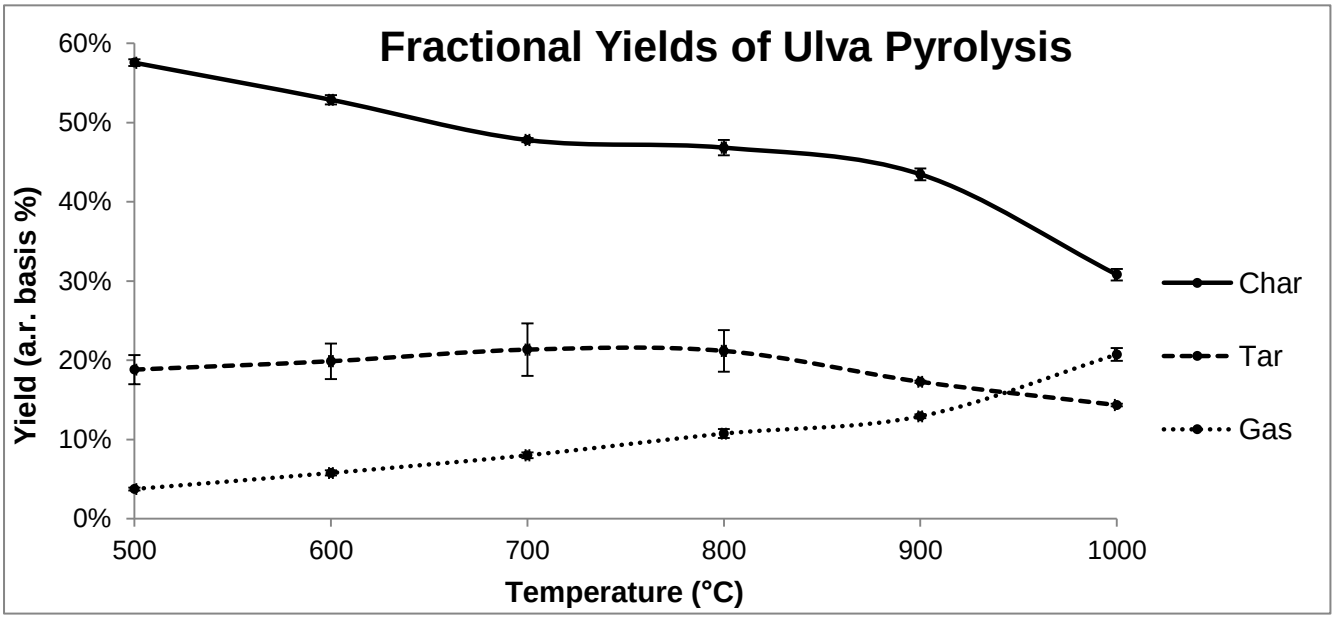

Figure 7.4. Fractional yields of Ulva pyrolysis for different pyrolysis temperatures.

It is expected that the char yields will go down for increasing temperature, since the temperature increase will cause more biomass to get devolatilised. The tar yields are expected to go up at first, due to the devolatilisation, but the yields peak at a certain temperature and then go down with increasing temperature due to secondary reactions that result in the release of non-condensable gases. The gas yields are expected to go up over the whole temperature range due to consecutively char formation reactions, fragmentation reactions and (secondary) cracking reactions [49]. For Miscanthus this was confirmed by studies on fast pyrolysis of similar biomass species (grass species, energy crops etc.) in the same temperature range [104-111]. For Ulva this was confirmed as well by studies on fast pyrolysis of similar biomass species (macro-algae, marine biomass etc.) [35, 112, 113].

7.2.1.1 Char Yields

For Miscanthus, the highest char yield was found at the lowest pyrolysis temperature (37.5 wt% at 500 °C). For Ulva, the char yield was at its maximum at the lowest pyrolysis temperature as well (57.6 wt% at 500 °C). Char product yields are at maximum levels at 500 °C when compared to the other temperatures investigated owing to uncompleted decomposition mechanisms (the lowest temperature investigated has the lowest level of pyrolysis conversion) [104].
For Miscanthus, the char yield decreased from 500 °C up to 800 °C. For Ulva, the char yield kept decreasing for all temperatures measured, with a minimum yield of 30.8 wt% at 1000 °C. As the temperature increased, the char yield decreased as a result of the competition between charring (accompanied by the release of water and non-condensable gases) and devolatilisation reactions (depolymerisation and fragmentation), which become successively more favoured [111].
For Miscanthus, the char yield was found to be nearly constant (approximately 15 wt%) between 800 °C and 1000 °C. It can be concluded that at these temperatures no more primary devolatilisation or char formation reactions occur [111]. Pyrolysis of Miscanthus produces higher yields of char (and therefore lower yields of volatile matter) as compared to, for instance, wood [6]. This behaviour may be explained in terms of different biochemical composition between the two different biomass types: the lignin content in Miscanthus is higher than that in wood [6]. Generally, in biomass, the char yield from lignin is the highest (in the region of 45-50 wt%), followed by the char yield from hemicellulose (around 30 wt%). The char yield from cellulose is the lowest. Biomass species with lower amounts of cellulose tend to have higher char yields [85]. However, since the amount of lignin in macro-algae is very low or even zero, there have to be different reasons for the high char yields of Ulva. According to different sources it could be attributed to the high mineral content in Ulva [35, 114, 115]. This has been proven by the fact that the char production is reduced upon demineralisation of the algal feedstock [116]. Furthermore, the presence of mineral components (such as sodium and potassium) can enhance the char formation during the pyrolysis process [114]. Generally, bio-char produced from seaweed has a high mineral content, but a low fixed carbon content of approximately 30-35%, whereas those produced from lignocellulosic biomass species typically have a carbon content of more than 70% [35]. The fact that the char yield decreases significantly at temperatures above 900 °C can be caused by the devolatilisation of some of the inorganic compounds (mainly carbonates) present in Ulva, as was also noticed in the slow pyrolysis experiments presented in *paragraph 7.1* [117, 118].

7.2.1.2 Tar Yields

For Miscanthus, the tar yield (here defined as the total liquid yield) firstly increased from 500 °C to 600 °C from 34 wt% to 38 wt%. For Ulva, the tar yield increased a little bit from 18.8 wt% at 500 °C to 21.3 wt% at 700 °C. Low tar yields are obtained at 500 °C due to the low level of pyrolysis conversion at this temperature [104]. The increases in the tar yields up to 600 °C can be attributed to (mainly) depolymerisation reactions [49]. At temperatures higher than 600 °C the tar yield of Miscanthus decreased to a minimum of 16.9 wt% at 1000 °C. From 800 °C to 1000 °C the tar yield of Ulva decreased from 21.1 to 14.3 wt%. At temperatures above 600 °C the long-chained primary pyrolysis tars can undergo secondary reactions. For both Miscanthus and Ulva (secondary) cracking reactions become more dominant at temperatures above 700 °C, resulting in the production of more light volatiles at the cost of the primary tar yield [104, 107, 109, 112]. Active minerals in Ulva could even promote secondary decomposition reactions of the produced volatiles [114]. At temperatures higher than 800 °C recombination reactions of tar components are likely to happen. These reactions are characteristic for the formation of PAH [49]. Analysis of the liquid product should show whether or not PAH are indeed present in the liquid yields for temperatures above 800 °C.
In general, the liquid yields of lignocellulosic biomass species are higher when the cellulose content is higher. This leads to the conclusion that cellulose has the biggest contribution to the amount of volatile matter produced during pyrolysis of biomass [85]. The tar yield of algal biomass is generally lower than that of lignocellulosic biomass at the temperatures investigated due to their difference in composition: the higher mineral content of algae compared to lignocellulosic biomass induces char production [117].

7.2.1.3 Gas Yields

For Miscanthus, the gas yield is only 8.3 wt% at 500 °C and increases for the whole spectrum of temperatures up to 29.1 wt% at 1000 °C. For Ulva, the gas yield is only 3.8 wt% at 500 °C and increases for the whole spectrum of temperatures as well up to 20.7 wt% at 1000 °C. Below 600 °C the increase in gas yield is mainly caused by the char formation mechanism, where non-condensable gases are released [49].
For both Miscanthus and Ulva, the increase in gas yield above 600 °C is most likely to be caused by fragmentation and (secondary) cracking of the condensable vapours into gas products [49, 52]. The increase in gas yield at these temperatures is coinciding with a decrease in char and tar yields [108]. In general, the pyrolysis of cellulose and hemicellulose produces more gaseous products than that of lignin at the same temperature [105]. As was found for the tar yields, the gas yields of lignocellulosic biomass species are higher if the cellulose content is higher [85].
Subparagraph 7.2.3 goes into more detail about the gaseous products and their compositions.

7.2.2 Mass Balances of Miscanthus and Ulva from Fast Pyrolysis

When the line chart in *figure 7.3* and *figure 7.4* are converted into column charts, the total mass balances and the mass balance deficits can be observed, see *figure 7.5* and *figure 7.6*. Theoretically, the mass balances should be at 100%, but in practice this is never achieved due to several losses According to both figures, the mass balance tends to decrease for higher pyrolysis temperatures. The highest mass balances were achieved at 500 °C for both Miscanthus (79.84%) and Ulva (80.12%). The lowest mass balances were achieved at 1000 °C: 60.91% for Miscanthus and 65.86% for Ulva.

There are a number of reasons why the mass balances did not reach 100% for the fast pyrolysis experiments performed in this study and why the mass balances decreased with temperature:

- A large deficit in the mass balances is caused by unquantified tars. Due to the short time that the tars are present in the trap some of the lighter tar compounds do not condense in the trap. Tar compounds that pass the trap are condensed in a condenser (impinger bottle) filled with isopropanol, in which the tars dissolve. The tars that are condensed in the trap cannot be quantified. This results in an incorrectly low tar yield and a deficit in the mass balance [69]. As condensation of the tars in the trap gets more difficult at higher temperatures, the mass balance deficits increase for increasing temperatures, as can be seen in *figures 7.5* and *7.6*. In order to reduce these losses, one could think of decreasing the flow rate in the Pyroprobe, which gives the tars more time to condense in the trap.
- Another large deficit is caused by the fact that part of the water produced during pyrolysis ends up in the condenser as well. During the experiments condensed water was observed until the end of the trap, indicating that some of the water passed the trap and condensed in the impinger bottle. According to different sources, pyrolytic water can account for 10-12 wt% of the dry feed [41, 45].
  In order to reduce these losses, one could think on analysing the content of the condenser, for instance by applying a Karl Fischer titration.
- A third reason for a deficit in the mass balance is caused by the fact that the micro-GC employed in the experiments is not able to detect gas species other than H_2, CO, CO_2, CH_4 and N_2. Therefore, higher hydrocarbons – mainly ethane, ethylene, acetylene, propane and propene [107, 109, 110] – cannot be measured. Their yields increase with increasing temperature as they are mostly derived from secondary pyrolysis reactions [119]. The total yield of these products are indicated at approximately 5 wt% depending on the experimental conditions and the biomass feedstock used [107, 108].
- Furthermore, it was observed during the cleaning of the Pyroprobe reactor, that some tars can condense in the tube (valve oven) before they exit the Pyroprobe reactor and enter the trap. The temperature in the valve oven is set to 325 °C and unfortunately cannot be increased to higher temperatures, causing a deficit in the mass balance due to small losses of tars.
- Minor losses may occur from the evaporation of very volatile compounds which manage to escape in the time interval between the trap removal from the reactor and the insertion in the isopropanol filled testing tube.
- Finally, there is always the possibility of error during the gravimetric measurements of the liquid and solid product as well as in the determination of the gaseous products through the micro-GC and the ideal gas law implementation.

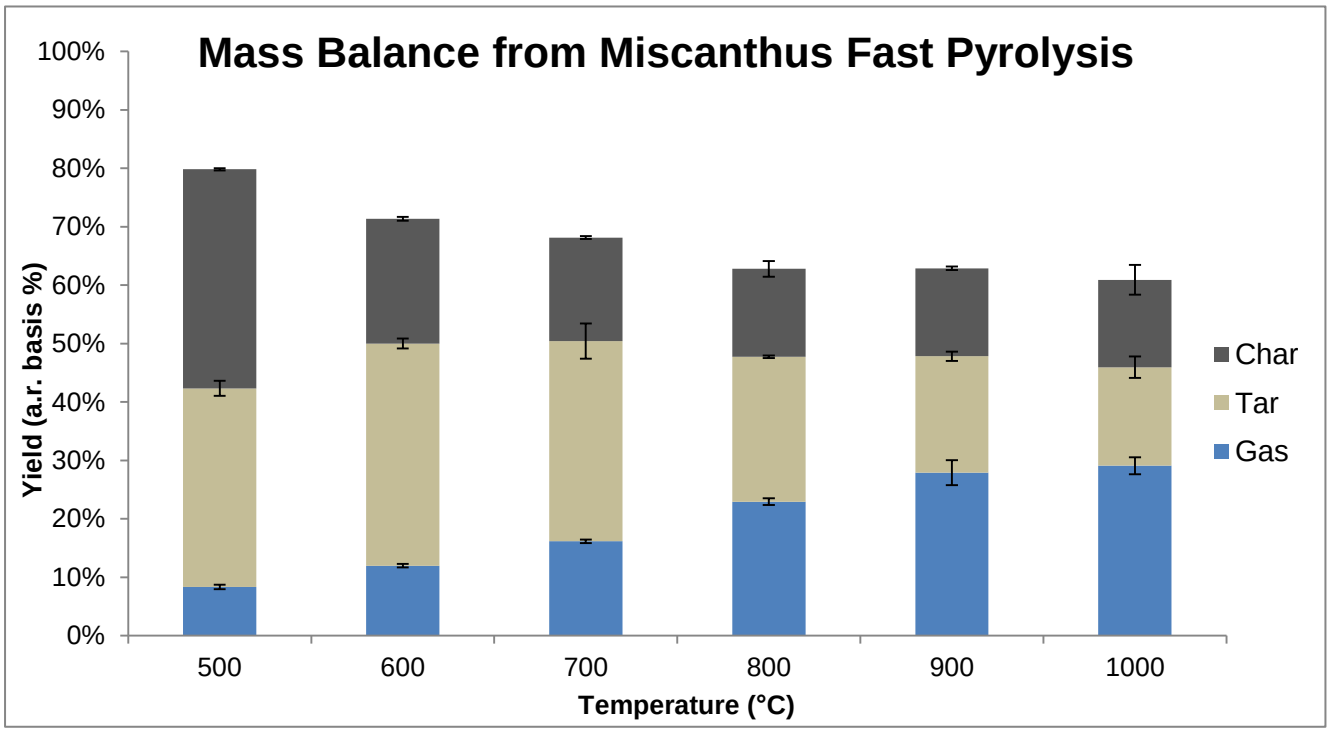

Figure 7.5. Mass balances of the fast pyrolysis experiments of Miscanthus for all temperatures.

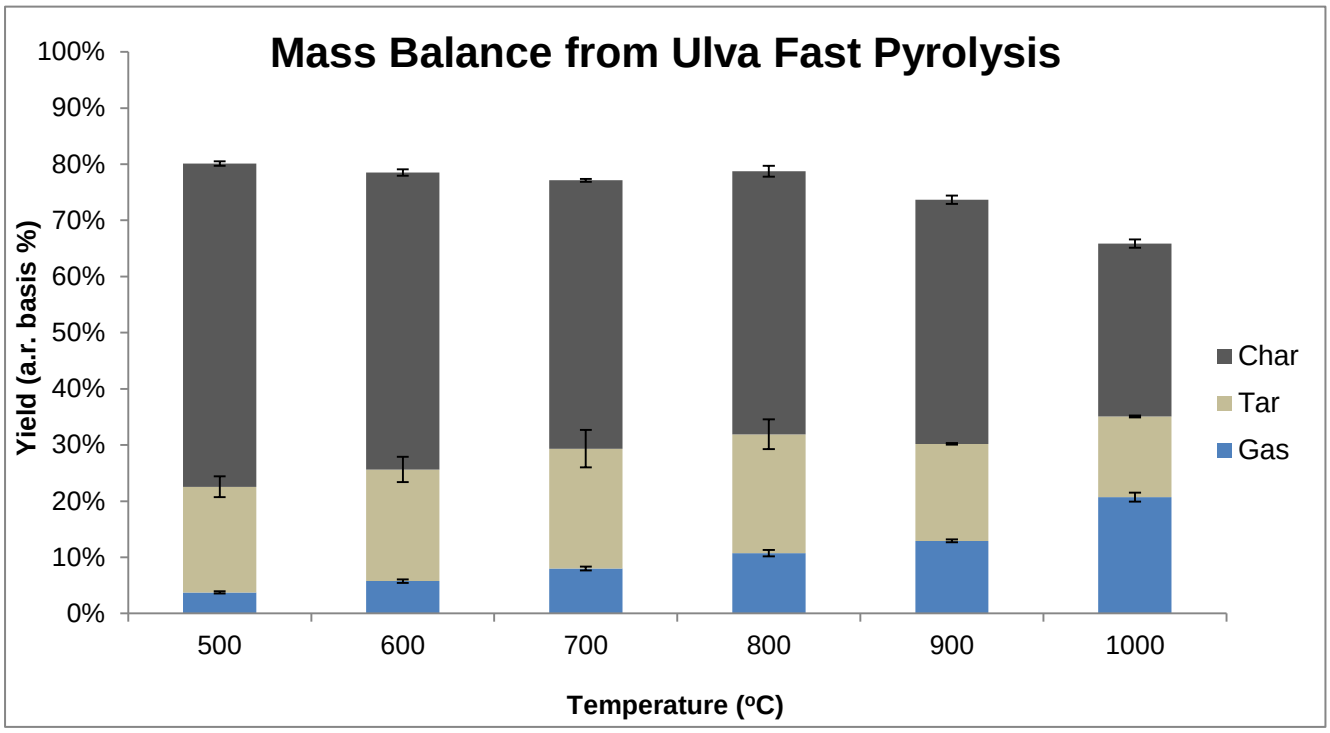

Figure 7.6. Mass balances of the fast pyrolysis experiments of Ulva for all temperatures.

7.2.3 Gas Compositions of Miscanthus and Ulva from Fast Pyrolysis

The gaseous products obtained from the Pyroprobe experiments at different pyrolysis temperatures are analysed using a micro gas chromatograph (micro-GC). Temperature has been found to have a positive effect on the total amount of gas generated. From the micro-GC analysis it was found that the yields of all individual gas components analysed, CO, CO_2, CH_4 and H_2, increased with temperature in the range of 500 – 1000 °C. This behaviour reflects the fact that the main pyrolysis gases are formed through thermally favoured reactions, such as cracking and depolymerisation [108].

As was mentioned in *paragraph 7.2.2*, higher hydrocarbons, such as ethane, ethylene, acetylene, propane and propene, contribute to the gaseous product as well (since they are non-condensable gases), but could not be measured with the micro-GC. Therefore, the yields of the gas components are presented as a fraction of the initial sample size and not as a fraction of the total gas product. The graphs of the gas fractions from the fast pyrolysis experiments of Miscanthus and Ulva can be found in *figure 7.7* and *figure 7.8*, respectively. Tables of the gas fractions for the individual experiments of Miscanthus and Ulva for all the temperatures (500 – 1000 °C) can be found in *Appendix D*. Tables and graphs of the compositions of the product gases as fractions of the total gas produced can be also found in *Appendix D*.

The trends for Miscanthus are similar to trends found in literature for similar lignocellulosic biomass species [105-111, 120]. For Ulva it is hard to find similar fast pyrolysis results in the same temperature range. Results for similar seaweeds were only found up to a pyrolysis temperature of 600 °C [112, 113]. These studies show that the yield of CO_2 was already decreasing relative to the other product gas components below temperatures of 500 °C.

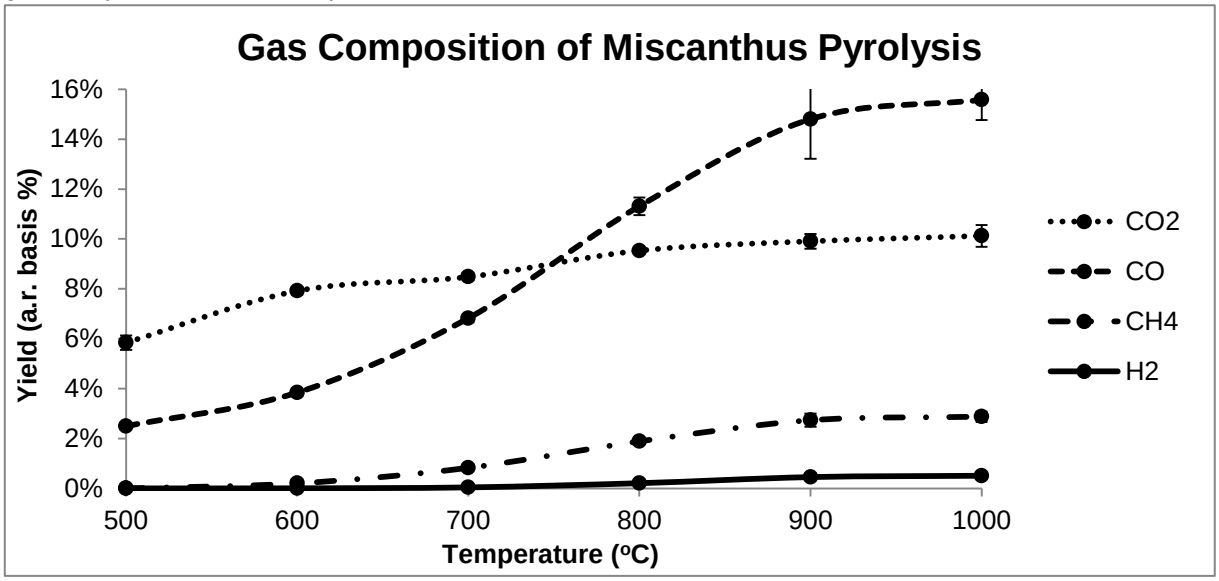

Figure 7.7. Gas composition of Miscanthus pyrolysis (wt% of initial sample size).

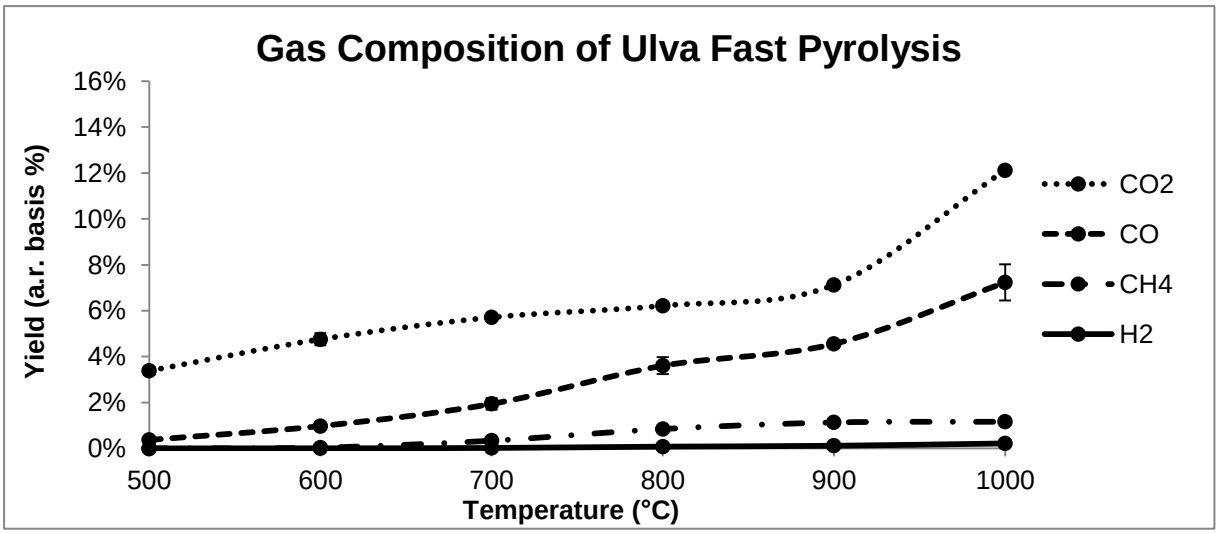

Figure 7.8. Gas composition of Ulva pyrolysis (wt% of initial sample size).

For both Miscanthus and Ulva the most abundant component at 500 °C is CO_2 (5.84 wt% and 3.38 wt%, respectively). The amounts of CO were 2.50 wt% and 0.37 wt%, respectively. At 500 °C the amounts of H_2 and CH_4 are negligible for both biomass species. The high fractions of CO_2 at 500 °C suggest that CO_2 is mainly derived from the direct degradation of the biomass species [107]. For lignocellulosic biomass, the relatively high amount of CO_2 at this low temperature can be related to primary pyrolysis of hemicellulose and cellulose. Mainly the char formation process of hemicellulose is known to produce mostly CO_2 and water vapour. This pathway becomes less favoured as the temperature increases [49, 108, 111]. For algal biomass, the CO_2 production can be attributed to the decomposition of carboxyl functional groups in proteins and carbohydrates [52, 113, 121].

From both *figure 7.7* and *figure 7.8* it can be seen that the yield of CO increases faster than the yield of CO_2 in the temperature range of 500 to 900 °C. This becomes even more clear when looking at the graphs of the relative gas compositions presented in *Appendix D*. For Miscanthus the amount of CO_2 increased from 5.84 wt% to 9.91 wt%, while the amount of CO increased from 2.50 wt% to 14.8 wt%. For Ulva the amount of CO_2 increased from 3.38 wt% to 7.12 wt%, while the amount of CO increased from 0.37 wt% to 4.55 wt%. From this it can be concluded that, relative to the production of CO_2, the production of CO increased with increasing temperature. Hence primary decomposition of the samples has essentially ceased, it is concluded that CO is mainly a product of secondary cracking reactions for both biomass species [107, 121]. For lignocellulosic biomass in particular, cracking reactions of cellulose tars are known to produce mainly CO [54].
For Miscanthus, the CO_2 yield seems to stabilise above 700 °C. The tendency of the CO_2 yield to stabilise can be attributed to the fact that CO_2 is a product of the primary pyrolysis by a path less favoured by increasing temperature [108]. The yield of CO in the gas product of Miscanthus seems to stabilise between 900 and 1000 °C, indicating that pyrolysis reactions at these temperatures do not contribute to the production of CO. For Ulva the yields of CO and CO_2 kept increasing for temperatures above 800 °C. As the changes in the yields at these temperatures were attributed to the devolatilisation of some of the inorganic compounds present in Ulva, it can be concluded that this devolatilisation results in the release of CO and CO_2.
At 1000 °C the most abundant gas component from Miscanthus was CO (15.57 wt%) followed by CO_2 (10.12 wt%). The most abundant component in the Ulva gas product was still CO_2 (12.12 wt%) and CO (7.23 wt%). The fact that CO_2 is the major component at all pyrolysis temperatures can be attributed to the high oxygen content (approximately 60 wt%) in the biomass material [52].

The amounts of H_2 in the product gases of Miscanthus and Ulva were small, but increased with temperature over the whole temperature spectrum for both biomass species. For Miscanthus the amount of H_2 increased from 0.01 wt% at 600 °C to 0.51 wt% at 1000 °C, while for Ulva the amount of H_2 increased from 0.00 wt% at 600 °C to 0.22 wt% at 1000 °C. The increase in H_2 was mainly noticed between 700 and 800 °C, where H_2 increased from 0.04 wt% to 0.21 wt% for Miscanthus and from 0.02 wt% to 0.08 wt% for Ulva. The increase of the H_2 yield at these temperatures for both lignocellulosic and algal biomass species, can be explained by the fact that hydrogen is mainly a product of secondary cracking reactions of the longer-chain hydrocarbons and aliphatic and aromatic structures in volatile vapours [52, 105, 108, 111, 113]. In general, biomass composed of more cellulose and hemicellulose is known to produce more hydrogen-rich gas than that composed of more lignin. However, depolymerisation of phenyl groups in lignin could also be responsible for some of the production of H_2 [105, 113]. For algal biomass, protein degradation (favoured at high temperatures) is one of the main mechanisms for H_2 production [113].
The H_2 yield of Ulva also increased sharply from 900 to 1000 °C (from 0.11 wt% to 0.22 wt%), indicating that the devolatilisation of some of the inorganic compounds is also responsible for the release of hydrogen.

The production of CH_4 started for both biomass species at 600 °C. For Miscanthus the fraction of CH_4 increased from 0.20 wt% at 600 °C to 2.88 wt% at 1000 °C, while for Ulva the fraction of CH_4 increased from 0.03 wt% at 600 °C to 1.16 wt% at 1000 °C. The main increase in CH_4 was also noticed from 700 to 800 °C, where CH_4 increased from 0.82 wt% to 1.89 wt% for Miscanthus and from 0.34 wt% to 0.84 wt% for Ulva. these observations are consistent with the view that, in analogy to CO evolution, secondary tar cracking reactions contribute to the high-temperature CH_4 yield. This implies that secondary tar cracking continues up to the highest temperature studied (1000 °C) [107, 108].
From the relatively small increase of CH_4 for Ulva at 1000 °C it can be concluded that the devolatilisation of inorganic compounds does not contribute to the CH_4 yield.

7.3 Modelling Results

7.3.1 Modelling Results for Miscanthus

As was explained in *paragraph 6.4*, a Matlab application was built to perform the modelling of the mass loss rates of Miscanthus using three independent parallel reactions. To obtain reliable results for the kinetic constants of Miscanthus, the Matlab application was run multiple times. To improve the accuracy of the constants obtained by the solver, the search ranges had to be narrowed down. The initial search ranges, stated in *table 6.4*, were very large in order to include all possible values for the 9 variables. After running the solver a few times it became clear which values the constants were approaching and the search ranges could be narrowed down accordingly. The final boundaries that were used are stated in *table 7.3*.

Table 7.3: Final boundaries for modelling the mass loss rates of lignocellulosic biomass species.

Activation Energies			Pre-exponential Factors			Fractions of Volatiles		
$E_{a,1}$	$100 - 115$	kJ/mol	A_1	$1 \cdot 10^8 - 1 \cdot 10^{11}$	$1/min$	c_1	$15 - 30$	%
$E_{a,2}$	$185 - 200$	kJ/mol	A_2	$1 \cdot 10^{15} - 1 \cdot 10^{17}$	$1/min$	c_2	$25 - 35$	%
$E_{a,3}$	$25 - 35$	kJ/mol	A_3	$1 \cdot 10^0 - 1 \cdot 10^2$	$1/min$	c_3	$10 - 25$	%

The final results for the desired constants obtained with the Matlab application that gave a mass loss rate graph with the lowest deviation from the experimental mass loss rate graph are shown in *table 7.4*. With these results the objective function was minimised to a value of $3.2306 \cdot 10^{-3}$. The corresponding deviation was 0.96%.

Table 7.4: Final values of the desired kinetic constants of Miscanthus at a heating rate of 5 °C/min

Activation Energies			Pre-exponential Factors			Fractions of Volatiles		
$E_{a,1}$	107.63	kJ/mol	A_1	$3.0339 \cdot 10^9$	$1/min$	c_1	16.960	%
$E_{a,2}$	186.52	kJ/mol	A_2	$5.7016 \cdot 10^{15}$	$1/min$	c_2	34.820	%
$E_{a,3}$	29.485	kJ/mol	A_3	$1.0580 \cdot 10^1$	$1/min$	c_3	20.020	%

The modelling results were plotted in two different graphs. In the first graph, the calculated total mass loss rate based on the optimised constants was plotted against the temperature together with the experimentally obtained mass loss rate so that the two graphs can be compared easily. The best modelling result obtained for Miscanthus is shown in the Matlab plot in *figure 7.9*.
To see how the calculated total mass loss rate is built up from the three independent reactions for the mass loss rates of the three main biomass components, a Matlab plot is made containing the total calculated mass loss rate together with the calculated mass loss rates of the independent parallel reactions. This plot is shown in *figure 7.10*. A figure of the interface after the run with the final modelling result can be found in *appendix E*.

From the final results of the modelling of Miscanthus it can be seen that the activation energy of lignin was the lowest (29.485 kJ/mol), followed by the activation energy of hemicellulose (107.63 kJ/mol) and the activation energy of cellulose (186.52 kJ/mol). These values make sense, because the decomposition of lignin is expected to start at the lowest temperature and therefore requires the lowest amount of energy, while the decomposition of cellulose is expected to start at the highest temperature and thus requires the highest amount of energy [50, 51, 85, 122].
The pre-exponential factor was also the lowest for lignin ($1.06 \cdot 10^1$) and the highest for cellulose ($5.70 \cdot 10^{15}$), with a value for the pre-exponential factor of hemicellulose in between ($3.03 \cdot 10^9$). A higher the pre-exponential factor of a component represents a higher the frequency of collisions. This results in a higher maximum reaction rate. Therefore, a higher pre-exponential factor leads to a steeper slope of the curve for the associated component in the mass loss rate graph. The results make sense, because the component with the highest pre-exponential factor, cellulose, is known to have the highest reaction rate and thus the smallest temperature range at which it decomposes. On the other hand, the component with the lowest pre-exponential factor, lignin, is known to decompose over the largest temperature range and does not present a clearly observable peak.
The fraction of volatiles from cellulose was, as expected, the largest (34.8%), since it is the most abundant component in Miscanthus according to literature [9]. The fraction of volatiles of lignin (20.0%) was somewhat higher than that of hemicellulose (17.0%). An explanation for this could be that the amount of lignin in the sample was simply higher than that of hemicellulose. Another reason could be that the fraction of volatiles due to the devolatilisation of extractives, which is assumed to be small (2.2-4.2%) [9] and occurs between 150 and 600 °C [123], is added to the fraction of volatiles from the lignin in the modelling results.

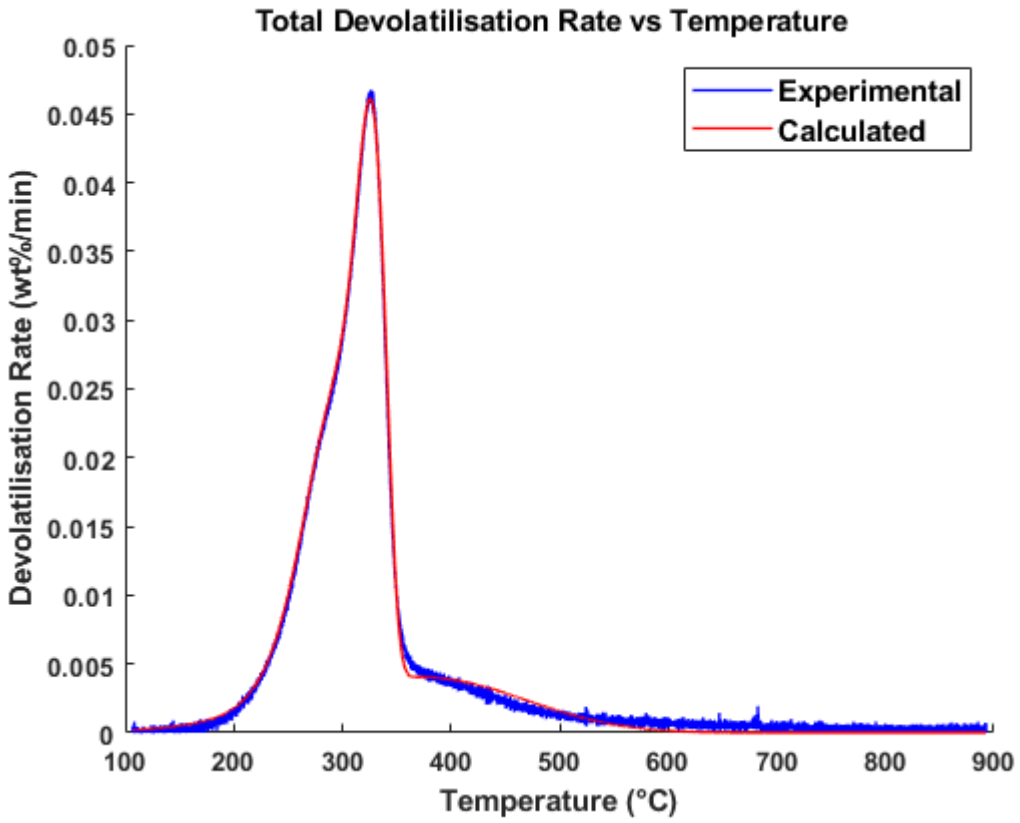

Figure 7.9. Matlab plot of the experimentally obtained mass loss rate and the calculated mass loss rate of Miscanthus at a heating rate of 5 °C/min plotted against the temperature.

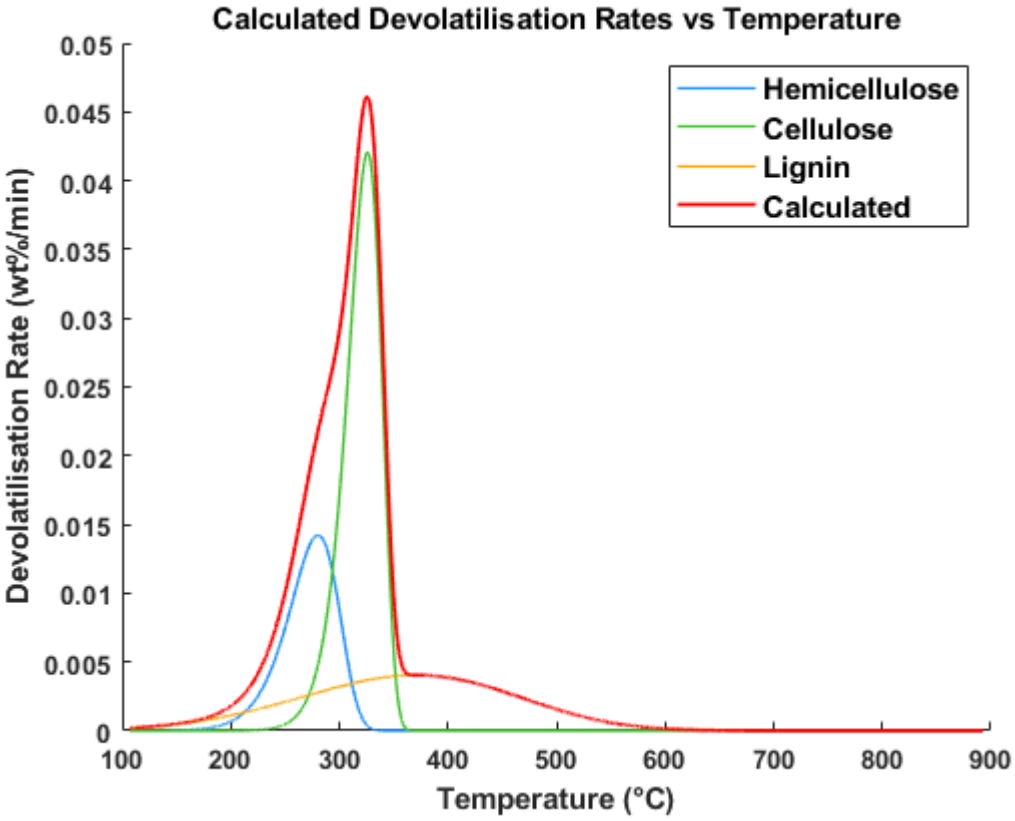

Figure 7.10. Matlab plot of the total calculated mass loss rate together with the calculated mass loss rates of the individual main biomass components of Miscanthus at a heating rate of 5 °C/min plotted against the temperature.

To investigate the influence of the heating rate on the kinetic constants, the mass loss rate graphs of Miscanthus for heating rates of 10 and 20 °C/min were modelled as well. The deviations from the experimentally obtained graphs were 0.94% and 0.70%, respectively. The results can be found in *table 7.5* and *table 7.6*, respectively. The associated graphs can be found in *Appendix F*.

Table 7.5: Final values of the desired kinetic constants of Miscanthus at a heating rate of 10 °C/min

Activation Energies			Pre-exponential Factors			Fractions of Volatiles		
$E_{a,1}$	111.41	kJ/mol	A_1	$7.9634 \cdot 10^9$	$1/min$	c_1	18.708	%
$E_{a,2}$	194.27	kJ/mol	A_2	$2.3768 \cdot 10^{16}$	$1/min$	c_2	34.099	%
$E_{a,3}$	29.599	kJ/mol	A_3	$1.8353 \cdot 10^1$	$1/min$	c_3	19.383	%

Table 7.6: Final values of the desired kinetic constants of Miscanthus at a heating rate of 20 °C/min

Activation Energies			Pre-exponential Factors			Fractions of Volatiles		
$E_{a,1}$	115.80	kJ/mol	A_1	$2.2491 \cdot 10^{10}$	$1/min$	c_1	18.438	%
$E_{a,2}$	209.28	kJ/mol	A_2	$3.9537 \cdot 10^{17}$	$1/min$	c_2	31.892	%
$E_{a,3}$	34.150	kJ/mol	A_3	$9.8651 \cdot 10^1$	$1/min$	c_3	20.070	%

When taking a look at the activation energies, it stands out that they increase for increasing heating rates. This difference can be explained by the thermal lag explained in *paragraph 7.1*: if the fact that the next temperature stage is reached before the heat of the previous temperature stage is uniformly distributed over the sample transfer, the decomposition of the individual components is actually visible at a higher temperature (lateral shift). When using a kinetic model, this leads to an increase in the values for the activation energies [86, 124].
When taking a look at the pre-exponential factors, it stands out that they also increase for increasing heating rates. This has an obvious reason, namely that the amount of collisions that lead to reactions per unit of time increases when the heating rate is increased [124].
The fractions of volatiles are very close between the modelling results obtained for the different heating rates. This makes sense, because the fractions of volatiles of the individual components are based on the composition of the biomass species and can only be changed if the pyrolysis mechanisms would change. This is not the case at the current heating rates of 5, 10 and 20 °C/min, which are all typical for slow pyrolysis. The results from the proximate analysis presented in *table 7.1* confirm this, as the total fraction of volatiles stays nearly constant.

It is hard to validate the kinetic results obtained in the present study by comparing with similar studies, because no studies were found that used the IPR model to model kinetic constants for Miscanthus. Several studies were found that used the IPR model to obtain kinetic constants for other lignocellulosic biomass species. The (wide) ranges for the different kinetic constants, which were used as an input for the model (see *table 6.4*), were already based on these studies. Therefore, to be able to compare the results for the kinetic constants in the present study, there was looked for literature presenting kinetic constants of biomass species similar to Miscanthus, namely energy crops. A table was made containing the kinetic parameters of studies applying the IPR model to model the decomposition of various energy crops at heating rates of 5, 10 and 20 °C/min. This table is presented in *Appendix G*. From the table it can be seen that the activation energies have a range of 93 – 129 kJ/mol for hemicellulose, 108 – 210 kJ/mol for cellulose and 31 – 64 kJ/mol for lignin. The pre-exponential factors have a range of $2.5 \cdot 10^8$ – $4.8 \cdot 10^{11}$ 1/min for hemicellulose, $2.3 \cdot 10^9$ – $1.4 \cdot 10^{18}$ for cellulose and $2.8 \cdot 10^1$ – $3.8 \cdot 10^3$ for lignin [75, 81, 83, 84, 86, 125]. The kinetic constants obtained in this study are all in the same ranges as the ones mentioned above.
The biomass species modelled with the IPR model that was the closest to Miscanthus was giant reed for a heating rate of 10 °C/min. The activation energies were 117, 176 and 33 kJ/mol and the pre-exponential factors were $3.1 \cdot 10^{10}$, $2.5 \cdot 10^{14}$ and $4.7 \cdot 10^1$ for hemicellulose, cellulose and lignin, respectively [86]. These results are close to the ones found for Miscanthus (see *table 7.5*). It can be concluded that the kinetic constants obtained in the present study at least have the right order of magnitude. However, the question whether they are correct could not be answered completely, as this model is purely based on mathematics. Isoconversional methods could help verifying the results obtained with the IPR model as they can give reliable indications for the activation energies based on TGA results [126].

7.3.2 Modelling Results for Ulva

In the present study, it was also tried to model the decomposition rate of Ulva based on its main components with the independent parallel reaction model. The high amount of variables (ten independent reactions resulted in 30 variables) made it not possible for the solver to find reliable solutions within a reasonable amount of running time. Even the modelling of just five independent reactions, associated with 15 variables, did not result in valuable results. On the one hand this was still caused by the amount variables resulting in high computation times. On the other hand, due to insufficient knowledge of the ranges of the kinetic constants for the different independent reactions (no literature was found on this matter regarding algal biomass), very large initial ranges had to be tried resulting in high computation times as well. When population sizes were kept small in order to maintain reasonable computation times, physically impossible results were continuously obtained: activation energies for reactions that started at higher temperatures were found to be lower than reactions starting at lower temperatures. Thus, due to the fact that the best results obtained still consisted of unreliable and physically impossible kinetic constants, it was chosen to not report any of the modelling results found for Ulva.

7.3.3 Evaluation of the Performance of the Model

The IPR model has some shortcomings. One of the shortcomings is that, due to the random number generator in the GA solver, it can never be assured that the best solution found is in fact the global minimum. The solver scans areas of solutions based on a set of random initial guesses. There is a chance that the absolute global minimum has not been found yet. However, due to the use of a large population size and due to the fact that the application was run many times, the chance of finding the best possible solution was maximised.
Furthermore, also due to the random number generator, it cannot be said with 100% certainty that the best results found are reproducible in every run. Obviously, the settings of the solvers are optimised in order to find the global minimum as much as possible, but there is always a chance that the best possible solution is in an area of solutions that is not explored by the solvers. Narrowing down the search ranges helps to minimise this problem.

Another shortcoming is that the model does not take into account the catalytic effect of possibly present inorganic components, which are known to alter the pathways of biomass pyrolysis. Inorganic components can potentially reduce the temperature threshold at which pyrolysis starts, especially for cellulose decomposition [83, 127]. Due to the fact that the inorganic components are not taken into account, different kinetic constants can be found for exactly the same biomass species (with exactly the same amounts of hemicellulose, cellulose and lignin), but containing a different amount of inorganic matter.

Also, the model is limited to a low amount of variables and thus to a low amount of independent reactions. When using three independent reactions, the model is applicable, but, as tried for Ulva, for ten parallel reactions, the model has too many variables to obtain valuable results. Due to the high amount of variables (30) the solvers in Matlab are not able to approach a meaningful minimum within a foreseeable running time.
For modelling Ulva with five parallel reactions, the large ranges applied for the variables were causing the model to not be able to find a meaningful minimum within a foreseeable running time. From this it can be concluded that an appropriate estimation of the ranges of the variables is essential for the model to work.

8. Conclusions & Recommendations

To conclude, answers to the research question and sub-questions found in the present study are summarised in *paragraph 8.1* and recommendations for further research are given in *paragraph 8.2*.

8.1 Conclusions

The research question was stated as follows: *"Can the decomposition of Miscanthus and Ulva during pyrolysis be explained based on the decomposition of their main components and can this decomposition be predicted using the independent parallel reaction model?"* To get a complete answer to this question, the sub-questions stated in *chapter 2* have been studied and the answers are summarised below.

The influence of the *biomass composition* on the slow pyrolysis was investigated for Miscanthus and Ulva. Their difference in composition was clearly visible in the mass loss rate curves of both biomass species. Miscanthus, mainly composed of hemicellulose, cellulose and lignin, was decomposed in the temperature range of 200 to 600 °C. It showed a shoulder-like peak, attributed to the decomposition of hemicellulose, followed by a main peak at approximately 330 °C, attributed to the decomposition of cellulose. Lignin was decomposed over the whole temperature range at low mass loss rates, without having a distinctive peak. Ulva, mainly composed of soluble and insoluble carbohydrates together with protein, but also containing a high mineral content, decomposed in the range of 180 to 1200 °C. The main peak at approximately 210 °C, attributed to the decomposition of soluble carbohydrates, was followed by two overlapping shoulder-like peaks up to 550 °C, attributed to the decomposition of insoluble carbohydrates, protein and lipids. The peaks in the range of 600 to 1200 °C can be attributed to the devolatilisation of part of the inorganic compounds.

The effect of the *heating rate* on the slow pyrolysis of Miscanthus and Ulva was investigated by performing experiments at three different heating rates: 5, 10 and 20 °C/min. It can be concluded that higher heating rates result in lateral shifts of the mass loss rate curves to higher temperatures due to thermal lag, probably caused by the strong endothermicity of the decomposition process. Furthermore, the mass loss rates seemed to be linearly increasing with increasing heating rates due to the lower residence times per temperature stage.

The influence of *final pyrolysis temperature* on the product yields of Miscanthus and Ulva was investigated by performing fast pyrolysis experiments in a Pyroprobe reactor for a temperature range of 500 – 1000 °C. For Miscanthus the char yield decreased with increasing temperature, the tar yield had a maximum at 600 °C and the gas yield increased for increasing temperatures. For Ulva the char yield decreased with increasing temperature as well, the tar yield had a maximum at 700 °C and the gas yield also increased for increasing temperatures. The behaviour described above was attributed to the pyrolysis mechanisms that were dominant under the different temperatures: at temperatures up to 600 °C char formation and depolymerisation dominated, whereas at temperatures higher than 600 °C fragmentation and (secondary) cracking reactions dominated. At temperatures higher than 800 °C also recombination reactions become part of the pyrolysis process.

The influence of *final pyrolysis temperature* on the compositions of the gas products obtained from the Pyroprobe experiments of Miscanthus and Ulva was investigated as well. For Miscanthus the most abundant component at 500 °C was CO_2 followed by CO. CH_4 and H_2 were not found at this temperature. At 1000 °C, CO was the most abundant component, followed by CO_2 and small amounts of CH_4 and H_2. For Ulva the most abundant component in the gas fraction at 500 °C was CO_2 followed by CO. Again, CH_4 and H_2 were not found at this temperature. At 1000 °C, CO_2 was still the most abundant component, followed by CO and small amounts of CH_4 and H_2. The behaviour described above was attributed to the pyrolysis mechanisms that were dominant under the different temperatures. For both biomass species, the production of CO_2 was linked to primary pyrolysis mechanisms, whereas the production of CO and CH_4 were linked to secondary pyrolysis mechanisms (mainly cracking). The production of H_2 was linked to depolymerisation and cracking for Miscanthus and to degradation of protein for Ulva.

The *biomass compositions* of Miscanthus and Ulva had great influence on the fast pyrolysis yields obtained. The char yield of lignocellulosic biomass species was found to be mainly caused by the decomposition of lignin. Therefore, lignocellulosic biomass with low amounts of lignin tend to have low char yields. The char yields of Ulva were significantly higher than those of Miscanthus. This was attributed to the high mineral content of Ulva. The fixed carbon content is known to be lower for algal biomass compared to lignocellulosic biomass. The tar and gas yields, obviously linked to the char yields, were found to be linked to the cellulose content of lignocellulosic biomass. A higher cellulose content results in higher tar and gas yields. Due to the high char yields of algal biomass as a result of their high mineral content, the tar and gas yields of algal biomass are generally lower than those of lignocellulosic biomass at the same pyrolysis temperature.

The mass balance deficits encountered during the fast pyrolysis experiments were between 60 and 81%. These values are considered to be satisfactory given the difficulties in measuring very volatile tars, pyrolytic water and higher hydrocarbon gases. The deficits seemed to increase for higher temperatures due to the fact that condensation of the volatile matter is counteracted by higher temperatures and yields of higher hydrocarbon gases increase with increasing temperature.

The thermal decomposition processes of Miscanthus were characterised by modelling its mass loss rates, obtained with thermogravimetric analysis, with the independent parallel reaction (IPR) model. As for all lignocellulosic biomass species, the mass loss rate of Miscanthus was modelled using three independent reactions, one for each of its main components: hemicellulose, cellulose and lignin. Kinetic constants (activation energies and pre-exponential factors) were found for each independent reaction together with the fractions of volatiles associated with each biomass component. This resulted in a calculated graph for the mass loss rate of Miscanthus that deviated only 0.96% from the experimentally obtained graph.

It was tried to model the mass loss rate of Ulva using the IPR model, but without success. At first it was tried to model the whole temperature range (100-1200 °C), which had as a consequence that ten independent reactions had to be used in order to model all the different peaks. As this was found to be impossible due to the infinitely long computation times, it was tried to model only the mass loss rate in the temperature range of 100-550 °C. For this, five independent reactions were required. This did not result in valuable kinetic constants as well. On the one hand this was again caused by the high amount variables, on the other hand, it was due to insufficient knowledge of the ranges of the kinetic constants for the different independent reactions. Both resulted in computation times that were still too high to obtain valuable results in a reasonable amount of time. From this it was concluded that an appropriate estimation for the ranges of the kinetic constants of the individual components of Ulva is essential for the IPR model to obtain valuable results.

The effect of the heating rate on the kinetic parameters for slow pyrolysis of Miscanthus was found by modelling the mass loss rates for three different heating rates, namely 5, 10 and 20 °C/min. For increasing heating rate a small increase in the activation energies was noticed. This was attributed to the lateral shift that was caused by thermal lag. The activation energies increased as well for increasing heating rate. This was attributed to the fact that the amount of collisions leading to reactions per unit of time – this is what the pre-exponential factor represents – increases for increasing heating rate.

To conclude, the pyrolysis characteristics of Miscanthus (lignocellulosic biomass) and Ulva (algal biomass) were investigated. Different temperature-dependent pyrolysis mechanisms were linked to the product yields and compositions of the two biomass species. The experimental results obtained on the pyrolysis of Miscanthus and Ulva help characterising the devolatilisation reactions of the two biomass species and contribute to the knowledge required to optimise thermal conversion methods of biomass in general. Making thermal conversion processes of biomass more efficient leads in the end to feasible application of biomass conversion processes at large-scale.
The kinetic study of the biomass pyrolysis is of relevant importance, since it constitutes the initial step of combustion and gasification processes. The knowledge of the kinetics for the thermal decomposition of different biomass species can not only be used as an input for other, more complex models, but is also required for the design of gasifiers and pyrolysis reactors.

8.2 Recommendations

Recommendations for further research on pyrolysis and kinetic modelling of Miscanthus and Ulva are discussed below.

For further research of the decomposition of Miscanthus and Ulva during fast pyrolysis reactions, it is recommended to investigate a wider range of operating conditions. Furthermore, different methods can be used to study product compositions or to reduce the mass balance deficit:

- Mass balance deficits encountered in the present study could be reduced by analysing the pyrolytic water in the liquid product using Karl Fischer titration. Furthermore, it could be tried to perform experiments with a lower nitrogen flow rate in order to promote the condensation of volatiles in the trap, which enhances the liquid yield obtained.
- Different particle sizes could be investigated. According to different sources the particle size may have a large influence on the product yields [37, 128]. Smaller particle sizes could lead to faster devolatilisation of the biomass samples and thus could lead to different product yields and compositions. By performing experiments with at least two different particle sizes of one biomass species, conclusions on the influence of the particle size can be drawn.
  Due to practical reasons Miscanthus and Ulva had different particle sizes in the fast pyrolysis experiments performed in the current study. If there is interest in comparing the product yields of the two biomass species, it is recommended to use similar particle sizes in the experiments of both biomass species. By performing experiments with the process conditions as equal as possible, the differences in the product yields can be entirely attributed to the difference in biomass composition between the two species.
- The influence of different heating rates can be investigated as well. In this study the heating rate was fixed at 600 °C/s. Other heating rates could give different results regarding the product yields and compositions.
- In the present study only the gas composition was investigated in order to track down the different pyrolysis mechanisms appearing at the different temperatures. It could be useful to investigate the tars produced in the fast pyrolysis experiments, since tars can influence the processes in for instance gasifiers. Different tar compounds could be identified using a high-performance liquid chromatograph (HPLC). It could also be useful to analyse the composition of the char produced, for instance with an elemental analyser. Char can be used to improve the quality of agricultural soils or it can be used as a source of bio-energy.

For further research of the mass loss rates of different biomass species and to increase the performance of the IPR model application, several recommendations can be made:

- To validate the obtained kinetic constants with the IPR model, it could be tried to apply isoconversional methods, such as the KAS method. This methods can give indications of the activation energies at fixed conversions, without having to make modelling assumptions. Therefore, they could also be used to set up the ranges of the kinetic constants that are used as an input for the IPR model.
- For the kinetic modelling of Ulva, it is recommended to collect more information on the ranges of the kinetic constants of the individual components that are desired to be found before using the IPR model. This is required in order to reduce the very large computation times. The KAS method mentioned above could be used for this purpose.
- It could be tried to increase the robustness (how often the best minimum is found) of the modelling application. This can maybe be done by testing different settings of the solvers.
  It is recommended to try different solvers for running the independent parallel reaction model. Apart from the GA solver, the global optimisation toolbox in Matlab contains five other global solvers that could be worth giving a try. These are GlobalSearch, MultiStart, patternsearch, particleswarm, and simulannealbnd. One of these solvers could provide similar or even better results within a reasonable amount of time.
- Furthermore the flexibility of the model application could be tested further. The flexibility could be tested by modelling mass loss rates at more different heating rates. The modelling of mass loss rates at heating rates up to 100 °C/min could be tested. The flexibility could also be tested by modelling more types of lignocellulosic biomass.

Bibliography

1. IEA, *Share of Total Primary Energy Supply in 2015 - Netherlands*, in *IEA Energy Statistics*. 2017, OECD/IEA.
2. IEA, *Share of Total Primary Energy Supply in 2015 - World*, in *IEA Energy Statistics*. 2017, OECD/IEA.
3. M. Zevenhoven-Onderwater, R.B., B.J. Skrifvars, M. Hupa, *The Ash Chemistry in Fluidised Bed Gasification of Biomass Fuels Part I: Predicting the Chemistry of Melting Ashes and Ash-Bed Material Interaction.* 2000.
4. Kwapinska, M., et al., *Fluidized Bed Gasification of Torrefied and Raw Grassy Biomass (Miscanthus×gigantenus). The Effect of Operating Conditions on Process Performance.* Energy & Fuels, 2015. **29**(11): p. 7290-7300.
5. Demirbas, A. and G. Arin, *An Overview of Biomass Pyrolysis.* 2002.
6. Dejong, W., A. Pirone, and M. Wojtowicz, *Pyrolysis of Miscanthus Giganteus and wood pellets: TG-FTIR analysis and reaction kinetics.* Fuel, 2003. **82**(9): p. 1139-1147.
7. Bridgwater, A.V., *Biomass Fast Pyrolysis.* 2004.
8. Kumar, A., D.D. Jones, and M.A. Hanna, *Thermochemical Biomass Gasification: A Review of the Current Status of the Technology.* Energies, 2009. **2**(3): p. 556-581.
9. Brosse, N., et al., *Miscanthus: a fast-growing crop for biofuels and chemicals production.* Biofuels, Bioproducts and Biorefining, 2012. **6**(5): p. 580-598.
10. Khanna, M., B. Dhungana, and J. Clifton-Brown, *Costs of producing miscanthus and switchgrass for bioenergy in Illinois.* Biomass and Bioenergy, 2008. **32**(6): p. 482-493.
11. Xue, G., et al., *Gasification of Miscanthus x giganteus in an Air-Blown Bubbling Fluidized Bed: A Preliminary Study of Performance and Agglomeration.* Energy & Fuels, 2014. **28**(2): p. 1121-1131.
12. Yorgun, S. and Y.E. Simsek, *Catalytic pyrolysis of Miscanthus x giganteus over activated alumina.* Bioresour Technol, 2008. **99**(17): p. 8095-100.
13. Khelfa, A., et al., *Catalytic pyrolysis and gasification of Miscanthus Giganteus: Haematite (Fe2O3) a versatile catalyst.* Journal of Analytical and Applied Pyrolysis, 2009. **84**(1): p. 84-88.
14. Kaknics, J., et al., *High-Temperature Interactions between MoltenMiscanthusAshes and Bed Materials in a Fluidized-Bed Gasifier.* Energy & Fuels, 2015. **29**(3): p. 1785-1792.
15. Sorensen, A., et al., *Hydrolysis of Miscanthus for bioethanol production using dilute acid presoaking combined with wet explosion pre-treatment and enzymatic treatment.* Bioresour Technol, 2008. **99**(14): p. 6602-7.
16. Christian, D.G., A.B. Riche, and N.E. Yates, *Growth, yield and mineral content of Miscanthus×giganteus grown as a biofuel for 14 successive harvests.* Industrial Crops and Products, 2008. **28**(3): p. 320-327.
17. Xue, G., et al., *Impact of Torrefaction on Properties of Miscanthus × Giganteus Relevant to Gasification.* Fuel, 2014. **121**: p. 189-197.
18. Lewandowski, I., et al., *Miscanthus: European Experience with a Novel Energy Crop.* 2000.
19. de Jong, W., et al., *Biomass and fossil fuel conversion by pressurised fluidised bed gasification using hot gas ceramic filters as gas cleaning.* Biomass and Bioenergy, 2003. **25**(1): p. 59-83.
20. Michel, R., et al., *Catalytic steam gasification of Miscanthus X giganteus in fluidised bed reactor on olivine based catalysts.* Fuel Processing Technology, 2011. **92**(6): p. 1169-1177.
21. Ceylan, S. and J.L. Goldfarb, *Green tide to green fuels: TG–FTIR analysis and kinetic study of Ulva prolifera pyrolysis.* Energy Conversion and Management, 2015. **101**: p. 263-270.
22. Nikolaisen, L.S. and P.D. Jensen, *Biomass feedstocks: categorisation and preparation for combustion and gasification*, in *Biomass Combustion Science, Technology and Engineering*. 2013. p. 36-57.
23. Saqib, A., et al., *Marine Macro Algae Ulva: A Potential Feedstock for Bio-Ethanol and Biogas Production.* 2013.
24. Bermúdez, J.M., et al., *Microwave-induced low temperature pyrolysis of macroalgae for unprecedented hydrogen-enriched syngas production.* RSC Adv., 2014. **4**(72): p. 38144-38151.

25. Lee, S.Y., J.H. Chang, and S.B. Lee, *Chemical composition, saccharification yield, and the potential of the green seaweed Ulva pertusa.* Biotechnology and Bioprocess Engineering, 2015. **19**(6): p. 1022-1033.
26. Kwon, E.E., Y.J. Jeon, and H. Yi, *New candidate for biofuel feedstock beyond terrestrial biomass for thermo-chemical process (pyrolysis/gasification) enhanced by carbon dioxide (CO2).* Bioresour Technol, 2012. **123**: p. 673-7.
27. Bruhn, A., et al., *Bioenergy potential of Ulva lactuca: biomass yield, methane production and combustion.* Bioresour Technol, 2011. **102**(3): p. 2595-604.
28. Yaich, H., et al., *Chemical composition and functional properties of Ulva lactuca seaweed collected in Tunisia.* Food Chemistry, 2011. **128**(4): p. 895-901.
29. Yu-Qing, T., et al., *Ulva Lactuca and Its Polysaccharides: Food and Biomedical Aspects.* 2016.
30. Morelli, A., D. Puppi, and F. Chiellini, *Perspectives on Biomedical Applications of Ulvan*, in *Seaweed Polysaccharides*. 2017. p. 305-330.
31. Trinh, T.N., et al., *Comparison of Lignin, Macroalgae, Wood, and Straw Fast Pyrolysis.* Energy & Fuels, 2013. **27**(3): p. 1399-1409.
32. Lahaye, M. and A. Robic, *Structure and Functional Properties of Ulvan, a Polysaccharide from Green Seaweeds.* 2007.
33. Carrasco, F. and P. Pagès, *Kinetics of the thermal decomposition of green alga Ulva by thermogravimetry.* Journal of Applied Polymer Science, 2004. **93**(4): p. 1913-1922.
34. Ripoll, N., et al., *Hydrogen production from algae biomass in rich natural gas-air filtration combustion.* International Journal of Hydrogen Energy, 2017. **42**(8): p. 5513-5522.
35. Roberts, D.A. and R. de Nys, *The effects of feedstock pre-treatment and pyrolysis temperature on the production of biochar from the green seaweed Ulva.* J Environ Manage, 2016. **169**: p. 253-60.
36. Lamare, M.D. and S.R. Wing, *Calorific content of New Zealand marine macrophytes.* New Zealand Journal of Marine and Freshwater Research, 2001. **35**(2): p. 335-341.
37. Demirbas, A., *Effects of temperature and particle size on bio-char yield from pyrolysis of agricultural residues.* Journal of Analytical and Applied Pyrolysis, 2004. **72**(2): p. 243-248.
38. Basu, P., *Pyrolysis*, in *Biomass Gasification, Pyrolysis and Torrefaction*. 2013. p. 147-176.
39. Basu, P., *Fluidized Bed Gasification*, in *Combustion and Gasification in Fluidized Beds*. 2006. p. 59-101.
40. Basu, P., *Gasification Theory*, in *Biomass Gasification, Pyrolysis and Torrefaction*. 2013. p. 199-248.
41. Mohan, D., C.U. Pittman, and P.H. Steele, *Pyrolysis of Wood/Biomass for Bio-oil: A Critical Review.* 2005.
42. Li, A.M., et al., *Pyrolysis of Solid Waste in a Rotary Kiln: Influence of Final Pyrolysis Temperature on the Pyrolysis Products.* 1999.
43. Newalkar, G., et al., *Effect of Temperature, Pressure, and Residence Time on Pyrolysis of Pine in an Entrained Flow Reactor.* Energy & Fuels, 2014. **28**(8): p. 5144-5157.
44. Mok, W.S.L. and M.J.A. Jr., *Effects of Pressure on Biomass Pyrolysis. I. Cellulose Pyrolysis Products.* 1983.
45. Bridgwater, A.V., D. Meier, and D. Radlein, *An Overview of Fast Pyrolysis of Biomass.* 1999.
46. Chen, G., et al., *Biomass Pyrolysis/Gasification for Product Gas Production: the Overall Investigation of Parametric Effects.* 2002.
47. Jahirul, M., et al., *Biofuels Production through Biomass Pyrolysis —A Technological Review.* Energies, 2012. **5**(12): p. 4952-5001.
48. Van de Velden, M., et al., *Fundamentals, kinetics and endothermicity of the biomass pyrolysis reaction.* Renewable Energy, 2010. **35**(1): p. 232-242.
49. Collard, F.-X. and J. Blin, *A review on pyrolysis of biomass constituents: Mechanisms and composition of the products obtained from the conversion of cellulose, hemicelluloses and lignin.* Renewable and Sustainable Energy Reviews, 2014. **38**: p. 594-608.
50. Manya, J.J., E. Velo, and L. Puigjaner, *Kinetics of Biomass Pyrolysis: a Reformulated Three-Parallel-Reactions Model.* 2003.
51. Yang, H., et al., *Characteristics of hemicellulose, cellulose and lignin pyrolysis.* Fuel, 2007. **86**(12-13): p. 1781-1788.

52. Ly, H.V., et al., *Fast pyrolysis of macroalga Saccharina japonica in a bubbling fluidized-bed reactor for bio-oil production.* Energy, 2015. **93**: p. 1436-1446.
53. Font Palma, C., *Modelling of tar formation and evolution for biomass gasification: A review.* Applied Energy, 2013. **111**: p. 129-141.
54. Anca-Couce, A., *Reaction mechanisms and multi-scale modelling of lignocellulosic biomass pyrolysis.* Progress in Energy and Combustion Science, 2016. **53**: p. 41-79.
55. Lu, Q., W.-Z. Li, and X.-F. Zhu, *Overview of fuel properties of biomass fast pyrolysis oils.* Energy Conversion and Management, 2009. **50**(5): p. 1376-1383.
56. Hernández, J.J., R. Ballesteros, and G. Aranda, *Characterisation of tars from biomass gasification: Effect of the operating conditions.* Energy, 2013. **50**: p. 333-342.
57. Siedlecki, M. and W. de Jong, *Biomass gasification as the first hot step in clean syngas production process – gas quality optimization and primary tar reduction measures in a 100 kW thermal input steam–oxygen blown CFB gasifier.* Biomass and Bioenergy, 2011. **35**: p. S40-S62.
58. Milne, T.A., *Biomass Gasifier "Tars": Their Nature, Formation and Conversion.* 1998.
59. Lee, H.K., *Polycyclic Aromatic Hydrocarbons - Gas Chromatography.* 2000.
60. Demirbas, M.F., *Current Technologies for Biomass Conversion into Chemicals and Fuels.* Energy Sources, Part A: Recovery, Utilization, and Environmental Effects, 2006. **28**(13): p. 1181-1188.
61. Xiu, S. and A. Shahbazi, *Bio-oil production and upgrading research: A review.* Renewable and Sustainable Energy Reviews, 2012. **16**(7): p. 4406-4414.
62. Sharma, A., V. Pareek, and D. Zhang, *Biomass pyrolysis—A review of modelling, process parameters and catalytic studies.* Renewable and Sustainable Energy Reviews, 2015. **50**: p. 1081-1096.
63. Laidler, K.J., *The Development of the Arrhenius Equation.* 1984.
64. White, J.E., W.J. Catallo, and B.L. Legendre, *Biomass pyrolysis kinetics: A comparative critical review with relevant agricultural residue case studies.* Journal of Analytical and Applied Pyrolysis, 2011. **91**(1): p. 1-33.
65. Diblasi, C., *Modeling chemical and physical processes of wood and biomass pyrolysis.* Progress in Energy and Combustion Science, 2008. **34**(1): p. 47-90.
66. Wang, S., et al., *Lignocellulosic biomass pyrolysis mechanism: A state-of-the-art review.* Progress in Energy and Combustion Science, 2017. **62**: p. 33-86.
67. PerkinElmer, I., *A Beginner's Guide to TGA.* 2015.
68. Instruments, T., *SDT Q600 Specifications.* 2010.
69. Tsekos, C., *Fast Pyrolysis of Woody Biomass in a Pyroprobe Reactor: Effect of Torrefaction on the Pyrolysis Products.* 2016.
70. Delft, T. *Pyroprobe*. 2017; Available from: https://www.tudelft.nl/3me/afdelingen/process-energy/facilities/pyroprobe/.
71. CDS Analytical, I., *CDS Analytic Pyroprobe Manual.*
72. JSB. *Pyroprobe 5200 (HPR)*. 13-9-2018]; Available from: http://www.go-jsb.nl/resources/images/assortiment/cds_model_5200_3.jpg.
73. Varian, I., *CP-4900 Micro-GC Data Sheet.* 2009.
74. Varian, I., *CP-4900 Micro-GC User Manual.* 2009.
75. Pantoleontos, G., et al., *A global optimization study on the devolatilisation kinetics of coal, biomass and waste fuels.* Fuel Processing Technology, 2009. **90**(6): p. 762-769.
76. Hastings, C., *Approximations for Digital Computers*. 1955.
77. The Mathworks, I. *Genetic Algorithm*. 2018 19-6-2018]; Available from: https://nl.mathworks.com/discovery/genetic-algorithm.html.
78. Orfao, J.J.M., F.J.A. Antunes, and J.L. Figueiredo, *Pyrolysis Kinetics of Lignocellulosic Materials - Three Independent Reactions Model.* 1998.
79. Watkins, D., et al., *Extraction and characterization of lignin from different biomass resources.* Journal of Materials Research and Technology, 2015. **4**(1): p. 26-32.
80. Anca-Couce, A., A. Berger, and N. Zobel, *How to determine consistent biomass pyrolysis kinetics in a parallel reaction scheme.* Fuel, 2014. **123**: p. 230-240.
81. Tsekos, C., et al., *Kinetic Modeling for the Pyrolysis of Biomass Fuels derived from Oil Crops.* 2015.

82. Grönli, M., M.J. Antal, and G. Varhegyi, *A Round-Robin Study of Cellulose Pyrolysis Kinetics by Thermogravimetry.* 1999.
83. Skodras, G., *Pyrolysis and Combustion Characteristics of Biomass and Waste-Derived Feedstock.* 2006.
84. Kastanaki, E., et al., *Thermogravimetric Studies of the Behavior of Lignite-Biomass Blends during Devolatilization.* 2002.
85. Raveendran, K., A. Ganesh, and K.C. Khilar, *Pyrolysis Characteristics of Biomass and Biomass Components.* 1996.
86. Vamvuka, D. and S. Sfakiotakis, *Effects of heating rate and water leaching of perennial energy crops on pyrolysis characteristics and kinetics.* Renewable Energy, 2011. **36**(9): p. 2433-2439.
87. Kim, J., et al., *Assessment of Miscanthus Biomass (miscanthus sacchariflorus) for Conversion and Utilization of Bio-oil by Fluidized Bed Type Fast Pyrolysis.* 2014.
88. Grierson, S., et al., *Thermal characterisation of microalgae under slow pyrolysis conditions.* Journal of Analytical and Applied Pyrolysis, 2009. **85**(1-2): p. 118-123.
89. Alves, A., et al., *Extraction and physico-chemical characterization of a versatile biodegradable polysaccharide obtained from green algae.* Carbohydr Res, 2010. **345**(15): p. 2194-200.
90. Zhao, H., et al., *The Pyrolysis Characteristics and Kinetics of the Marine MacroalgaeEnteromorpha proliferaUsing a Thermogravimetric Analyzer.* Energy Sources, Part A: Recovery, Utilization, and Environmental Effects, 2012. **34**(21): p. 1958-1966.
91. Kebelmann, K., et al., *Intermediate pyrolysis and product identification by TGA and Py-GC/MS of green microalgae and their extracted protein and lipid components.* Biomass and Bioenergy, 2013. **49**: p. 38-48.
92. Heo, H.S., *Influence of Operation Variables on Fast Pyrolysis of Miscanthus Sinensis var. Purpurascens.* 2009.
93. Bok, J.P., et al., *Fast Pyrolysis of Miscanthus Sinensis in Fluidized Bed Reactors: Characteristics of Product Yields and Biocrude Oil Quality.* 2013.
94. Mos, M., et al., *Impact of Miscanthus x Giganteus Senenscence Times on Fast Pyrolysis Bio-oil Quality.* 2012.
95. Mészáros, E., G. Várhegyi, and E. Jakab, *Thermogravimetric and Reaction Kinetic Analysis of Biomass Samples from an Energy Plantation.* 2004.
96. Jeguirim, M., et al., *Devolatilization Kinetics of Miscanthus Straw from Thermogravimetric Analysis.* International Journal of Green Energy, 2010. **7**(2): p. 164-173.
97. Dorge, S., M. Jeguirim, and G. Trouvé, *Thermal degradation of Miscanthus pellets: kinetics and aerosols characterization.* Waste and Biomass Valorization, 2011. **2**(2): p. 149-155.
98. Cortés, A.M. and A.V. Bridgwater, *Kinetic study of the pyrolysis of miscanthus and its acid hydrolysis residue by thermogravimetric analysis.* Fuel Processing Technology, 2015. **138**: p. 184-193.
99. Wang, J., et al., *A comparative study of thermolysis characteristics and kinetics of seaweeds and fir wood.* Process Biochemistry, 2006. **41**(8): p. 1883-1886.
100. Jmel, M.A., et al., *Variations in Physicochemical Properties and Bioconversion Efficiency of Ulva lactuca Polysaccharides After Different Biomass Pretreatment Techniques.* Appl Biochem Biotechnol, 2018. **184**(3): p. 777-793.
101. Kristensen, E., *Characterization of Biogenic Organic Matter by Stepwise Thermogravimetry (STG).* 1990.
102. Ye, N., et al., *Comparative studies of the pyrolytic and kinetic characteristics of maize straw and the seaweed Ulva pertusa.* PLoS One, 2010. **5**(9).
103. Niu, H. and N. Liu, *Effect of Particle Size on Pyrolysis Kinetics of Forest Fuels in Nitrogen.* Fire Safety Science, 2014. **11**: p. 1393-1405.
104. Ates, F. and M.A. Isikdag, *Evaluation of the Role of the Pyrolysis Temperature in Straw Biomass Samples and Characterization of the Oils by GC/MS.* 2008.
105. Li, S., et al., *Fast pyrolysis of biomass in free-fall reactor for hydrogen-rich gas.* Fuel Processing Technology, 2004. **85**(8-10): p. 1201-1211.
106. Garcia, A., R. Font, and A. Marcilla, *Kinetic Studies of the Primary Pyrolysis of Municipal Solid Waste in a Pyroprobe 1000.* 1992.

107. Nunn, T.R., et al., *Product Compositions and Kinetics in the Rapid Pyrolysis of Sweet Gum Hardwood.* 1985.
108. Becidan, M., Ø. Skreiberg, and J.E. Hustad, *Products distribution and gas release in pyrolysis of thermally thick biomass residues samples.* Journal of Analytical and Applied Pyrolysis, 2007. **78**(1): p. 207-213.
109. Figueiredo, J.L., et al., *Pyrolysis of Holm-Oak Wood: Influence of Temperature and Particle Size.* 1989.
110. Dufour, A., et al., *Synthesis gas production by biomass pyrolysis: Effect of reactor temperature on product distribution.* International Journal of Hydrogen Energy, 2009. **34**(4): p. 1726-1734.
111. Blasi, C.D., et al., *Product Distribution from Pyrolysis of Wood and Agricultural Residues.* 1999.
112. Bae, Y.J., et al., *The characteristics of bio-oil produced from the pyrolysis of three marine macroalgae.* Bioresour Technol, 2011. **102**(3): p. 3512-20.
113. Norouzi, O., et al., *Promotion of hydrogen-rich gas and phenolic-rich bio-oil production from green macroalgae Cladophora glomerata via pyrolysis over its bio-char.* Bioresour Technol, 2016. **219**: p. 643-651.
114. Wang, J., M. Chen, and S. Liu, *Pyrolysis of Ulva Rigida by Microwave Heating.* 2011.
115. Bird, M.I., et al., *Algal biochar–production and properties.* Bioresour Technol, 2011. **102**(2): p. 1886-91.
116. Ross, A.B., et al., *Investigation of the pyrolysis behaviour of brown algae before and after pre-treatment using PY-GC/MS and TGA.* Journal of Analytical and Applied Pyrolysis, 2009. **85**(1-2): p. 3-10.
117. Yanik, J., et al., *Pyrolysis of algal biomass.* Journal of Analytical and Applied Pyrolysis, 2013. **103**: p. 134-141.
118. Yang, H., et al., *Influence of mineral matter on pyrolysis of palm oil wastes.* Combustion and Flame, 2006. **146**(4): p. 605-611.
119. Hajaligol, M.R., et al., *Product Compositions and Kinetics for Rapid Pyrolysis of Cellulose.* 1982.
120. Caballero, J.A., R. Font, and A. Marcilla, *Comparative Study of the Pyrolysis of Almond Shells and their Fractions, Holocellulose and Lignin. Product Yields and Kinetics* 1995.
121. Ferrera-Lorenzo, N., et al., *Pyrolysis characteristics of a macroalgae solid waste generated by the industrial production of Agar–Agar.* Journal of Analytical and Applied Pyrolysis, 2014. **105**: p. 209-216.
122. Sanchez-Silva, L., et al., *Thermogravimetric-mass spectrometric analysis of lignocellulosic and marine biomass pyrolysis.* Bioresour Technol, 2012. **109**: p. 163-72.
123. Guo, X., et al., *Influence of Extractives on Mechanism of Biomass Pyrolysis.* 2010.
124. Skodras, G., et al., *A kinetic study on the devolatilisation of animal derived byproducts.* Fuel Processing Technology, 2007. **88**(8): p. 787-794.
125. Radmanesh, R., et al., *A unified lumped approach in kinetic modeling of biomass pyrolysis.* Fuel, 2006. **85**(9): p. 1211-1220.
126. Šimon, P., *Isoconversional methods.* Journal of Thermal Analysis and Calorimetry, 2004. **76**(1): p. 123-132.
127. Gronli, M., *A Theoretical and Experimental Study of the Thermal Degradation of Biomass*. 1996.
128. Shen, J., et al., *Effects of particle size on the fast pyrolysis of oil mallee woody biomass.* Fuel, 2009. **88**(10): p. 1810-1817.

Appendices

Appendix A – Pyroprobe Protocol

1. PYROLYSIS EXPERIMENT

Prior to conducting the experiment, the biomass sample should be ground and sieved to, at least, 0.2mm size. Furthermore, for a more thorough analysis of the results, the conduction of TGA experiments for sample characterization is suggested.

The experimental procedure described below is of an instructive character. The user should modify it as he/she sees fit, as long as the basic guidelines are followed.

In order to avoid contamination of the various removable parts (especially the holder and the trap) the user is requested to use plastic gloves during the entire experimental procedure.

1. Firstly, the sample holder should be cleaned. This is done by searing it with the use of a torch and then with pressurized air or nitrogen. **In order to avoid accidents, the user should wait until the sample holder cools down after its searing.**
2. Again, with the use of the torch, the wool should be seared in order to remove contaminants.
3. The sample holder, apart from the biomass sample, will contain to pieces of quartz wool on each side, in order to prevent the sample from escaping. So, the next step is to insert the first piece of wool on one side of the holder. It would be the best if the inserted glass wool is one piece. 4! Try to keep the wool intact as it can break easily and subsequently contaminate the sample. This can affect a future analysis of the extracted char.
4. The sample holder together with the inserted piece of wool should be weighed.
5. Roughly 30mg of sample should be inserted in the holder and subsequently weighed. The sample mass must be large enough if permanent gases are to be samples and analysed.
6. The user should try not to compress the inserted sample. After inserting the sample, the walls of the holder have to be cleaned with a paper tissue for the inside walls and pressurized air for the outside ones.
7. Insert the second piece of wool in the sample holder and clean it with pressurized air or nitrogen.

Try not to waste wool!

8. Weigh the full sample holder.
9. Turn on Pyroprobe, from back switch.
10. On the PC press communications tab and then connect.
11. Measure the nitrogen flow which has to be higher than 15ml/min and lower than 20ml/min. This measurement is performed with the use of a test tube filled with soaped water. **Make sure there is no air flow for pyrolysis experiments.** The user should also keep in mind that in order to measure the flow the probe has to be tightly closed.
12. Prepare the trap.
    a) Clean the condenser assembly with isopropanol (IPA).
    b) Dry the condenser with pressurized air or nitrogen. **The user should make sure that there is no IPA left in the last part of the assembly (where the gas extraction takes place).**
    c) Insert 2ml of IPA in the condenser.

d) Weigh the empty trap**. The user should keep in mind that the trap should be always weighed standing, in a vertical position. Furthermore, due to initial vibration after its placement, it might take the scale a while to reach to the right weight value. The trap should be weighed with the same orientation before and after the experiment.**
e) Insert trap and tighten the screws carefully. The filter of the trap should be on the outside and exactly on the Pyroprobe orifice.
f) Connect the condenser to the trap

13. Unscrew the probe and insert the sample holder. **The holder should not be in contact with the wick on the bottom and the probe coils should not be in contact with each other.** Subsequently, screw the probe tightly.
14. Make sure that the syringe for the gas sampling works properly. This is done by connecting it to the nitrogen outflow from Pyroprobe.
15. On the PC, go to the Pyroprobe tab and select the heating rate and the final temperature according to test parameters. Furthermore, adjust if needed the parameters on the Accessory tab. Then save and subsequently load the current method.

The pyrolysis temperature set in Pyroprobe is different from the actual temperature in which pyrolysis takes place. The corresponding values are included in Chapter 1. Additionally the holding time set in Pyroprobe does not correspond to the interval on which the sample is heated at the pyrolysis temperature. Instead it includes the time needed to achieve the specified temperature. The time that needs to be set for 10s of holding time is also presented also in Chapter 1.

16. Before initiating the experiment it should be made sure that every component is tightly closed (e.g. probe, gas sampler, etc.).
17. Press RUN.

If the experiment is proceeding smoothly, bubbles should appear in the condenser. Furthermore, during and a little bit after pyrolysis the user might notice smoke in the vial.

18. Before the temperature of the accessory reaches 300 °C, the syringe is inserted. **The syringe should not contain any air, but pushing it out should be done with care in order for it not to get stuck.**
19. During the test, there might be a smell of “burning”. The smell should not be strong as this would mean that there is a leakage.
20. Wait until the test is over. **Then, first separate the condenser from the trap immediately in order to avoid IPA back-flow into the trap and afterwards remove the syringe and put its lid on also immediately.**
21. Note the volume of the gases collected in the syringe, as it will be used for the gas products determination.
22. Measure the weight of the trap. **The trap should be weighed as fast as possible after the completion of the experiment in order to prevent major losses of very volatile tar compounds.** For the same reason, the part of the trap that contains the filter should be placed at the bottom of the balance.
23. Wait for the accessory to cool down at 50oC in order to remove the sample holder safely.
24. Tar collection:
    a) Insert 3ml of IPA in a testing tube and add the 2ml of IPA that were already in the condenser.
    b) Insert the trap into the testing tube.
    c) Stir the tube carefully. **Make sure that the bottom part of the trap is at the side of the testing tube where the IPA is, so the trapped tars are removed as efficiently as possible.**
    d) Leave it in a standing position for at least 30 minutes. Longer residence time in the IPA solution can improve tar analysis and the subsequent trap cleaning.
25. When the temperature falls below 50oC, open the probe and retrieve the sample holder using tweezers.
26. Weigh the sample holder, in order to measure the amount of reacted biomass.

27. Carefully remove the wool and the char from the sample holder. The char must be stored. **Stored char should not contain traces of wool if possible.**
28. Resume tar collection:
    a) Empty the tar solution through a paper filter into a clean testing vessel. Make sure that the part of the solution that is in the trap is also collected.
    b) Collect the tar solution (with a pipet) into a small vial and seal it.
29. Clean all used vessels with acetone.
30. The trap should be cleaned with IPA both on the inside and on the outside. Carefully, clear any remaining tars from the bottom part of the trap. Also, by pushing gently IPA through the filter, the user should try to remove from it any particles that might be stuck there. **After cleaning the trap should be dried immediately using pressurized nitrogen. In order for it to be completely dried, the trap should also be inserted into the Pyroprobe, this time with the filter facing the inside of the Pyroprobe and left there for some minutes. An oven set at temperatures around 150 °C can also be used for this purpose.**
31. Measure the nitrogen flow again. If a big deviation from the former value is observed, it probably means that there is a blockage of the device and cleaning should be performed before the conduction of more experiments.

2. Gas Analysis

Gas analysis is performed manually in a Micro GC using the Galaxie software.

1. Insert the syringe into the Micro-GC reception.
2. Press quick start.
3. Change name (i.e. save the results with the selected name)
4. Change identifier (i.e. 1,2,3,4 because there will be multiple injections).
5. Press start.
6. When a distinctive sound is heard from the Micro GC (i.e. the mGC is injecting) press the syringe slightly in order to push out an amount of gas sample. Keep pressing repeatedly until the sound goes off. **Be very careful not to remove the reception tube due to the gas-pushing; it should be held firmly while pushing.**
7. Repeat the process above at least 3-4 times. Every time keep the same name and change the identifier. The last run gives the final values for the gas analysis.
8. In order to view the results go to File: open chromatogram: file name (on the left side of the screen).

Appendix B – Protocol Matlab Application

The Matlab application was made with MATLAB R2018a®. It is recommended to have at least Matlab version R2016a. Operating the application on earlier versions might not work, since the Matlab App Designer did not exist in earlier versions. Furthermore, for the application to work, it is required to have the Global Optimization Toolbox, which is not in the standard Matlab package.

Starting the application

1. Open Matlab.
2. Browse for the folder in which you saved the Matlab Application file. It is required to have the Excel file with the TGA results that have to modelled in the same folder as the Matlab Application file.
3. To run the application, double click on the application file in the 'Current Folder' window. If it is desired to take a look at the code, hit right-click on the application file and select 'open'. The application can be run from here as well by pressing the 'Run' button.

Interface settings

4. In the interface that appeared after running the application, information about the Excel file with the TGA results has to be filled in:
    a. Fill in the name of the Excel file.
    b. Fill in the name of the Excel tab containing the TGA results.
    c. Fill in the heating rate and the total fraction of volatiles.
    d. Fill in the start cell and the end cell of the Excel row with the mass loss rates. Do the same for the Excel row with the temperatures.
    e. Fill in the Excel column with the mass loss rates. Do the same for the Excel column with the temperatures.
    f. Choose the correct units for the mass loss rates and temperatures used in Excel.

If the same Excel file will be used multiple times, it is recommended to change the pre-set data of the interface in the code* (or to not close the application in between runs)

5. The GA Solver Options in the interface are pre-set to values that appeared to work best for modelling with the IPR model.
    a. The 'Function Tolerance' is the value of the change of the objective function and is used a stopping criterion for the genetic algorithm solver.
    b. The 'Population Size' gives the size of each generation for the genetic algorithm solver. For a larger generation, the search area of the combinations of the kinetic constants is more extensive. The pre-set population size is a compromise between search area and computation time. When the modelling results deviate very much from the experimental results, a higher population size could be tried in order to find better modelling results.
6. The input ranges for finding the kinetic constants of hemicellulose, cellulose and lignin that are shown in the interface are pre-set values for the maximum ranges of the kinetic constants (activation energies, pre-exponential factors and fractions of volatiles) found in literature for lignocellulosic biomass species. The values can be changed based on the biomass species. It is recommended to run the first time with the pre-set values. Based on the results, the ranges can be narrowed down in order to improve the modelling results
7. The reaction orders were all fixed to 1 as first order reactions proved to give valuable results. The reaction orders could be changed or set to be variable if there is a reason to do so.

Running the application

8. Close all open Excel files on your computer.
9. Press the 'Run' button in the centre of the interface. By pressing the 'Run' button, the text on the button changes to 'Running…'. The running time of the application is found to be between 30 to 60 minutes. This time increases when the population size is increased.
10. When the application is done running, the results of the kinetic constants and the associated graphs are shown on the interface. The results for the kinetic constants are also shown in the Matlab command window for facilitating the ease of copying the results. The graphs are also shown in separate figures for facilitating the ease of saving them.

*To change the pre-set interface data, the code of the Matlab application has to be opened. The data can be changed by clicking on the particular field in the 'Design View' and changing the text (text fields) or the number (numeric fields).

Appendix C – Pyroprobe Results

Results for Miscanthus pyrolysis

T=500 °C	#	Gas	Tar	Char	Mass balance
	1	8.60 wt%	34.88 wt%	37.66 wt%	81.14 wt%
	2	8.09 wt%	33.07 wt%	37.38 wt%	78.54 wt%
	Average	8.34 wt%	33.98 wt%	37.52 wt%	79.84 wt%
	Stdev	0.36 wt%	1.28 wt%	0.19 wt%	1.84 wt%

T=600 °C	#	Gas	Tar	Char	Mass balance
	1	11.75 wt%	38.62 wt%	21.11 wt%	71.48 wt%
	2	12.19 wt%	37.42 wt%	21.61 wt%	71.22 wt%
	Average	11.97 wt%	38.02 wt%	21.36 wt%	71.35 wt%
	Stdev	0.31 wt%	0.85 wt%	0.35 wt%	0.19 wt%

T=700 °C	#	Gas	Tar	Char	Mass balance
	1	16.38 wt%	32.11 wt%	17.54 wt%	66.04 wt%
	2	15.96 wt%	36.37 wt%	17.90 wt%	70.23 wt%
	Average	16.17 wt%	34.24 wt%	17.72 wt%	68.13 wt%
	Stdev	0.30 wt%	3.01 wt%	0.26 wt%	2.97 wt%

T=800 °C	#	Gas	Tar	Char	Mass balance
	1	22.52 wt%	24.65 wt%	14.09 wt%	61.27 wt%
	2	23.36 wt%	24.93 wt%	16.00 wt%	64.29 wt%
	Average	22.94 wt%	24.79 wt%	15.05 wt%	62.78 wt%
	Stdev	0.59 wt%	0.20 wt%	1.35 wt%	2.14 wt%

T=900 °C	#	Gas	Tar	Char	Mass balance
	1	26.39 wt%	20.48 wt%	15.27 wt%	62.14 wt%
	4	29.40 wt%	19.38 wt%	14.83 wt%	63.61 wt%
	Average	27.89 wt%	19.93 wt%	15.05 wt%	62.87 wt%
	Stdev	2.13 wt%	0.78 wt%	0.31 wt%	1.04 wt%

T=1000 °C	#	Gas	Tar	Char	Mass balance
	2	29.98 wt%	18.24 wt%	12.07 wt%	60.28 wt%
	3	29.87 wt%	14.77 wt%	16.01 wt%	60.66 wt%
	4	27.39 wt%	17.58 wt%	16.82 wt%	61.79 wt%
	Average	29.08 wt%	16.86 wt%	14.97 wt%	60.91 wt%
	Stdev	1.46 wt%	1.84 wt%	2.54 wt%	0.78 wt%

Results for Ulva pyrolysis

T = 500 °C	#	Gas	Tar	Char	Mass balance
	6	3.88 wt%	17.51 wt%	57.25 wt%	78.65 wt%
	7	3.62 wt%	20.12 wt%	57.85 wt%	81.59 wt%
	Average	3.75 wt%	18.82 wt%	57.55 wt%	80.12 wt%
	Stdev	0.19 wt%	1.84 wt%	0.42 wt%	2.08 wt%

T = 600 °C	#	Gas	Tar	Char	Mass balance
	4	5.54 wt%	21.46 wt%	53.29 wt%	80.28 wt%
	6	6.00 wt%	18.29 wt%	52.46 wt%	76.75 wt%
	Average	5.77 wt%	19.88 wt%	52.87 wt%	78.52 wt%
	Stdev	0.32 wt%	2.24 wt%	0.58 wt%	2.50 wt%

T = 700 °C	#	Gas	Tar	Char	Mass balance
	1	8.25 wt%	19.00 wt%	47.98 wt%	75.23 wt%
	2	7.76 wt%	23.69 wt%	47.61 wt%	79.05 wt%
	Average	8.00 wt%	21.34 wt%	47.79 wt%	77.14 wt%
	Stdev	0.35 wt%	3.32 wt%	0.26 wt%	2.70 wt%

T = 800 °C	#	Gas	Tar	Char	Mass balance
	1	11.14 wt%	19.31 wt%	46.15 wt%	76.61 wt%
	2	10.33 wt%	23.04 wt%	47.51 wt%	80.88 wt%
	Average	10.74 wt%	21.17 wt%	46.83 wt%	78.74 wt%
	Stdev	0.57 wt%	2.64 wt%	0.96 wt%	3.02 wt%

T = 900 °C	#	Gas	Tar	Char	Mass balance
	2	12.75 wt%	17.18 wt%	42.94 wt%	72.86 wt%
	4	13.10 wt%	17.39 wt%	44.00 wt%	74.49 wt%
	Average	12.92 wt%	17.28 wt%	43.47 wt%	73.68 wt%
	Stdev	0.25 wt%	0.15 wt%	0.75 wt%	1.15 wt%

T = 1000 °C	#	Gas	Tar	Char	Mass balance
	1	21.29 wt%	14.22 wt%	31.32 wt%	66.83 wt%
	2	20.16 wt%	14.46 wt%	30.29 wt%	64.90 wt%
	Average	20.72 wt%	14.34 wt%	30.80 wt%	65.87 wt%
	Stdev	0.80 wt%	0.17 wt%	0.73 wt%	1.37 wt%

Appendix D – Micro-GC results

Gas composition for Miscanthus fast pyrolysis (wt% of initial sample size)

T = 500	#	H_2	CO	CH_4	CO_2
	1	0.00 wt%	2.54 wt%	0.00 wt%	6.05 wt%
	2	0.00 wt%	2.45 wt%	0.00 wt%	5.64 wt%
	Average	0.00 wt%	2.50 wt%	0.00 wt%	5.84 wt%
	Stdev	0.00 wt%	0.07 wt%	0.00 wt%	0.29 wt%

T = 600	#	H_2	CO	CH_4	CO_2
	1	0.01 wt%	3.74 wt%	0.20 wt%	7.81 wt%
	2	0.01 wt%	3.95 wt%	0.21 wt%	8.02 wt%
	Average	0.01 wt%	3.84 wt%	0.20 wt%	7.92 wt%
	Stdev	0.00 wt%	0.15 wt%	0.01 wt%	0.15 wt%

T = 700	#	H_2	CO	CH_4	CO_2
	1	0.04 wt%	6.94 wt%	0.82 wt%	8.58 wt%
	2	0.04 wt%	6.71 wt%	0.83 wt%	8.38 wt%
	Average	0.04 wt%	6.82 wt%	0.82 wt%	8.48 wt%
	Stdev	0.00 wt%	0.17 wt%	0.00 wt%	0.14 wt%

T = 800	#	H_2	CO	CH_4	CO_2
	1	0.20 wt%	11.06 wt%	1.84 wt%	9.43 wt%
	2	0.22 wt%	11.56 wt%	1.94 wt%	9.63 wt%
	Average	0.21 wt%	11.31 wt%	1.89 wt%	9.53 wt%
	Stdev	0.02 wt%	0.35 wt%	0.07 wt%	0.15 wt%

T = 900	#	H_2	CO	CH_4	CO_2
	1	0.47 wt%	13.68 wt%	2.55 wt%	9.70 wt%
	4	0.44 wt%	15.92 wt%	2.92 wt%	10.11 wt%
	Average	0.45 wt%	14.80 wt%	2.73 wt%	9.91 wt%
	Stdev	0.02 wt%	1.59 wt%	0.27 wt%	0.30 wt%

T = 1000	#	H_2	CO	CH_4	CO_2
	2	0.54 wt%	15.94 wt%	3.00 wt%	10.50 wt%
	3	0.52 wt%	16.14 wt%	2.99 wt%	10.22 wt%
	4	0.47 wt%	14.64 wt%	2.64 wt%	9.64 wt%
	Average	0.51 wt%	15.57 wt%	2.88 wt%	10.12 wt%
	Stdev	0.04 wt%	0.81 wt%	0.21 wt%	0.44 wt%

Gas composition for Ulva fast pyrolysis (wt% of initial sample size)

T = 500	#	H_2	CO	CH_4	CO_2
	6	0.00 wt%	0.37 wt%	0.00 wt%	3.51 wt%
	7	0.00 wt%	0.36 wt%	0.00 wt%	3.25 wt%
	Average	0.00 wt%	0.37 wt%	0.00 wt%	3.38 wt%
	Stdev	0.00 wt%	0.01 wt%	0.00 wt%	0.18 wt%

T = 600	#	H_2	CO	CH_4	CO_2
	4	0.00 wt%	0.97 wt%	0.00 wt%	4.56 wt%
	6	0.00 wt%	0.98 wt%	0.07 wt%	4.94 wt%
	Average	0.00 wt%	0.97 wt%	0.03 wt%	4.75 wt%
	Stdev	0.00 wt%	0.01 wt%	0.05 wt%	0.27 wt%

T = 700	#	H_2	CO	CH_4	CO_2
	1	0.02 wt%	2.12 wt%	0.33 wt%	5.79 wt%
	2	0.02 wt%	1.76 wt%	0.34 wt%	5.63 wt%
	Average	0.02 wt%	1.94 wt%	0.34 wt%	5.71 wt%
	Stdev	0.00 wt%	0.25 wt%	0.01 wt%	0.11 wt%

T = 800	#	H_2	CO	CH_4	CO_2
	1	0.08 wt%	3.86 wt%	0.87 wt%	6.33 wt%
	2	0.07 wt%	3.34 wt%	0.82 wt%	6.10 wt%
	Average	0.08 wt%	3.60 wt%	0.84 wt%	6.22 wt%
	Stdev	0.01 wt%	0.37 wt%	0.03 wt%	0.16 wt%

T = 900	#	H_2	CO	CH_4	CO_2
	2	0.11 wt%	4.50 wt%	1.10 wt%	7.05 wt%
	4	0.12 wt%	4.61 wt%	1.17 wt%	7.20 wt%
	Average	0.11 wt%	4.55 wt%	1.13 wt%	7.12 wt%
	Stdev	0.01 wt%	0.08 wt%	0.05 wt%	0.11 wt%

T = 1000	#	H_2	CO	CH_4	CO_2
	1	0.23 wt%	7.79 wt%	1.11 wt%	12.17 wt%
	2	0.20 wt%	6.67 wt%	1.21 wt%	12.07 wt%
	Average	0.22 wt%	7.23 wt%	1.16 wt%	12.12 wt%
	Stdev	0.02 wt%	0.79 wt%	0.08 wt%	0.07 wt%

Relative gas composition for Miscanthus fast pyrolysis (wt% of total gas yield)

Temperature (°C)	H_2	CO	CH_4	CO_2
500	0.03 wt%	29.93 wt%	0.00 wt%	70.03 wt%
600	0.06 wt%	32.11 wt%	1.70 wt%	66.13 wt%
700	0.26 wt%	42.19 wt%	5.10 wt%	52.44 wt%
800	0.92 wt%	49.31 wt%	8.23 wt%	41.55 wt%
900	1.64 wt%	52.99 wt%	9.79 wt%	35.57 wt%
1000	1.72 wt%	53.75 wt%	9.82 wt%	34.71 wt%

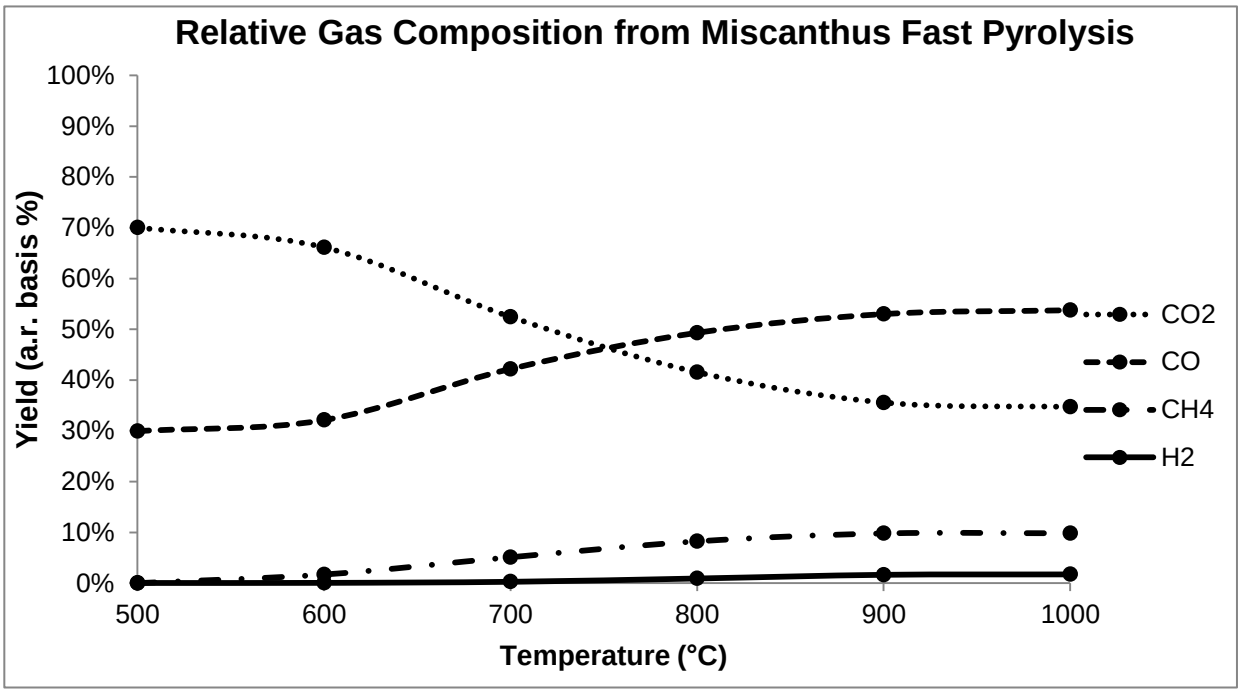

Figure D1. Gas composition of Miscanthus pyrolysis (wt% of total gas product).

Relative gas composition for Ulva fast pyrolysis (wt% of total gas yield)

Temperature (°C)	H_2	CO	CH_4	CO_2
500	0.000 wt%	9.617 wt%	0.000 wt%	90.383 wt%
600	0.066 wt%	16.903 wt%	0.579 wt%	82.452 wt%
700	0.241 wt%	24.195 wt%	4.203 wt%	71.361 wt%
800	0.714 wt%	33.490 wt%	7.870 wt%	57.926 wt%
900	0.886 wt%	35.233 wt%	8.749 wt%	55.131 wt%
1000	1.04 wt%	34.83 wt%	5.61 wt%	58.52 wt%

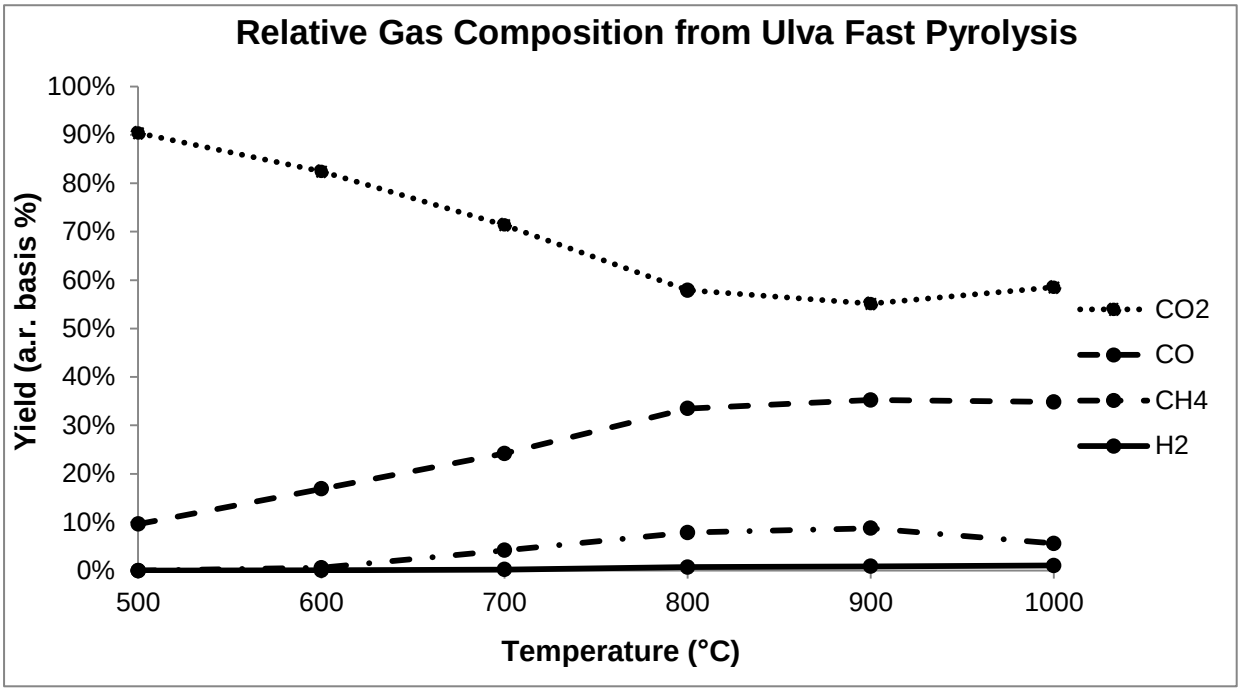

Figure D2. Gas composition of Ulva pyrolysis (wt% of total gas product).

Appendix E – Interface of Matlab Application with Results

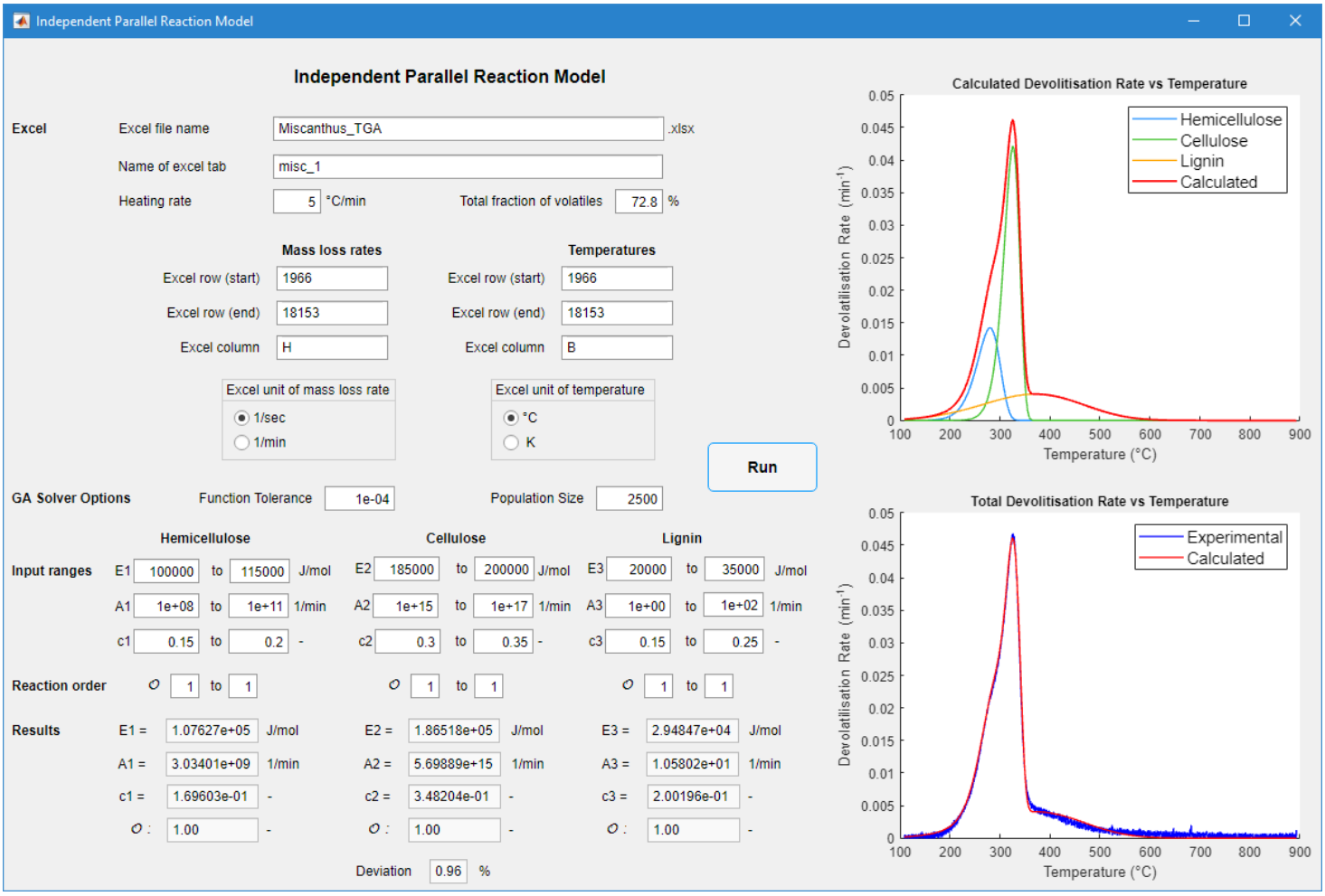

Figure E1. Interface of Matlab application with optimal modelling results found for the mass loss rate of Miscanthus for a heating rate of 5 °C/min.

Appendix F – Modelled Mass Loss Rates of Miscanthus (10 and 20 °C/min)

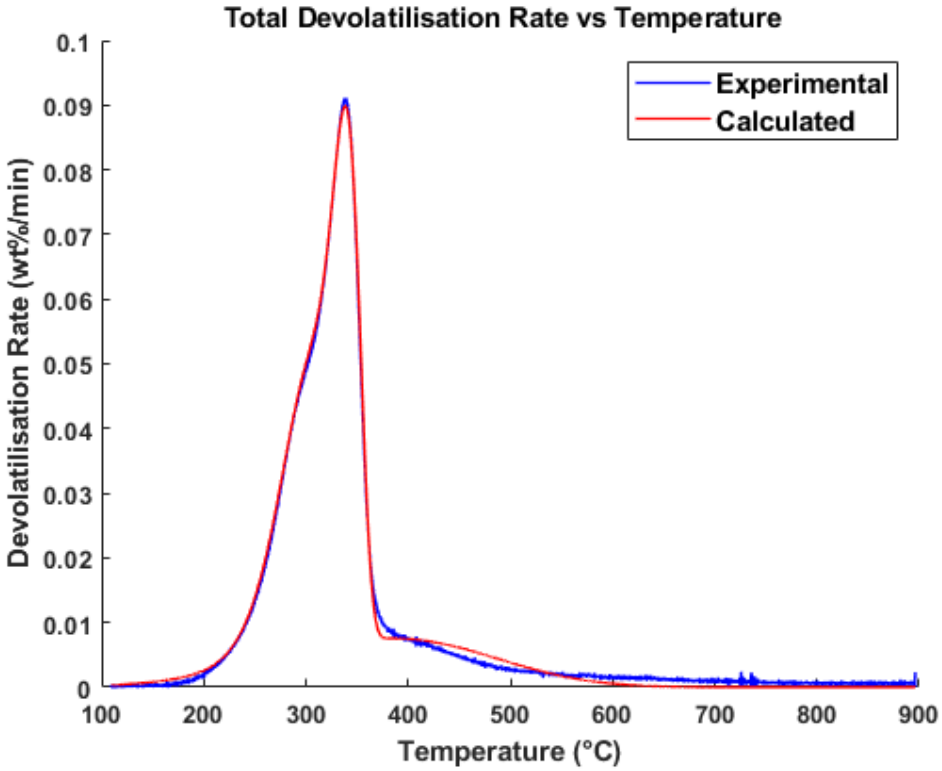

Figure F1. Matlab plot of the experimentally obtained mass loss rate and the calculated mass loss rate of Miscanthus at a heating rate of 10 °C/min plotted against the temperature.

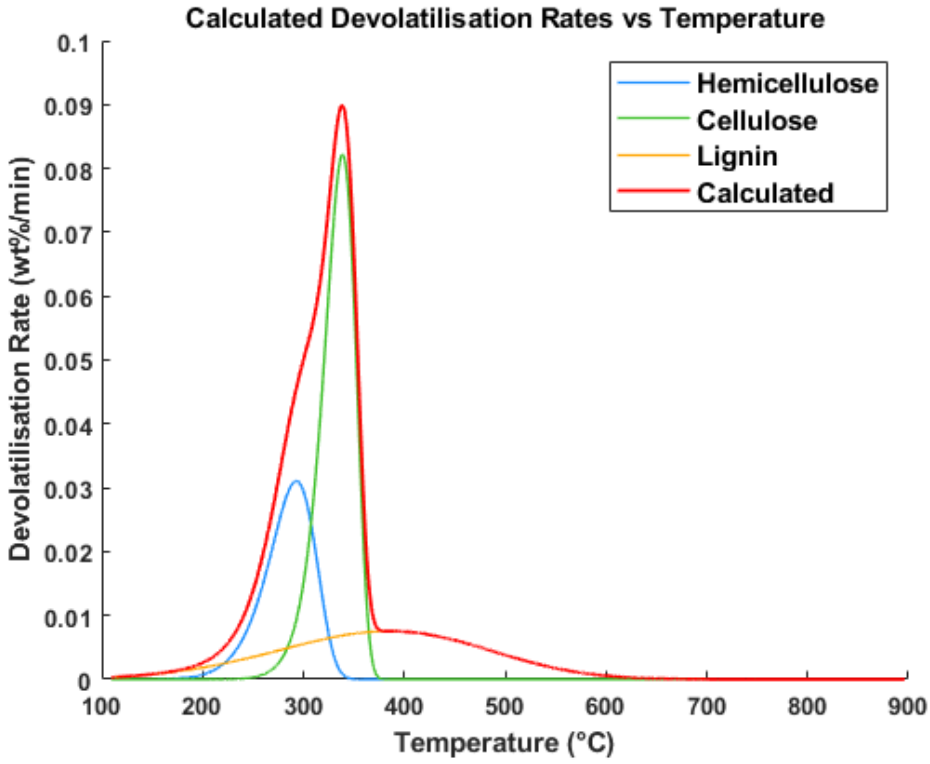

Figure F2. Matlab plot of the total calculated mass loss rate together with the calculated mass loss rates of the individual main biomass components of Miscanthus at a heating rate of 10 °C/min plotted against the temperature.

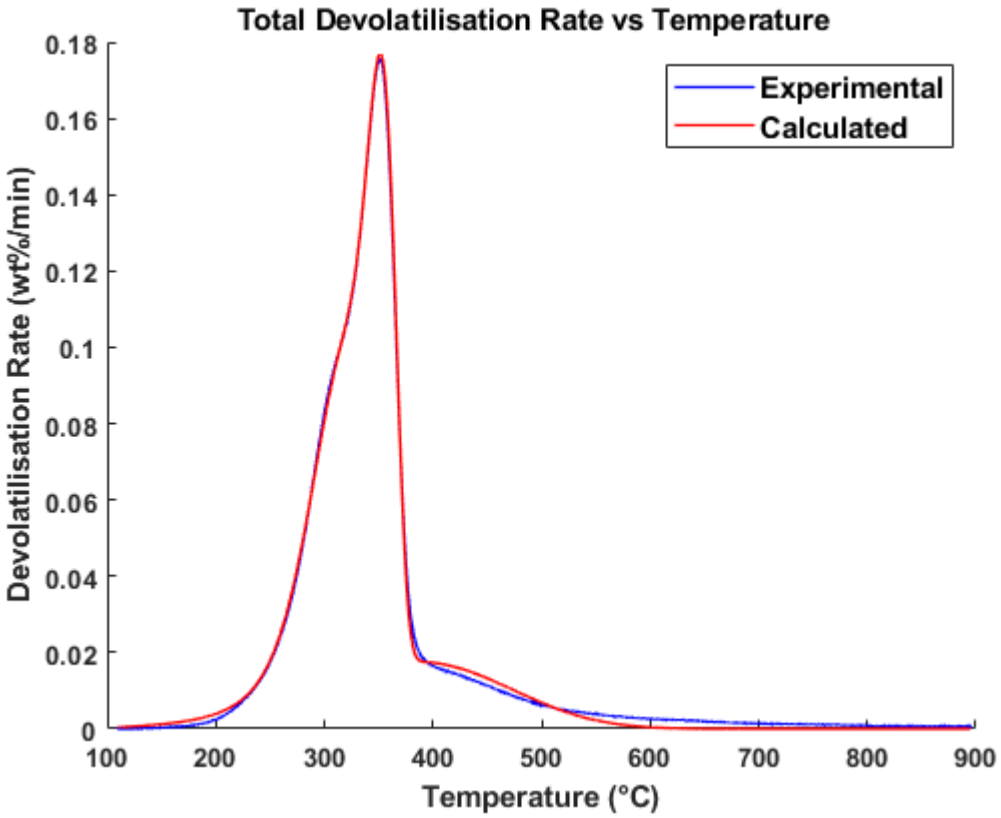

Figure F3. Matlab plot of the experimentally obtained mass loss rate and the calculated mass loss rate of Miscanthus at a heating rate of 20 °C/min plotted against the temperature.

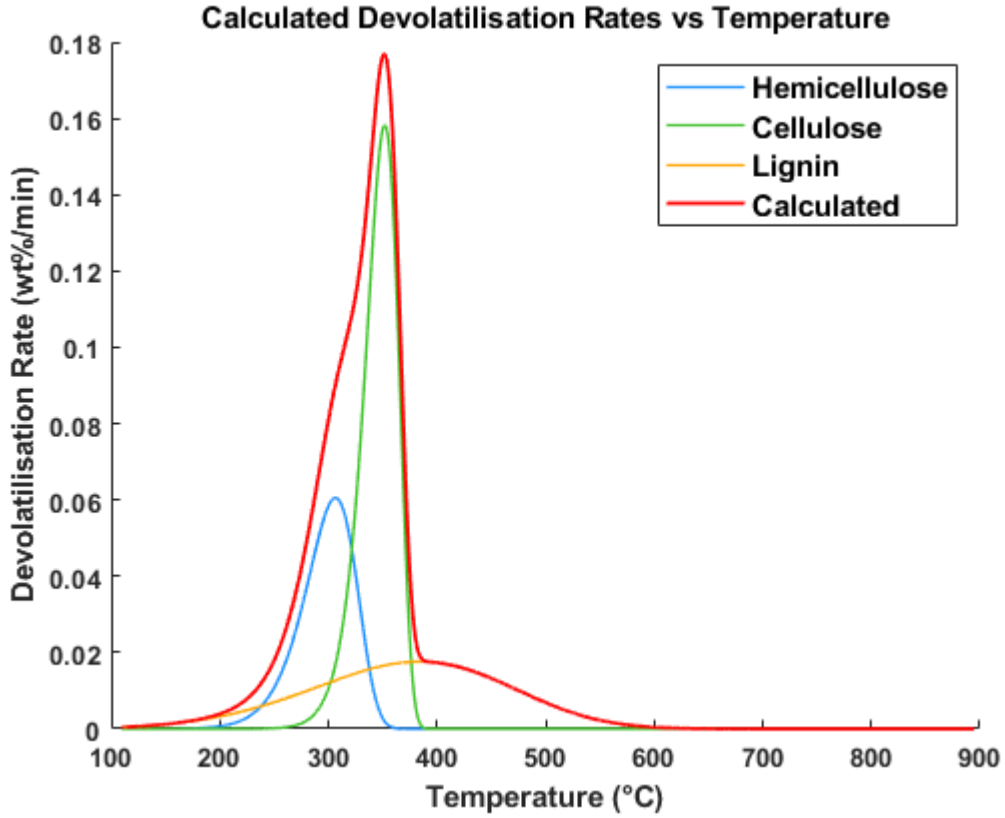

Figure F4. Matlab plot of the total calculated mass loss rate together with the calculated mass loss rates of the individual main biomass components of Miscanthus at a heating rate of 20 °C/min plotted against the temperature.

Appendix G – Literature Review on Energy Crops Modelled with the IPR Model

Table G1: Summary of Kinetic Constants Obtained with the IPR model for Various Energy Crops

Heating rate	Energy Crop	Hemicellulose			Cellulose			Lignin		
		E (kJ/mol)	A (1/min)	c (%)	E (kJ/mol)	A (1/min)	c (%)	E (kJ/mol)	A (1/min)	c (%)
5 °C/min										
Radmanesh et al.	Rice husk	129	4.8e11	0.22	184	1.5e15	0.59	64	3.8e3	0.18
Pantoleontos et al.	Olive kernel	116	4.7e10	0.14	143	1.5e12	0.51	41	1.2e2	0.35
10 °C/min										
Vamvuka et al.	Switch grass	122	5.6e10	0.29	175	1.7e14	0.55	39	1.7e2	0.15
	Giant reed	117	3.1e10	0.19	176	2.5e14	0.45	33	4.7e1	0.36
Tsekos et al.	Sunflower	97	4.4e9	0.09	108	2.3e9	0.38	31	3.1e2	0.26
Kastanaki et al.	Olive kernel	93	2.5e8	0.18	210	1.4e18	0.28	31	2.8e1	0.29
20 °C/min										
Skodras et al.	Olive kernel	109	1.7e10	0.10	131	1.6e11	0.56	46	5.8e2	0.34
Pantoleontos et al.	Olive kernel	119	1.5e11	0.11	137	5.5e11	0.54	33	7.1e1	0.36